crack. For example, the anchorage length available for the diagonal crack at A is $(L_p)_A$, if this is greater than L_e then the full IC debonding resistance can be achieved. When the anchorage length L_p is less than L_e, then the IC debonding resistance reduces until, at the critical diagonal crack at C where $L_p = 0$, the IC debonding resistance is zero.

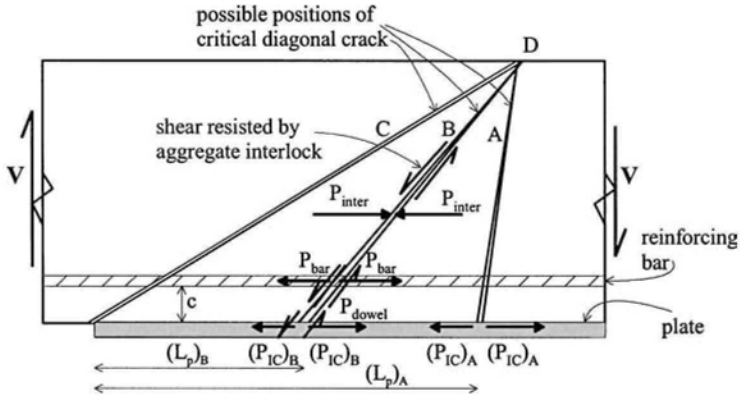

Figure 4.3 Affect of IC resistance on CDC debonding

4.2.2 Examples of CDC debonding of tension face plates

Examples of CDC debonding of tension face plated beams without stirrups are shown in Figs 1.18 and 1.38; in these tests, the tension face plate was terminated just short of the support. It was explained and shown that a critical diagonal crack can suddenly appear in a previously uncracked zone of a beam and, simultaneously, cause plate debonding. For example, the cracks marked 120 in Fig. 1.18, 188 in Fig. 1.19 and 20 in Fig. 1.38 were not the extension of flexural-shear cracks, such as those shown in Fig. 2.2, but suddenly formed and caused CDC debonding.

An example of CDC debonding in a tension face plated beam with stirrups is shown in Fig. 4.4. The presence of stirrups tends to cloud the debonding mechanism because, unlike plated beams without stirrups where the formation of the critical diagonal crack causes the beam to fail at V_c, the presence of stirrups allows the beam to resist the shear load after the critical diagonal crack has formed. The failure mechanism may appear at first sight to be different. However numerous direct comparisons of the same plated beam with and without stirrups have shown that the shear load at debonding $V_{c\text{-plate}}$ is the same; in fact in one series of tests, sufficient stirrups were provided to increase the shear capacity of the unplated beam to $4V_c$ but on plating these beams, the plated beams were found to debond at the same shear load $V_{c\text{-plate}}$ as the beams without stirrups.

The beam in Fig. 4.4 was loaded under displacement control. The diagonal shear crack marked *A* first formed, but as it did not intercept the plate, it did not initiate debonding. Critical diagonal crack debonding first occurred at the formation of the CDC marked *B* which caused CDC debonding from the root of the CDC to the plate end shown by the arrow marked 1. As with IC debonding, the debonding crack propagates towards the plate end. Because of the formation of these new cracks, the stiffness of the beam reduced, thereby, reducing the applied load as the hydraulic jack was under displacement control. The applied load was then increased and when it reached near to the previous level, the CDC marked *C* formed, followed immediately

by crack propagation marked 2 and the load reduced again. The same sequence of loading produced the remaining critical diagonal cracks and debonding cracks. Of importance, the critical diagonal cracks formed at about the same shear load $V_{c\text{-plate}}$, the debonding cracks always propagated from the root of the CDC to the plate end. However, the CDC debonding cracks spread away from the supports. Hence in reality, although the distribution of the cracks in the beam with stirrups in Fig. 4.4 would at first glance appear to be different from those beams without stirrups in Figs 1.19, 1.38 and 4.1, the mechanism of debonding is exactly the same.

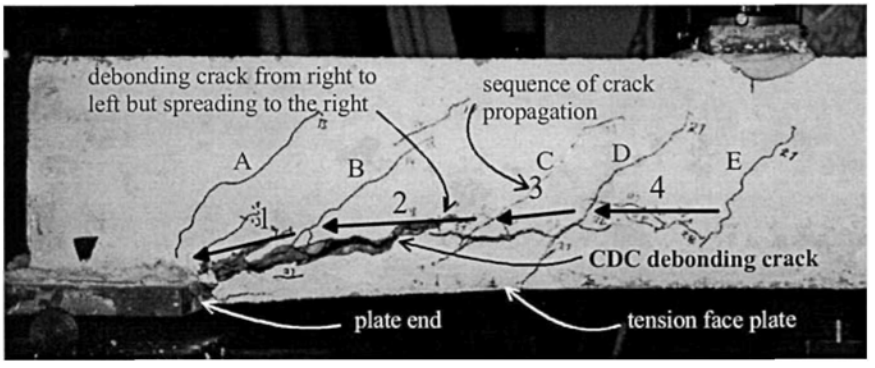

Figure 4.4 CDC debonding of a tension face plated beam with stirrups

It is also worth comparing, the distribution of cracks in Fig. 4.4, that were induced by CDC debonding in a beam with stirrups with those in Fig. 2.19 that were induced by IC debonding. They would appear to be similar with *concrete teeth* forming between the cracks, but the mechanisms that formed them, as has been explained, are totally different. IC debonding in Fig. 2.19 is induced by axial forces in the plate, starts at several positions in the region of maximum moment, and propagate and spread towards the plate end. In contrast, CDC debonding in Fig. 4.4 is induced by the rigid body shear displacement across a diagonal crack, starts at the root of a diagonal crack, propagates towards the plate end and spreads away from the plate end.

4.3 Concrete shear capacity of unplated beams or slabs

It has been shown that CDC debonding of a plated beam at $V_{c\text{-plate}}$ is controlled by the same mechanism that controls the concrete shear capacity V_c. Hence a good starting point, to develop a mathematical model for CDC debonding, is to start with the mathematical model for the shear capacity of a beam or slab without stirrups, that is V_c. In this section, we will first look at examples of the formation of critical diagonal cracks in RC beams and then qualitatively describe a procedure by Zhang (1997) for determining the concrete shear capacity V_c. Zhang's procedure has been chosen as it not only quantifies the capacity of V_c but also the position of the critical diagonal crack, which is an important criterion in determining P_{IC} and, hence, the extent of plating. It may be worth noting that Zhang's approach is a semi-empirical approach and consequently has a few dimensionally incorrect equations, but it has been calibrated with well over a hundred tests and, hence can be used with confidence.

4.3.1 Critical diagonal cracks in RC beams

Figure 4.5 shows shear failure of an RC beam without stirrups. The numbers on the beam are the applied loads. It can be seen that a series of vertical flexural and slightly inclined flexural-shear cracks first formed in the lower half of the beam and in the vicinity of the applied load. Then in a completely uncracked region, a critical diagonal crack formed through the depth of the beam and, as the beam did not have stirrups, this one critical diagonal crack caused failure. The shear failure is the concrete shear capacity of the beam V_c.

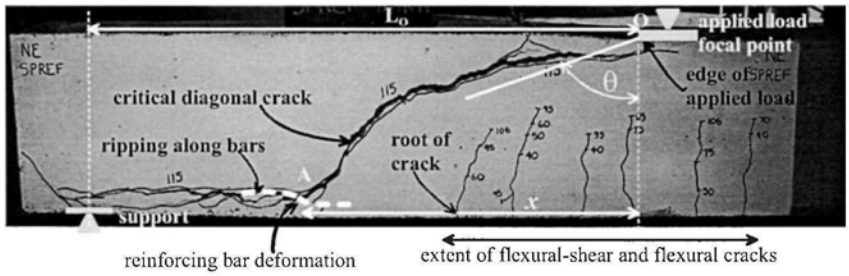

Figure 4.5 Critical diagonal crack in beam without stirrups

The critical diagonal crack in Fig. 4.5 spans between the edge of the applied load at point O, which will be referred to as the focal point, to the root of the crack at point A, that is over a length x of the shear span of length L_o. The horizontal cracking, along the level of the reinforcing bars from point A to the support, is due to the ripping action, as the reinforcing bars on the left side of A are pushed down due to the rigid body shear displacement across the two sides of the critical diagonal crack. The deformation of the reinforcing bar across the CDC is shown as the broken white line next to point A. It is this deformation, due to the rigid body displacement across the CDC, that causes the bars to the left of the CDC to break away from the beam as their cover is relatively small. As a matter of interest, it is this same action that causes plates that cross the CDC to debond as can be seen in Figs 1.19, 1.38 and 4.4.

For beams with concentrated loads, the focal point O usually occurs at the edge of the concentrated load as shown in Fig. 4.5 and it is a question of finding the inclination of the critical diagonal crack θ that gives the weakest strength. For convenience, the critical diagonal crack is represented by a straight line. For beams with uniformly distributed loads, the position of the focal point O of the critical diagonal crack is not so easy to define as it depends on the rate of change of the applied shear, so it may be necessary to try several positions to determine the weakest position, relative to the applied shear, that of the critical diagonal crack.

The formation of the critical diagonal cracks in beams with stirrups in Fig. 4.6 would appear to be much more confusing when compared to the single critical diagonal crack in Fig. 4.5 in a beam without stirrups. However, the first critical diagonal crack in Fig. 4.6 will form at the same position as in a beam without stirrups, as the presence of stirrups has virtually no effect on the formation of cracks, as stirrups only start to resist significant force when they span a crack. It is the formation and then rigid body displacement of this first critical diagonal crack that causes a plate to debond and not the ensuing diagonal cracks. After the formation of the first critical diagonal crack, and because the beam does not fail due to the presence of stirrups, other diagonal cracks can form as can be seen in Fig. 4.6.

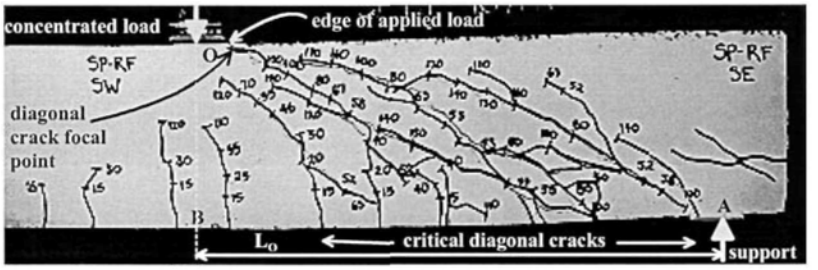

Figure 4.6 Critical diagonal cracks in beam with stirrups

4.3.2 Qualitative description of CDC analysis

An RC beam or slab without stirrups fails in vertical shear by first forming a diagonal crack after which failure occurs when the vertical shear resistance of that diagonal crack is exceeded. Hence, the shear capacity at a given section of a beam depends on two parameters: the vertical shear load that is required to form a diagonal crack $(V_{dat})_{cr}$ and the shear capacity that that diagonal crack can resist $(V_{dat})_u$. The CDC analysis for the hogging region of a beam follows the same procedure as that for the sagging region.

As an example of the analysis for vertical shear failure, let us consider one shear span of a hogging region of a plated beam as shown in Fig. 4.7(a). In the analysis, it is convenient to determine the shear load at any convenient datum point V_{dat} at which shear cracking or failure occurs within the shear span. In this example, we will assume that the datum point is at the point of contraflexure as shown and also that there is no applied load between the point of contraflexure and the support, so that in this example the vertical shear force is constant along the shear span at V_{dat}.

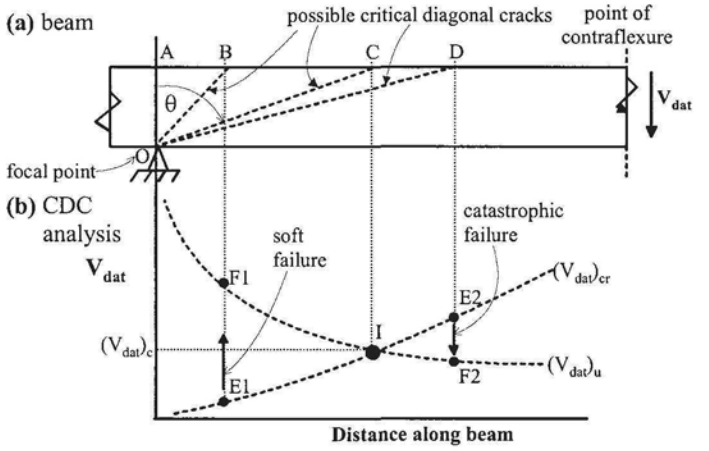

Figure 4.7 CDC analysis of unplated RC beam

Consider the diagonal crack O-B in the unplated beam in Fig. 4.7(a). The shear load V_{dat}, at the point of contraflexure, required to induce the diagonal crack is shown as point E1 in Fig. 4.7(b). The shear load V_{dat} to overcome the shear resistance of the crack is at point F1. Hence when the beam is gradually loaded, the diagonal

crack will first form at $(V_{dat})_{cr}$ = E1, but the diagonal crack will not fail until the shear has increased to $(V_{dat})_u$ = F1. It can be seen that there is prior warning of failure, so that this is called a soft failure. For the diagonal crack O-D in Fig. 4.7(a), the shear load to cause cracking is E2 and the shear load V_{dat} required to overcome the shear resistance of that diagonal crack is F2. Hence, for the diagonal crack O-D, nothing would happen until the shear crack formed at $(V_{dat})_{cr}$ = E2 and, immediately, there would be a catastrophic failure as the shear load to achieve the shear capacity $(V_{dat})_u$ = F2 is less than that to cause cracking.

It can be seen in Fig. 4.7(b) that for every position of the diagonal crack (that is as the diagonal crack rotates θ in Fig. 4.7(a) about the focal point O) the shear load at the datum point V_{dat} to cause cracking can be plotted as a line which is shown as $(V_{dat})_{cr}$. Similarly V_{dat} to cause the diagonal crack to fail can be plotted as $(V_{dat})_u$ (these iterative analyses are ideally suited for spreadsheets, however, direct but less accurate approaches are also presented in Section 4.5). Where the lines $(V_{dat})_{cr}$ and $(V_{dat})_u$ intercept at point I in Fig. 4.7(b) gives the weakest strength and, hence, the shear load at the datum point to cause shear failure in a beam without stirrups $(V_{dat})_c$, as well as the position of the critical diagonal crack A-C in Fig. 4.7(a). In this example, because we have assumed that V is constant along the hogging region, it will be shown in the next section that the shear force $(V_{dat})_c$ is also the shear capacity of the beam without stirrups V_c. It is also worth noting that cracking is a fairly random occurrence depending on the vagaries of the concrete properties. Hence, it is unlikely that the critical diagonal crack will occur exactly at point I in Fig. 4.7(b). If it occurs to the left there will be a soft failure and if it occurs to the right there will be rapid failure; this analysis explains what has been found to occur in practice and in tests.

4.3.3 Zhang's iterative approach

Zhang (1997) derived a lower bound to the shear capacity which is equivalent to a characteristic strength that can be used in design. The CDC analysis procedure has been described in qualitative terms in Section 4.3.2 and illustrated in Fig. 4.7. Consider the shear span B-C in Fig. 4.8. In theory, it would be necessary to determine the shear capacity at any position of the focal point, such as O_1, O_2 and O_3, and for each position it would be necessary to consider all possible inclinations θ of the crack. The weakest or critical diagonal crack will give V_c. The generic procedure for doing this will be described in this section. However, it is worth bearing in mind, that the position of the focal point is often known, such as at the position of the concentrated load in Fig. 4.5.

Let us consider the CDC analysis of the shear span A-B in Fig. 4.8 with the focal point at O, as shown, so that we need to determine the angle θ of the critical diagonal crack that gives the weakest shear capacity. The datum point is at a distance L_o from the focal point, where the shear load is V_{dat} as shown in Fig. 4.8(a) and the moment is M_{dat}. It is required to determine the shear load V_{dat} at the datum point to cause cracking for every possible rotation θ of the critical diagonal crack, which is shown as $(V_{dat})_{cr}$ in Fig. 4.7 as described in Section 4.3.2. We also need to determine the shear at the datum point V_{dat} to cause shear failure or crack sliding through an existing diagonal crack in any part of the shear span which is shown as $(V_{dat})_u$ in Fig. 4.7. We will be analysing the sagging region in Fig. 4.8, but the same analysis applies to the hogging region.

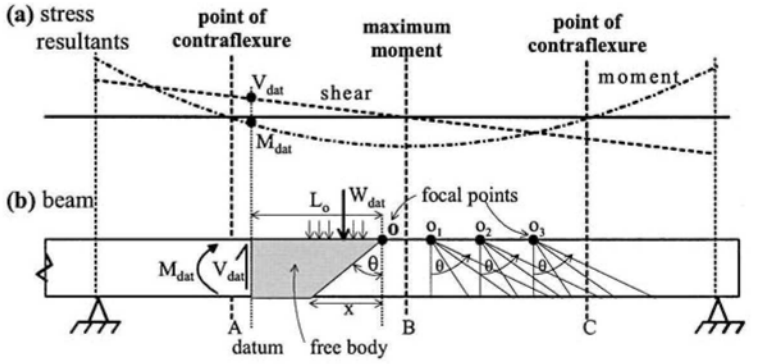

Figure 4.8 CDC analysis of free body

4.3.3.1 Vertical shear to cause cracking

The free body diagram in Fig. 4.8(b) has been shown enlarged in Fig. 4.9. It is necessary to determine the shear load at the datum point $(V_{dat})_{cr}$, that will cause the diagonal crack at an angle θ to form, that is the vertical shear to cause cracking. The beam is assumed to be prestressed with the prestressing tendon at a vertical distance d_{ps} from the focal point and a prestressing force of F_{ps}. The axial force in the longitudinal reinforcement is ignored as prior to cracking the stresses in the reinforcing bars are negligible. The shear load at the datum point to cause cracking $(V_{dat})_{cr}$ is our reference stress resultant. Hence $(M_{dat})_{cr}$ is the moment at the datum point when $(V_{dat})_{cr}$ is acting. Therefore, $(M_{dat})_{cr}$ is a function of $(V_{dat})_{cr}$, that is $(M_{dat})_{cr} = K_M(V_{dat})_{cr}$. Furthermore, $(W_{dat})_{cr}$ is the resultant of the applied loads acting on the free body of length L_o when $(V_{dat})_{cr}$ is acting and, hence, it is also proportional to $(V_{dat})_{cr}$ such that $(W_{dat})_{cr} = K_W(V_{dat})_{cr}$. The resultant applied load $(W_{dat})_{cr}$ acts at a distance e from the focal point. The depth of the beam is h, the inclination θ of the diagonal crack is defined by the distance *x* and the effective tensile strength of the concrete is f_{tef}.

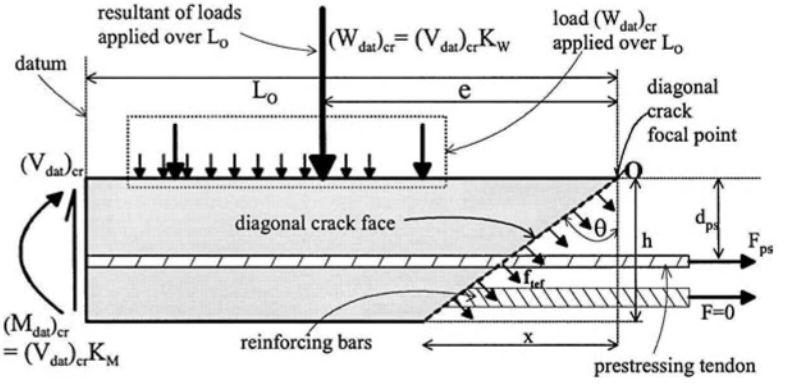

Figure 4.9 Shear load to cause cracking

From rotational equilibrium of the stress resultants in Fig. 4.9, the shear load at the datum point required to cause cracking is given by

$$(V_{dat})_{cr} = \frac{\left(\left(x^2 + h^2\right)\left(\frac{b_c f_{tef}}{2}\right)\right) + \left(F_{ps} d_{ps}\right)}{L_O + K_M - K_W e} \qquad 4.1$$

where b_c is the width of the slab, or 1 m width of slab for convenience, or the width of the web of a beam, and the effective tensile strength of the concrete is given by

$$f_{tef} = 0.156 f_c^{2/3}\left(\frac{h}{100}\right)^{-0.3} \qquad \text{[N and mm]} \qquad 4.2$$

which is not the actual tensile strength of the concrete but an effective tensile strength that has been derived empirically to allow for the non-uniform stress distribution of tensile stress within the depth of the beam. Hence the shear load at the datum point to cause cracking for various positions of the root of the diagonal crack x in Fig. 4.9 can be plotted as in Fig. 4.7(b) for $(V_{dat})_{cr}$.

Equation 4.1 may appear to be unduly complicated but it has been deliberately written to encompass all forms of loading and positions of the datum point. In general, the datum point will be taken at a point of contraflexure so that $(M_{dat})_{cr}$ is zero, that is $K_M = 0$. Furthermore, $(W_{dat})_{cr}$ is either a uniformly distributed load so that its relationship to $(V_{dat})_{cr}$, that is K_W, is known or it can be assumed to be negligible.

4.3.3.2 Vertical shear to cause crack sliding

After the diagonal crack has formed in Fig. 4.9, the vertical shear capacity of the diagonal crack V_u in Fig. 4.10 needs to be determined. As described in Section 4.2.1 and Figs 4.2 and 4.3, the shear capacity depends on the reinforcing bars crossing the crack and the prestress force F_{ps} across the crack, as they induce passive interface forces.

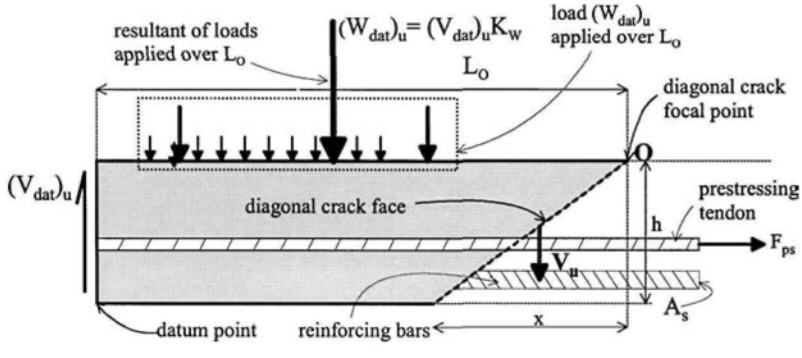

Figure 4.10 Vertical loads to cause crack sliding at failure

The shear load at the datum point to cause failure $(V_{dat})_u$, better referred to as crack sliding, can be determined from vertical equilibrium of the free body in Fig. 4.10. The applied load $(W_{dat})_u$ acts over the length L_o of the free body when $(V_{dat})_u$ is acting. Hence, $(W_{dat})_u$ is a function of $(V_{dat})_u$, that is $(W_{dat})_u = (V_{dat})_u K_W$. The vertical shear resistance across the diagonal crack is V_u. From vertical equilibrium

$$(V_{dat})_u = \frac{V_u}{1 - K_w} \tag{4.3}$$

where the shear capacity across the diagonal crack is given by

$$V_u = \frac{1}{4}\gamma_O f_c b_c h\left(\sqrt{1+\left(\frac{x}{h}\right)^2} - \frac{x}{h}\right) \tag{4.4}$$

and where the cohesive effectiveness factor γ_O is given by

$$\gamma_O = \lambda f_1(f_c) f_2(h) f_3(\rho) f_4\left(\frac{\sigma_{ps}}{f_c}\right) \tag{4.5}$$

The functions in Eq. 4.5 are given below with their units, as well as the ranges in which they have been calibrated and within which their use should be restricted. The concrete contribution to the strength is given by

$$f_1(f_c) = \frac{3.5}{\sqrt{f_c}} \qquad \text{[N and mm]} \quad 5 < f_c < 60\,MPa \tag{4.6}$$

the size effect by

$$f_2(h) = 0.27\left(1 + \frac{1}{\sqrt{h}}\right) \qquad \text{[m]} \quad 0.08 < h < 0.7 \tag{4.7}$$

the contribution of the longitudinal reinforcement by

$$f_3(\rho) = 0.15\rho + 0.58 \qquad \rho = \frac{A_s}{b_c h} \times 100 \;\; and \;\; \rho < 4.5 \tag{4.8}$$

where A_s is the cross-section area of all of the longitudinal reinforcement crossing the critical diagonal crack, that is at all levels of the beam and it is suggested those within b_c. The contribution through prestressing is given by

$$f_4\left(\frac{\sigma_{ps}}{f_c}\right) = 1 + 2\frac{\sigma_{ps}}{f_c} \qquad where\ \sigma_{ps} = \frac{F_{ps}}{b_c h} \tag{4.9}$$

Zhang proposed that the coefficient λ in Eq. 4.5 should be taken as 1.6 for concentrated applied loads and 1.2 for uniformly distributed applied loads. There does not appear to be any theoretical justification for this difference and it can only be assumed that these coefficients were derived empirically through calibration of the mathematical model with test results. It is suggested that λ = 1.6 should be used throughout for all types of loads and load combinations as: most shear failures are associated with concentrated loads such as at supports of continuous beams where the vertical shear is at its highest; a brief comparison with code values shows reasonable

correlation when using $\lambda = 1.6$; and more importantly, it will be suggested later in Section 4.4 that the CDC analysis should, preferably, be used to determine only the increase in V_c due to plating $\Delta V_{c\text{-plate}}$, to be used in conjunction with $(V_c)_{code}$ from the national code so that any differences in the overall strength will be minimised.

The shear load at the datum point to cause failure after a diagonal crack has formed can be derived as follows from Eqs 4.3 and 4.4 with $\lambda = 1.6$

$$(V_{dat})_u = \frac{0.4\left(f_1(f_c)f_2(h)f_3(\rho)f_4\left(\frac{\sigma_{ps}}{f_c}\right)\right)f_c b_c h\left(\sqrt{1+\left(\frac{x}{h}\right)^2}-\frac{x}{h}\right)}{1-K_W} \qquad 4.10$$

and can be plotted as $(V_{dat})_u$ in Fig. 4.7(b).

4.3.3.3 Concrete shear capacity of RC beams and slabs

Let us consider a beam or slab without stirrups so that the formation of the critical diagonal crack will cause failure as the concrete shear component V_c has been exceeded. Equations 4.1 and 4.10 can be used to plot both the shear load at the datum point to cause cracking at any position along the beam which is $(V_{dat})_{cr}$ in Fig. 4.7(b), and the shear load at the datum point to cause crack sliding or failure at any position along the beam which is $(V_{dat})_u$ in Fig. 4.7(b). The intercept of these two lines is the shear load at the datum point to cause the region of the beam being analysed to form a critical diagonal crack and fail which is shown as $(V_{dat})_c$.

If the applied shear load at the datum point $(V_{dat})_{applied}$ is less than $(V_{dat})_c$, then the region will not fail, that is a critical diagonal crack will not form in this region, and vice versa. Furthermore specifically for the critical diagonal crack, in Eq. 4.3 $(V_{dat})_u$ is $(V_{dat})_c$ and V_u is V_c. Hence the concrete shear capacity is given by

$$V_c = (1-K_W)(V_{dat})_c \qquad 4.11$$

It may be worth noting that when the applied load along the shear span L_O in Fig. 4.10 is zero then $K_W = 0$ in Eq. 4.11 so that $V_c = (V_{dat})_c$ in Eq. 4.11 and Fig. 4.7(b). It may also be worth noting that for a beam with stirrups that V_c may not be the failure load, but it is the shear load at which the first diagonal crack or critical diagonal crack slides which is also the shear load at which CDC debonding of plates occurs as described in Section 4.4.

4.4 CDC debonding of tension face plates

Zhang's analysis, in Section 4.3.3, for determining the vertical shear capacity of a beam or slab without stirrups is adapted in Section 4.4.1 to allow for the contributions of adhesively bonded tension face plates. The CDC analysis is then incorporated into a general CDC design procedure in Section 4.4.2 based on either the hinge approach in Section 2.5.2 or the anchorage approach in Section 2.5.1. As this approach for plated beams is based directly on Zhang's lower bound analysis, it can be considered to give a characteristic or lower bound value suitable for design.

4.4.1 Iterative CDC analysis

It has been shown that critical diagonal crack debonding of an externally bonded plate is exactly the same mechanism as that which governs the concrete shear capacity of a beam without stirrups V_c. Hence, it is a question of determining the enhanced concrete shear capacity due to plating $V_{c\text{-}plate}$. Furthermore, $V_{c\text{-}plate}$ also governs the CDC debonding of plates bonded to beams with stirrups, as the rigid body deformation across the critical diagonal crack or crack sliding, associated with CDC debonding, is required to stretch the stirrups so that they can resist shear as quantified by the stirrup shear component V_s. However, tests have shown that, before any significant portion of V_s can be achieved, the rigid body deformation or crack sliding causes CDC debonding.

The generic CDC analysis for an unplated RC beam or slab has been described in Sections 4.3.2 and 4.3.3. In theory, the critical diagonal crack can emanate from any position along the beam, such as the focal points O_1 to O_3 in the shear span B-C in Fig. 4.8. To reduce the amount of analyses, guidelines are given in Section 4.4.1.1 to the probable positions of the focal points. Externally bonded plates inhibit or delay the formation of the critical diagonal crack and this is covered in Section 4.4.1.2. After the critical diagonal crack has formed, the plate can be considered to act as additional longitudinal reinforcement in Section 4.4.1.3, where the shear is resisted by dowel action and through aggregate interlock as described in Section 4.2.1 and Figs 4.2 and 4.3. Alternatively after diagonal cracking, the plate resistance is considered to act as a passive prestressing force in Section 4.4.1.4, where the axial force in the plate induces the passive normal force P_{inter} in Fig. 4.2 that is required to resist the shear by aggregate interlock.

4.4.1.1 Position of diagonal crack focal and datum points

The first requirement of the CDC analysis is to identify the *focal point* of the diagonal crack that has the weakest shear capacity. The *focal point* is always on the compression face of the beam. For beams with concentrated or point loads on the compression face, the focal point is assumed to occur adjacent to the edge of the concentrated load on the compression face, such as in Figs 1.19, 4.1 and 4.6. Illustrations of focal points that emanate from concentrated loads that are applied to the compression faces of continuous beams are shown in Fig. 4.11. For example, the support reaction at E is a concentrated or point load that is being applied to the compression face of the hogging region of the beam. Hence, point E at the edge of the support is a focal point for determining the shear capacity of a beam without stirrups V_c or crack sliding in a plated beam that induces CDC debonding $V_{c\text{-}plate}$. Large concentrated loads applied to the beam, as may occur in vehicular bridge beams, can also be the focal point for critical diagonal cracks. An example is shown in shear span B-C where the concentrated load or point load is being applied to the compression face in the sagging region.

For sagging regions subjected to predominantly uniformly distributed loads (udl), as shown in shear span C-D in Fig. 4.11, the position of the focal point is not as clearly defined as that for concentrated loads so it may be necessary to vary the position of the focal point to find the CDC. It needs to be stressed that if it is not clear where the critical focal point is, that is the focal point where the weakest diagonal crack emanates, then the CDC analyses can be applied to several points along the beam, such as O_1 to O_3 in Fig. 4.8, to find the critical focal point. This may occur when there are combinations of loads to be dealt with. It is also worth remembering

that the weakest diagonal crack is the weakest diagonal crack relative to the applied shear at that position.

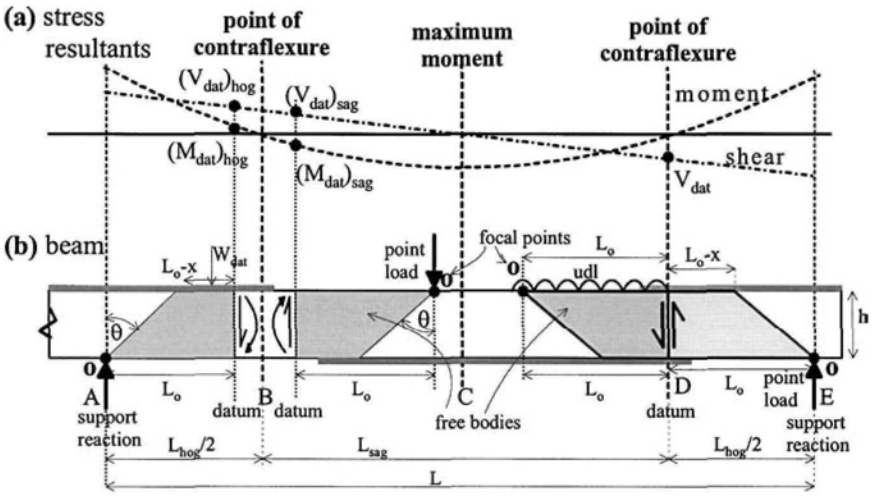

Figure 4.11 Diagonal crack focal points and datum points in continuous beams

The focal point establishes one side of the free body required in the CDC analysis as shown in Fig. 4.11. The other side, which is the datum point, can be anywhere. The shear load at the datum point to cause cracking, as in Eq. 4.1 for $(V_{dat})_{cr}$ in the unplated beam and later in Eq. 4.18 for $(V_{dat})_{cr\text{-}plate}$ in the plated beam depends on the following coefficient

$$K_M = \frac{M_{dat}}{V_{dat}} \qquad 4.12$$

where K_M can be derived directly from the ratio of the stress resultants at the datum point as shown in Fig. 4.11(a) and which is not difficult to determine. However, as $K_M = 0$ at a point of contraflexure, it is convenient to choose a point of contraflexure as a datum point as shown for the free bodies in the shear spans C-D and D-E in Fig. 4.11.

The shear load at the datum point to cause cracking in Eqs 4.1 and 4.18 as well as the shear load to cause crack sliding or failure that is $(V_{dat})_u$ in the unplated beam in Eq. 4.10 and later $(V_{dat})_{u\text{-}metal}$ for the plated beam in Eq. 4.21 depends on load shear ratio

$$K_W = \frac{W_{dat}}{V_{dat}} \qquad 4.13$$

where W_{dat} is the portion of the applied load, that induces V_{dat}, that is acting on the free body as shown in the shear span A-B in Fig. 4.11.

For example, if there is no applied load acting along the free body, such as on the free body in shear span B-C and D-E in Fig. 4.11, where the concentrated load is not acting along the body but on the edge at the focal point, then

$$K_W = \frac{W_{dat}}{V_{dat}} = 0 \qquad 4.14$$

Furthermore, if the continuous beam in Fig. 4.11 is only subjected to a uniformly distributed load of w per unit length, then for the CDC analysis of the free body in the shear span C-D, the shear load at the datum point D is

$$\left(\left(V_{dat}\right)_{poc}\right)_{udl} = \frac{wL}{2} - \frac{wL_{hog}}{2} \qquad 4.15$$

so that the factor K_W for the free body in the sagging shear span C-D is given by

$$\left(\left(K_W\right)_{sag}\right)_{udl} = \frac{wL_O}{\frac{wL}{2} - \frac{wL_{hog}}{2}} = \frac{2L_O}{L_{sag}} \qquad 4.16$$

and similarly for the free body in the hogging shear span D-E

$$\left(\left(K_W\right)_{hog}\right)_{udl} = \frac{w\left(L_O - x\right)}{\frac{wL}{2} - \frac{wL_{hog}}{2}} = \frac{2\left(L_O - x\right)}{L_{sag}} \qquad 4.17$$

4.4.1.2 Shear to cause cracking of tension face plated sections

The stress resultants involved in determining the vertical shear to cause a diagonal crack to form in an unplated beam in a sagging region is shown in Fig. 4.9. This can be compared with those required in a tension face plated beam in the sagging region B-C in Fig. 4.11 which is shown fully in Fig. 4.12. The only difference between the unplated beam in Fig. 4.9 and the plated beam in Fig. 4.12 is the additional force in the tension face plate $(F_{plate})_{cr}$ that has to be overcome to allow the concrete to crack. This force was determined by simply transforming the plate into an equivalent area of concrete.

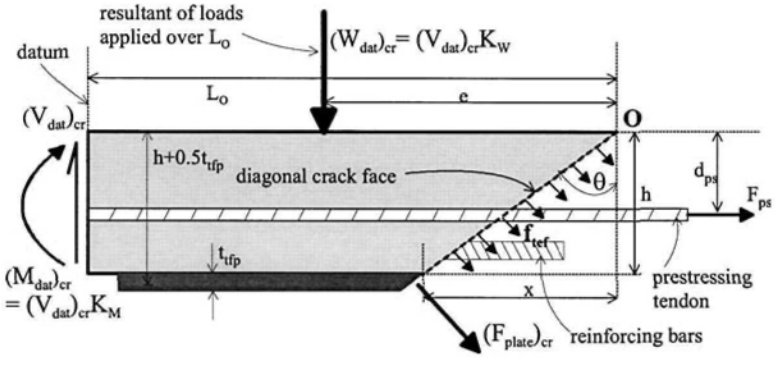

Figure 4.12 Shear load to cause cracking in a tfp beam in the sagging region

The shear load at the datum point to cause cracking in a tension face plated beam or slab in the sagging region is given by

$$\left(\left(V_{dat}\right)_{cr-plate}\right)_{sag} = \frac{\left(\left(x^2+h^2\right)\left(\frac{b_c f_{tef}}{2} + \frac{m_p f_t b_{tfp} t_{tfp}\left(h+0.5t_{tfp}\right)}{h^2}\right)\right) + \left(F_{ps} d_{ps}\right)}{L_O + K_M - K_W e} \qquad 4.18$$

where m_p is the modular ratio of the plate material stiffness to that of the concrete E_p/E_c. f_t is the tensile strength of the concrete in the beam which if not measured directly can be taken as $0.4\sqrt{f_c}$ [N/mm^2], b_{tfp} and t_{tfp} are the width and thickness of the tension face plate such that their product is the cross-sectional area of plate, and $(h + 0.5t_{tfp})$ is the vertical distance from the plate centroid to the focal point which for tension face plates can be taken as h, but it will be left in this form to show later how Eqs 4.1 and 4.18 are special cases of a generic equation which will be developed in Chapter 5.

The stress resultants in the free body in shear span A-B in the hogging region in Fig. 4.11(b) are shown in Fig. 4.13. The only real difference between Fig. 4.12 (sagging region) and Fig. 4.13 (hogging region) is that in Fig. 4.13 the moment of the applied load $W_{dat}e$ about the focal point acts in the opposite direction to the remaining moments on the free body as compared with that in Fig. 4.12. Furthermore, W_{dat} in Fig. 4.13 is applied over a smaller length L_O-x as compared with L_O in Fig. 4.12.

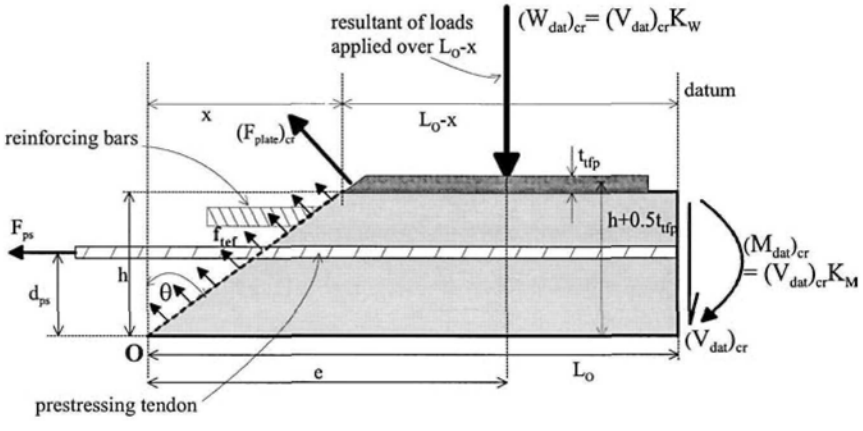

Figure 4.13 Shear load to cause cracking in a tfp beam in the hogging region

From rotational equilibrium of the stress resultants in Fig. 4.13, the shear load at the datum point to cause cracking for a tension face plated beam in the hogging region is given by

$$\left(\left(V_{dat}\right)_{cr-plate}\right)_{hog} = \frac{\left(\left(x^2+h^2\right)\left(\frac{b_c f_{tef}}{2} + \frac{m_p f_t b_{tfp} t_{tfp}\left(h+0.5t_{tfp}\right)}{h^2}\right)\right) + \left(F_{ps} d_{ps}\right)}{L_O + K_M + K_W e} \qquad 4.19$$

The difference between the sagging result in Eq. 4.18 and the hogging result in Eq. 4.19 is the change in sign of the $K_w e$ term in the denominator, which is due to the reversal in the moment $W_{dat}e$ relative to the other moments as explained previously.

It can be seen that both Eqs 4.18 and 4.19 can be used to determine the shear load at the datum point to cause cracking for unplated beams $(V_{dat})_{cr}$ by simply substituting $t_{tfp} = 0$ into the equations. There is now no need to revert back to Eq. 4.1 or its equivalent for the hogging region for a CDC analysis of an unplated beam.

4.4.1.3 Shear to cause crack sliding in tension face plated sections – longitudinal reinforcement approach

The shear to cause crack sliding in an unplated beam in a sagging region is described in Section 4.3.3.2 and the stress resultants involved are shown in Fig. 4.10. Those required to cause crack sliding in a tension face plated beam or slab in a sagging region are shown in Fig. 4.14. The only additional force is the maximum possible force in the plate P_{plate}. The maximum force in the plate P_{plate} is the lesser of: the yield capacity, if it is a metal plate, of $A_p f_{yp}$; the IC debonding force P_{IC} whose magnitude depends on the available anchorage length L_p in Fig. 4.14 which depends on the effective length L_e in Eq. 2.3 and the IC debonding resistance of the plate in Eq. 2.1; and the fracture strength $A_p f_{FRP}$ if it is an FRP plate. It may be worth noting that the plate force $(F_{plate})_{cr}$ in Figs 4.12 and 4.13 does not depend on the anchorage length L_p as it is the force in the plate just prior to cracking, whereas P_{plate} in Fig. 4.14 is the force the plate can resist after cracking which depends on, for example, the resistance to IC debonding and hence L_p.

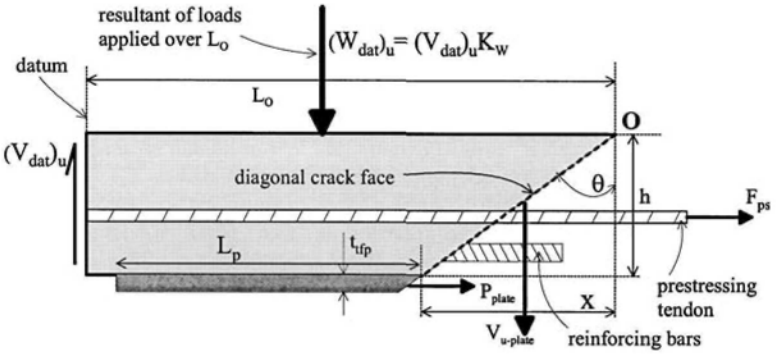

Figure 4.14 Shear load to cause crack sliding in a tfp beam in the sagging region

The plate force P_{plate} in Fig. 4.14 can be assumed to act as additional longitudinal reinforcing bars as described in Section 4.2.1. The function which governs this contribution in an unplated beam is given by Eq. 4.8 which depends on the cross-sectional area of all of the longitudinal reinforcing bars A_s. Hence P_{plate} has to be converted to an equivalent area of longitudinal reinforcement. This conversion can be made for metal plates as they have a yield capacity as do reinforcing bars, but it is difficult to make this conversion for FRP plates as they do not yield and, hence, this *longitudinal reinforcement approach* is restricted to metal plates. To be on the conservative side, so as not to over-estimate the equivalent area of reinforcing bar, we can assume that P_{plate} is equivalent to an area of metal plate that has yielded at its yield capacity f_{yp}, so that the longitudinal reinforcement function for unplated beams in Eq. 4.8 becomes

$$f_3(\rho_{plate}) = \frac{15}{b_c h}\left(A_s + \frac{P_{plate}}{f_{yp}}\right) + 0.58 \le 1.26 \qquad 4.20$$

The shear load to cause crack sliding in unplated beams in Eq. 4.10 now becomes for metal tension face plated beams

$$\left((V_{dat})_{u-metal}\right)_{sag} = \frac{0.4\left(f_1(f_c)f_2(h)f_3(\rho_{plate})f_4\left(\frac{\sigma_{ps}}{f_c}\right)\right)f_c b_c h\left(\sqrt{1+\left(\frac{x}{h}\right)^2} - \frac{x}{h}\right)}{1 - K_W} \qquad 4.21$$

To complete the picture, the stress resultants in the hogging region are shown in Fig. 4.15, and the shear load at the datum point to cause crack sliding is given by Eq. 4.22 which differs from Eq. 4.21 by the sign of the K_W coefficient.

$$\left((V_{dat})_{u-metal}\right)_{hog} = \frac{0.4\left(f_1(f_c)f_2(h)f_3(\rho_{plate})f_4\left(\frac{\sigma_{ps}}{f_c}\right)\right)f_c b_c h\left(\sqrt{1+\left(\frac{x}{h}\right)^2} - \frac{x}{h}\right)}{1 + K_W} \qquad 4.22$$

Equations 4.21 and 4.22 can only be used for metal plates. Furthermore, they can also be used for determining the shear load at the datum point to cause crack sliding in an unplated beam $(V_{dat})_u$ by simply substituting $P_{plate} = 0$ in Eq. 4.20. Hence there is no need to use Eq. 4.10 or its equivalent for the hogging region for an unplated beam.

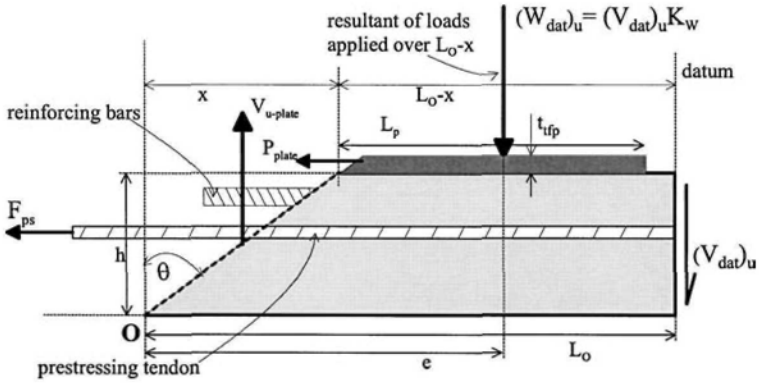

Figure 4.15 Shear load to cause crack sliding in a tfp beam in the hogging region

4.4.1.4 Shear to cause crack sliding in tension face plated sections – passive prestress approach

An alternative to converting the maximum plate force P_{plate} into an equivalent area of longitudinal reinforcement, as in Section 4.4.1.3, is to assume that the maximum plate force P_{plate} directly applies a passive prestress across the diagonal crack as explained in Section 4.2.1 and in Figs 4.2 and 4.3. In which case, the prestress force term F_{ps} in

the prestress function of Eq. 4.9 for unplated beams is increased to $F_{ps}+P_{plate}$. A comparison of this increase in the shear capacity with tests in which critical diagonal cracks were known to occur (Oehlers et al 2004a) showed that the coefficient 2 in Eq. 4.9 gives a conservative estimate of the increase in the shear to cause CDC debonding. A coefficient of 4 was found to correlate well with test data and also with prestressed code approaches described in Section 4.5.2. Hence, the prestress function of Eq. 4.9 has been adapted as follows to include a passive prestress term.

$$f_4\left(\frac{\sigma_{ps}}{f_c}\right)_{plate} = 1 + 2\frac{F_{ps}}{f_c b_c h} + 4\frac{P_{plate}}{f_c b_c h} \qquad 4.23$$

where the passive prestress $\sigma_{pp} = P_{plate}/b_c h$. This approach has the benefit that it can be used for both metal and FRP plates and that the plate force P_{plate} can be used directly instead of having to be converted into an equivalent area of longitudinal reinforcing.

The shear force at the datum point to cause crack sliding in a sagging region in Fig. 4.14 using the passive prestress approach is given by

$$\left((V_{dat})_{u-pres}\right)_{sag} = \frac{0.4\left(f_1(f_c)f_2(h)f_3(\rho)f_4\left(\frac{\sigma_{ps}}{f_c}\right)_{plate}\right)f_c b_c h\left(\sqrt{1+\left(\frac{x}{h}\right)^2}-\frac{x}{h}\right)}{1-K_W} \qquad 4.24$$

and for the hogging region in Fig. 4.15

$$\left((V_{dat})_{u-pres}\right)_{hog} = \frac{0.4\left(f_1(f_c)f_2(h)f_3(\rho)f_4\left(\frac{\sigma_{ps}}{f_c}\right)_{plate}\right)f_c b_c h\left(\sqrt{1+\left(\frac{x}{h}\right)^2}-\frac{x}{h}\right)}{1+K_W} \qquad 4.25$$

It needs to be emphasised that the passive prestress induced by the plate P_{plate} does not act before an intermediate diagonal crack has formed as it is induced by the aggregate interlock sliding action across the crack. Hence, the passive prestress P_{plate} does not affect the shear load to cause cracking $(V_{dat})_{cr\text{-}plate}$ as it simply does not exist prior to cracking. In contrast, the active prestressing force F_{ps} in Fig. 4.12 acts prior to cracking and that is why it is included in the shear load to cause cracking in Eqs 4.18 and 4.19.

Equations 4.24 and 4.25 can be used for metal and FRP plates, in fact plates of any material. Furthermore and to stress and reiterate a point, they can also be used for determining the shear load at the datum point to cause crack sliding in an unplated beam or slab $(V_{dat})_u$ by simply substituting $P_{plate} = 0$ in Eq. 4.23. Hence there is no need to use Eq. 4.10 or its equivalent for the hogging region for an unplated beam.

4.4.1.5 Shear capacity analysis

An application of the CDC analysis for a tension face plated beam is shown in Fig. 4.16. The equations used in the analysis of the hogging region are given in Fig. 4.16(b), as well as those that would be required for the analysis of a sagging region for reference.

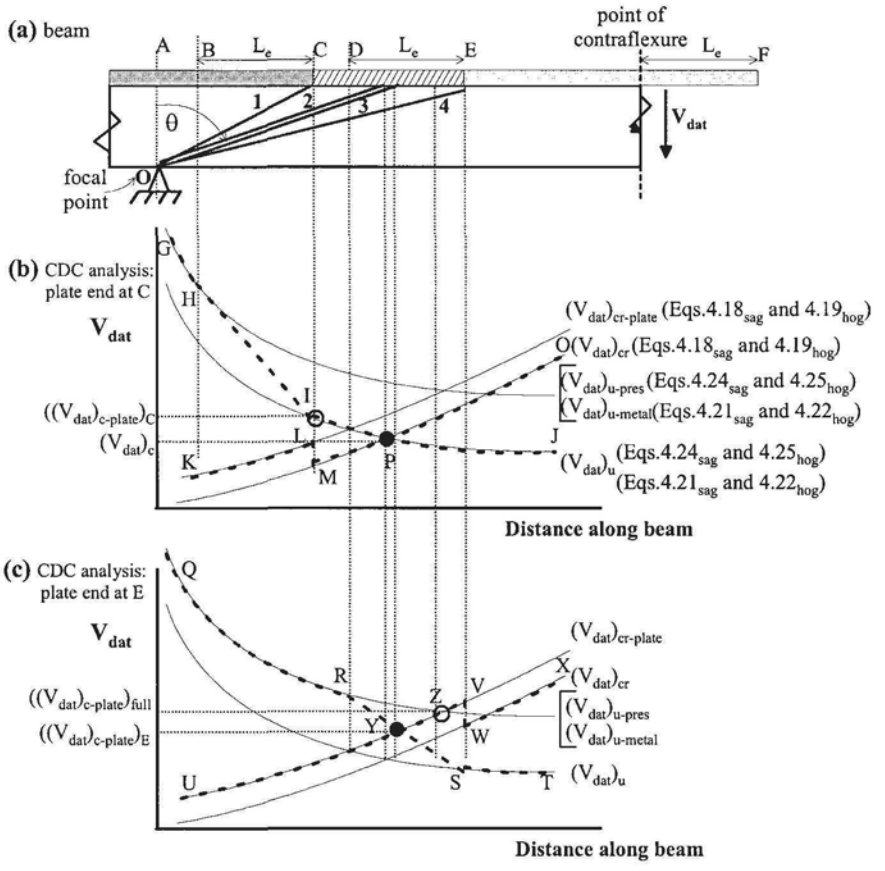

Figure 4.16 Shear capacity of partially plated beams

The beam has been analysed first as unplated so that Eq. 4.19, with the plate thickness equal to zero, has been used to determine the variation of the shear load at the datum point to cause a diagonal crack $(V_{dat})_{cr}$ in Figs 4.16(b) and (c). Equations 4.22 or 4.25, with P_{plate} equal to zero, can be used to determine the variation of the shear load at the datum point to cause crack sliding or failure $(V_{dat})_u$. The beam has then been assumed to be fully plated and also that the plate is fully anchored in the hogging region so that the plate has been extended past the point of contraflexure in Fig. 4.16(a) by an effective length L_e. Hence at every possible position of the CDC along the hogging region, the full plate strength P_{plate} can be achieved. The shear load at the datum point to cause cracking is given by Eq. 4.19 and that to cause crack sliding by Eqs 4.22 or 4.25 with P_{plate} constant and at its maximum value. Just to illustrate the procedure, we will assume that the maximum plate strength P_{plate} is the IC debonding resistance P_{IC} that requires a minimum anchorage length of L_e. Hence, it could be said that the two unplated curves and the two fully plated curves form the bounds of the 'failure envelopes'.

Let us first consider a short tension face plate of length A-C in Fig. 4.16(a); so that A-B is fully anchored and the force in the plate reduces over the effective length L_e from its maximum at B, being fully anchored, to zero at C, where there is no

anchorage. Hence in Fig. 4.16(b), the load to cause cracking follows the path K-L, along the plated section, and then at the plate end at L drops to M and follows the path M-O along the unplated section. The load to cause crack sliding follows the path G-H and then from H on the fully anchored curve to I on the unplated curve, over the effective length L_e, after which it follows the path I-J on the unplated beam. The paths cross at point P, $(V_{dat})_c$, which lies beyond the plate. This means that a critical diagonal crack will first form in the unplated region as shown by the diagonal crack marked 2 in Fig. 4.16(a) which would cause failure in beams without stirrups. If the beam had stirrups so that the shear load could be increased, then the diagonal crack marked 1 would occur at the plate end at the shear load marked I, $((V_{dat})_{c\text{-}plate})_C$ in Fig. 17(a) and this would be the shear load to cause debonding in the plated region.

Let us now extend the plate to E in Fig. 4.16(a). The load to cause cracking follows the plated path U-V in Fig. 4.16(c) to the plate end, then drops to W in the unplated beam and then W-X along the unplated beam. The load to cause crack sliding follows the plated path Q-R, then from R to S, over the effective length L_e, and then S-T along the unplated beam. The paths cross at Y, $((V_{dat})_{c\text{-}plate})_E$. Hence the critical diagonal crack is the diagonal crack marked 3 in Fig. 4.16(a) which occurs within the anchorage zone of the plate.

It is also worth considering the fully anchored analyses in Fig. 4.16(c) which is given by the lines $(V_{dat})_{cr\text{-}plate}$ and $(V_{dat})_{u\text{-}pres/metal}$. These lines cross at point Z which is, therefore, the position of the critical diagonal crack for the fully plated member with a shear capacity of $((V_{dat})_{c\text{-}plate})_{full}$, in Fig. 4.16(c). This gives the maximum possible strength. Hence, extending the plate a further distance L_e to the right of Z is all that is required to achieve the greatest benefit from this plate; this is the minimum extent of plating required to achieve the greatest increase in $V_{c\text{-}plate}$. It may be worth noting that there is a tendency for plating to move the position of the root of the critical diagonal crack towards the datum, that is to increase the inclination of the critical diagonal crack θ. This does not always occur but does tend to occur as illustrated in the example in Fig. 4.16 where the critical diagonal crack moves from *P* in the unplated beam to *Y* in the partially plated beam and then to Z in the fully anchored plated beam.

If the concrete shear capacity of the plated beam $V_{u\text{-}plate}$ in Figs 4.14 and 4.15 is required, then from Eq. 4.11 and also from Eqs 4.24 and 4.25

$$V_{c-plate} = (1 \pm K_W)(V_{dat})_{c-plate} \qquad 4.26$$

where $(V_{dat})_{c\text{-}plate}$ is shown on the ordinates of Figs 4.16(b) and (c) which includes $(V_{dat})_c$ for the unplated beam as a special case of the plated beam. The factor K_W is negative in the sagging regions and positive in hogging regions. This is because in the sagging region, as in Fig. 4.11, the shear load at the datum point, which is always nearer to the point of contraflexure than the focal point, is always larger than at the focal point. Hence, V_{dat} at the datum point has to be reduced to determine the shear force at the focal point. Conversely, in the hogging region in Fig. 4.11, the shear load at the datum point is lower than at the focal point so that K_W is positive to allow for the increased shear at the diagonal crack. It is also worth noting that $V_{c\text{-}plate}$ in Eq. 4.26 is the shear load to cause crack sliding and hence debonding in a plated beam.

4.4.2 Design approach for CDC debonding

At this stage of the analysis, the plates required at the positions of maximum moment in Figs 4.17(b) and (c) have been designed to resist the maximum moments in Fig.

4.17(a) and this has been based in Chapter 3 on IC debonding. The next step is to design against CDC debonding along a region of the beam, that is within the hogging or sagging region, which depends on the magnitude and distribution of the vertical shear force in Fig. 4.17(a) and which also controls the extent of plating. Having already described the CDC analysis, we will now describe a CDC design procedure. The design procedure depends on the design philosophy that is being adopted as explained in Section 2.5: the anchorage approach is shown in Fig. 4.17(b); and the hinge approach in Fig. 4.17(c).

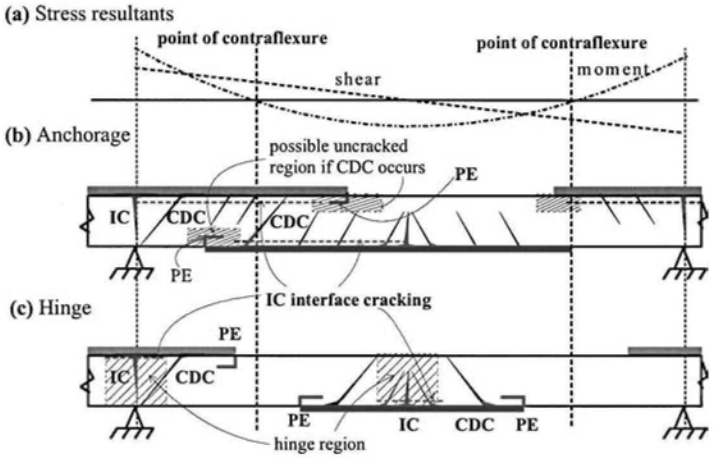

Figure 4.17 Design philosophies

4.4.2.1 CDC design procedure in hinge approach

Let us start with the *hinge approach* in Fig. 4.17(c). The hinge approach restricts the IC interface crack to within a relatively small region or hinge. This allows the plates to be terminated short of the points of contraflexure, so that it will be necessary to determine the extent of plating as well as the resistance to CDC debonding. The extent of plating is also controlled by plate end debonding and this is covered in Chapter 6. The CDC design procedure is the same in the hogging region and the sagging region, so let us consider the hogging region over the left support in Fig. 4.17(c) which is shown in Fig. 4.18.

The design procedure for the hinge approach is illustrated in Fig. 4.18(a) and consist of the following steps.

1. First assume that the beam is fully plated along the region and for every possible position θ of the diagonal crack, such as O-C in Fig. 4.18(a), assume that the plate is fully anchored beyond the diagonal crack, that is it extends at least the effective length L_e beyond the root of the diagonal crack. Hence the maximum plate force P_{plate} can be assumed to be constant along the region which simplifies the analysis.
2. From a CDC analysis as described in Section 4.4.1 determine the position A-C of the weakest diagonal crack that is the critical diagonal crack, and the shear force $(V_{dat})_{c\text{-}plate}$ at the datum point to cause shear failure or crack sliding.
3. If the shear force at the datum point required to cause crack sliding $(V_{dat})_{c\text{-}plate}$ exceeds the applied shear force at the datum point $(V_{dat})_{applied}$, then the plate will

not debond. Otherwise, the design load cannot be achieved and some other plating arrangement or system of plating such as bolting may need to be considered.

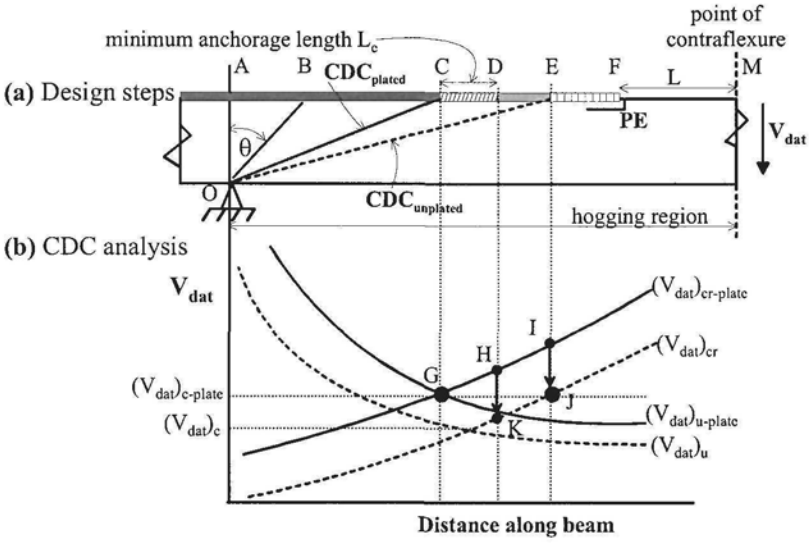

Figure 4.18 CDC design procedure using hinge approach

4. If the plated structure is strong enough, extend the plate at least one effective length L_e (Eq. 2.3) to Point D, to ensure that the plate is fully anchored as per the assumption in the CDC analysis in step (1).
5. A critical diagonal crack could also occur in the unplated region D-M in Fig. 4.18(a). However, this is not a debonding problem as a critical diagonal crack in the unplated region will not induce plate debonding. For beams with stirrups, it may be necessary to ensure that the shear in the unplated region is less than $V_c + V_s$. For a slab without stirrups, a critical diagonal crack in the unplated region may be undesirable particularly if the increase in the shear capacity due to plating is required to resist the increased applied load that this plating rehabilitation allows. In which case, the plate should be extended as in the following steps, to ensure that the critical diagonal crack occurs within the plated region.
6. To ensure that a critical diagonal crack does not occur within the unplated region, a CDC analysis of the unplated beam, as described in Section 4.4.1 and using the same equations as for the plated beam, needs to be performed to give the lines $(V_{dat})_{cr}$ and $(V_{dat})_u$ in Fig. 4.18(b).
7. As the root of the critical diagonal crack moves from C to D in Fig. 4.18(a), the path of the shear load to cause failure moves from G to H along $(V_{dat})_{cr\text{-}plate}$ in Fig. 4.18(b), and then to K on $(V_{dat})_{cr}$ at the plate end. Hence at position D, the shear to cause failure in the unplated region may be less than that to cause failure of the fully anchored plate at point C. Hence, it will be necessary to extend the plate to point E where the shear to cause failure J in the unplated beam is the same as that in the fully anchored plated beam at C.
8. It may be necessary to extend the plate beyond E to say point F to ensure plate end debonding does not occur as described in Section 1.3.3 and quantified in Chapter 6. However, it may be worth noting that PE debonding will rarely if ever prevent

adhesive bonding plates as it can be easily prevented by simply terminating the plate at the point of contraflexure.

These analyses have determined the extent of plating A-E in Fig. 4.18(a). They have also determined the shear load at the datum point to cause failure which is $(V_{dat})_{c\text{-}plate}$ in Fig. 4.18(b), from which can be deduced the vertical shear capacity within the plated region $V_{c\text{-}plate}$ in Eq. 4.26. The same can be said for the unplated beam. From $(V_{dat})_c$ in Fig. 4.18(b), can be deduced the vertical shear capacity of the unplated beam V_c from Eq. 4.11, which is really the same as Eq. 4.26. Hence the increase in the shear capacity $\Delta V_{c\text{-}plate} = V_{c\text{-}plate} - V_c$ due to plating is given by

$$\Delta V_{c-plate} = (1 \pm K_W)\left((V_{dat})_{c-plate} - (V_{dat})_c\right) \qquad 4.27$$

where K_W is defined in Eq. 4.13 and is negative in sagging regions and positive in hogging regions. For a continuous beam such as in Fig. 4.11 subjected to a uniformly distributed load, K_W has the values in Eqs 4.16 or 4.17. Furthermore, for a portion of the beam where no concentrated loads are acting within the free body of the CDC analysis then $K_W = 0$ as in Eq. 4.14.

It is suggested for design, that the value of the concrete shear capacity of the unplated beam from the national code should be used $(V_c)_{code}$ with the increase in the shear capacity due to plating $\Delta V_{c\text{-}plate}$ in Eq. 4.27. Hence the concrete shear capacity of the plated section is given by

$$V_{c-plate} = (V_c)_{code} + \Delta V_{c-plate} \qquad 4.28$$

which is also the shear load to cause crack sliding and, hence, CDC debonding in a plated beam. This will help overcome the probability that there may be slight differences between the national code values for $(V_c)_{code}$ and those calculated using the CDC analysis V_c.

4.4.2.2 CDC design procedure in anchorage approach

The anchorage approach is in many ways more straightforward than the hinge approach, as described in Section 4.4.2.1, because the anchorage approach requires the plate end to be fully anchored in an uncracked region as shown in the left hogging region in Fig. 4.17(b) and in Fig. 4.19(a). This requirement, of anchoring the plate in an uncracked region, would suggest that the plate is terminated at least up to the point of contraflexure if not beyond.

For the anchorage approach, the design steps for the hinge approach simplifies to the following.

1. The beam is fully plated and the plate fully anchored along the region A-E in Fig. 4.19(a) so that the plate extends an anchorage length L_e to point F.
2. From a CDC analysis, Section 4.4.1, determine the shear force $(V_{dat})_{c\text{-}plate}$ at the datum point to cause crack sliding.
3. If the shear force at the datum point $(V_{dat})_{c\text{-}plate}$ required for crack sliding exceeds the applied shear force at the datum point $(V_{dat})_{applied}$, then the plated structure is strong enough. Otherwise, the design load cannot be achieved and some other plating arrangement or system may need to be considered.

4. Determine the increase in the shear capacity due to plating from a CDC analysis of the unplated beam to give the lines $(V_{dat})_{cr}$ and $(V_{dat})_u$ in Fig. 4.19(b) and $(V_{dat})_c$ at point L in Fig. 4.19(b). Hence $\Delta V_{c\text{-}plate}$, the increase in the concrete shear capacity due to plating, can be obtained from Eq. 4.27 and the overall shear strength from Eq. 4.28.
5. It may be necessary to check for plate end debonding at F in Fig. 4.19(a) as described in Section 1.3.3 and quantified in Chapter 6.
6. It may be necessary to check that CDC debonding does not occur in the sagging region such as the diagonal crack J-G in Fig. 4.19(a) and this can be determined from a CDC analysis of the sagging region. This is unlikely to be a problem for the hogging plate in Fig. 4.17(b), as the shear at the plate end diminishes as the plate is extended into the sagging region. However it may be a problem in extending the tension face plate in the sagging region in Fig. 4.17(b) into the hogging region, as the vertical shear force at the plate end increases as the plate is extended; so that it may not be possible to find a region that is uncracked in both shear and flexure, that is it may not be possible to prevent the cracking shown in Figs 1.38 and 1.39.

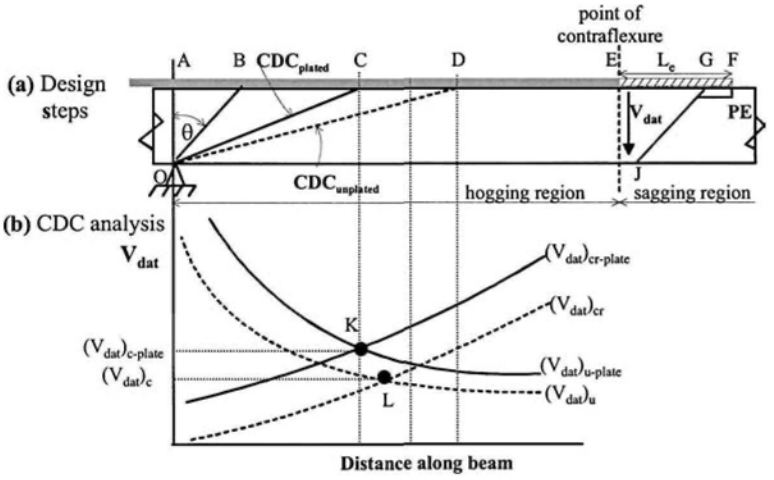

Figure 4.19 CDC design procedure using anchorage approach

4.5 Direct CDC debonding analysis

The critical diagonal crack analysis technique described in Section 4.4 is a highly adaptable iterative procedure suitable for spreadsheet analyses; it can cope with a wide variety of structures, applied loads, beam restraints, plating configurations and extent of plating. However, although easy to apply using spread sheets, it is iterative.

The direct approaches described in this section tend to be less accurate. Furthermore because they do not predict the position of the CDC, the whole region, that is the hogging region or the sagging region has to be fully plated as well as being fully anchored by an effective length L_e as in Fig. 4.20. However as they are direct approaches, they may be more suitable for design, particularly for the early stages. A comparison is also made of the CDC approaches in the guidelines in Table 1.1.

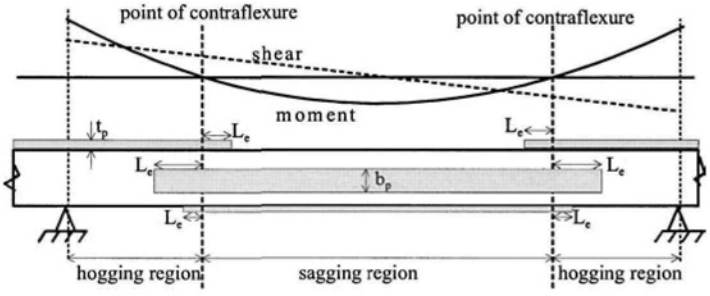

Figure 4.20 Extent of plating for direct approaches

4.5.1 Mean approach

4.5.1.1 Development of mean approach procedure

A relatively simple and conservative approach (Farrant et al 2002) for directly determining the shear capacity can be deduced from the typical shapes of the curves derived in the CDC analyses such as those in Figs 4.16(b) and (c) and 4.21(b). The shear load at the datum point required to cause cracking $(V_{dat})_{cr\text{-}plate}$ is at its lowest when the crack is vertical, that is $\theta = 0$ in Fig. 4.21(a); simply because this represents a flexural crack which commonly occurs at low applied loads. As the inclination θ of the crack increases, the crack gets longer and is less influenced by flexure so that the shear required to induce the crack increases, giving the typical increasing path with x for $(V_{dat})_{cr\text{-}plate}$ in Fig. 4.21(a). In contrast, the shear load to cause failure or crack sliding after cracking $(V_{dat})_{u\text{-}pres/metal}$ in Fig. 4.21(b) has its maximum value when the crack is vertical because the passive interface forces acting across the crack as shown in Figs 4.2 and 4.3, induced by the plate and the longitudinal reinforcing bars, act perpendicular to the crack face and so have their greatest effect. As the angle θ of the crack face increases as in Fig. 4.21(a), the passive interface forces become inclined to the face and become less effective as well as the dowel force shown in Figs 4.2 and 4.3 which will have less resistance from the surrounding concrete due to the inclination of the surface. Hence as the angle of the diagonal crack θ increases, we get the typical reducing path with x for $(V_{dat})_{u\text{-}pres/metal}$ in Fig. 4.21(a). Where these paths cross at point C in Fig. 4.21 is the capacity of the critical diagonal crack.

On either side of point C in Fig. 4.21(b), where the critical diagonal crack occurs, one of the shear capacity components, $(V_{dat})_{cr\text{-}plate}$ or $(V_{dat})_{u\text{-}pres/metal}$, will always overestimate and the other shear capacity will always underestimate the capacity of the CDC at point C. Hence it may be expected that the mean of $(V_{dat})_{cr\text{-}plate}$ and $(V_{dat})_{u\text{-}pres/metal}$ shown as $(V_{dat})_{mean}$ in Fig. 4.21 will approximate the CDC capacity. An extensive parametric study (Farrant et al 2002) of the shape of the mean curve $(V_{dat})_{mean}$ in Fig. 4.21(b) showed that it had the consistent and typical shape shown. There was always a region B-C where the mean value slightly underestimated the strength and the position of this region was always between the focal point and the position of the critical diagonal crack at C and always adjacent to the position of the critical diagonal crack as needs be as $(V_{dat})_{mean}$ will always pass through the position of the critical diagonal crack by definition of this crack.

If an inclination θ of a critical diagonal crack can be found that always lies within the conservative zone B-C in Fig. 4.21(b), that is within the range θ_{min} and θ_{max} in Fig. 4.21(a), then this could be used to provide a direct solution to the iterative procedure described in Section 4.4. An example of a part of an extensive parametric

study (Farrant et al 2002) to determine the range θ_{min} and θ_{max} is shown in Fig. 4.22; the position of a concentrated load L_O was varied in a shear span, such as in the free body depicted in the shear span B-C in Fig. 4.11 but with the datum point at the point of contraflexure, and the beam was analysed as fully plated and fully anchored.

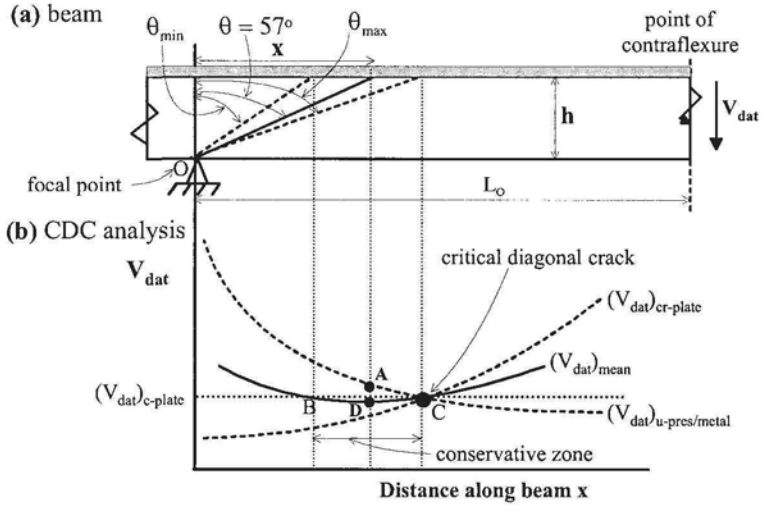

Figure 4.21 CDC debonding analysis – mean approach

In Fig. 4.22, the vertical distance between the lines marked *maximum angle* (θ_{max} in Fig. 4.21(a)) and *minimum angle* (θ_{min}) represents the conservative or safe zone B-C in Fig. 4.21. It can be seen in Fig. 4.22 that as L_O/h increases both θ_{max} and θ_{min} increase. However, the crack inclination from 56° to 57° always falls within θ_{max} and θ_{min}. From further parametric studies, the angle $\theta = 57°$ was chosen as an angle of a critical diagonal crack that would always give a conservative estimate of the strength of the critical diagonal crack. This is shown in Fig. 4.21(a) as the diagonal crack at $\theta = 57°$. This position of crack will have a capacity shown as point *A* in Fig. 4.21(b) which is greater than the strength of the critical diagonal crack at *C* but the *mean strength* is given by point *D* which is smaller than the strength of the CDC. This relationship between the strengths at points A, D and C needs to be emphasised. The critical diagonal crack at $\theta_{mean} = 57°$ given in the following equation, is chosen because the *mean strength* is conservative. Hence for the *mean approach*, a conservative estimate of the shear capacity is given by

$$\tan\theta_{mean} = \frac{x}{h} = 1.54 \qquad 4.29$$

It is also worth noting in Fig. 4.22, that the line marked *maximum angle* (θ_{max}) gives the position of the critical diagonal crack that is point C in Fig. 4.21 which also governs the extent of plating. This position is much more difficult to define and, hence, this *mean approach* procedure should be restricted to regions of the beam that are fully plated and fully anchored; that is the hogging region or sagging region must have a plate covering its full length and extended beyond the points of contraflexure

by at least the effective length L_e which is similar to the requirement of the anchorage approach in Section 4.4.2.2.

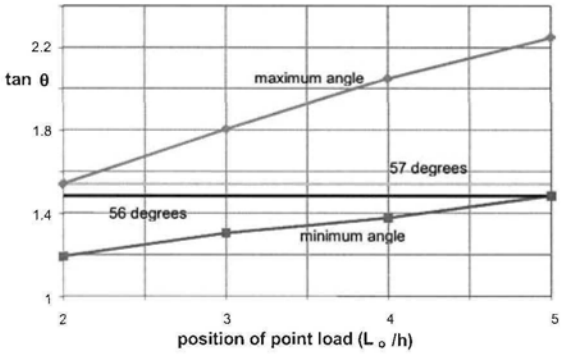

Figure 4.22 Determining conservative design region

4.5.1.2 Mean approach analysis

As the angle of inclination of the critical diagonal crack has now been defined by Eq. 4.29, the equations in the iterative approach in Section 4.4 can be used directly.

The shear load at the datum point to cause cracking $(V_{dat})_{cr\text{-}plate}$ are given in Eqs 4.18 and 4.19 for the sagging and hogging regions. In these equations, the following parameter, which controls the inclination of the crack, can be simplified as shown using Eq. 4.29.

$$\left(x^2 + h^2\right) = 3.37h^2 \quad \text{(for use in Eqs 4.18 and 4.19)} \tag{4.30}$$

The shear load at the datum point to cause crack sliding or failure is given in Eqs 4.21 and 4.22 for the *longitudinal reinforcement* approach $(V_{dat})_{u\text{-}metal}$, and in Eqs 4.24 and 4.25 for the *passive prestress* approach $(V_{dat})_{u\text{-}pres}$. The following parameter that controls the crack inclination can be simplified as shown by substituting Eq. 4.29.

$$\sqrt{1+\left(\frac{x}{h}\right)^2} - \frac{x}{h} = 0.296 \quad \text{(for use in Eqs 4.21, 4.22, 4.24 and 4.25)} \tag{4.31}$$

The *mean strength* at $\theta_{mean} = 57^\circ$ is given by

$$\left(V_{dat}\right)_{c-plate-mean} = \frac{\left(V_{dat}\right)_{cr-plate} + \left(V_{dat}\right)_{u-pres/metal}}{2} \tag{4.32}$$

where $(V_{dat})_{cr\text{-}plate}$ can be determined from Eq. 4.30 and $(V_{dat})_{u\text{-}pres/metal}$ can be determined from Eq. 4.31. The subscript *pres/metal* in Eq. 4.32 simply refers to the fact that the designer can choose either Eqs 4.21 and 4.22 where the *longitudinal reinforcement approach* is used, or Eqs 4.24 and 4.25 where the *passive prestress approach* is used.

To achieve consistency in the notation, Eq. 4.27 becomes

$$\Delta V_{c-plate} = \left(1 \pm K_w\right)\left(\left(V_{dat}\right)_{c-plate-mean} - \left(V_{dat}\right)_{c-mean}\right) \tag{4.33}$$

where $\Delta V_{c\text{-}plate}$ is the increase in the shear capacity or resistance to sliding due to plating; $(V_{dat})_{c\text{-}plate\text{-}mean}$ is the shear load at the datum point to cause failure or crack sliding in the plated beam given by Eq. 4.32; $(V_{dat})_{c\text{-}mean}$ is the shear load at the datum point to cause failure or crack sliding of the unplated beams that can be derived using the same equations as those used to derive $(V_{dat})_{c\text{-}plate\text{-}mean}$ but with the plate thickness equal to zero; and the coefficient K_W has been defined in Eqs 4.13 to 4.17 and which is negative in sagging regions and positive in hogging regions. It may also be worth noting that K_W, and hence e, should also be derived using Eq. 4.29.

4.5.2 Prestressed code approach

National concrete codes prescribe methods of determining the shear capacity of prestressed concrete beams by incorporating the stress due to prestressing into the shear strength equation which lends itself well to the passive prestress approach. Unlike the crack sliding model, code approaches generally do not require iteration to solve for the shear capacity but, unfortunately, are unable to predict the position of the CDC requiring the entire hogging or sagging region to be fully plated and anchored as in Fig. 4.20 and which is similar to the anchorage design approach in Section 2.5.1.

Not all national prestress code models are suitable for predicting CDC debonding. As an example, let us compare the ACI (2002) and Eurocode (1992) models for predicting the concrete component of the shear capacity of prestressed beams. These are given in Eqs. 4.34 and 4.35 for the case of a beam or slab with a rectangular cross-section of width b_c and effective depth d.

$$\left(V_{pp}\right)_{ACI} = \left(0.29\sqrt{f_c} + 0.3\sigma_{ps}\right)b_c d \qquad 4.34$$

$$\left(V_{pp}\right)_{Euro} = \left(\tau_{Rd}\left(1.6-d\right)\left(1.2+\frac{40A_{st}}{b_c d}\right)+0.15\sigma_{ps}\right)b_c d \qquad 4.35$$

where the compressive prestress in the concrete due to the prestressing force F_{ps} is $\sigma_{ps} \approx F_{ps}/b_c d$, A_{st} = cross-sectional area of tension reinforcing bars and τ_{Rd} is a basic design shear strength.

The ACI approach of Eq. 4.34 predicts an increase in the shear capacity due to prestress of $0.3\sigma_{ps}b_c d$ which is twice that predicted by the Eurocode approach of Eq. 4.35 of $0.15\sigma_{ps}b_c d$. Hence there would appear to be a very large difference between these two approaches. However, it should be remembered that the ACI approach of Eq. 4.34, as with the ACI rigorous approach based on principal stresses (ACI 2002), is based on predicting the formation of a critical diagonal crack in a prestressed beam and is not suitable, or cannot be used, for predicting the shear capacity of unprestressed beams. In contrast, the Eurocode approach of Eq. 4.35 is applicable to both prestressed and unprestressed beams and is based on the shear capacity of the critical diagonal crack. As the increase in the shear capacity due to the passive prestress approach is mainly based on the increase in the shear resistance to crack sliding, that is on the shear capacity after the CDC has formed, the Eurocode approach can only be adapted for the passive prestress approach, that is, only nation standard models that predict the concrete component of the shear capacity of both prestressed and unprestressed beams can be adapted for the passive prestress approach.

It needs to be stressed that there is nothing wrong with the conceptual approaches of the ACI. It would appear that the ACI is recognising the fact that for

prestressed beams the shear load to cause cracking V_{cr}, as represented by Eqs 4.18 and 4.19, is generally greater than the shear load to cause crack sliding after the crack has formed V_u, as represented by Eqs 4.21 and 4.22, and, hence, the importance of determining when diagonal cracks occur in prestressed beams. In contrast, the *Eurocode approach* (1992) is primarily based on the capacity after the critical diagonal crack has formed V_u, as represented by Eqs 4.21 and 4.22.

From Eq. 4.35, the increase in the shear capacity due to prestress is $0.15\sigma_{ps}b_cd \approx 0.15F_{ps}$. Hence, it can be assumed that the increase in the shear capacity due to the passive prestress P_{plate} is $0.15P_{plate}$, that is 15% of P_{plate}. A comparison of this 15% theoretical increase with tests on tension face and side plated beams (Oehlers et al 2004b) gave very good correlation. It is also worth noting that a parametric comparison of the increase in the shear capacity based on the Eurocode approach of Eq. 4.35 with $0.15P_{plate}$ with that of Zhang's adapted approach in Eq. 4.23 can show that the coefficient shown as 4 in Eq. 4.23 can vary from about 4.2 to 5.6. Hence there is also good correlation between the indirect crack sliding approach of Eq. 4.23 and the direct code approach of Eq. 4.35. A lower bound of 4 was used for the coefficient in Eq. 4.23, as this was 10% less than that determined from tests. It is suggested that a lower bound of 0.13 should be used for the coefficient in Eq. 4.35. Hence the increase in the shear capacity due to passive prestress is given by

$$(V_{incr})_{pp} = 0.13\sum P_{plate} \qquad 4.36$$

that is the increase in the concrete shear capacity is directly proportional to the total maximum axial force in all the plates ΣP_{plate} which for each individual plate is the lesser of the yield capacity of metal plates A_pf_{yp}, the fracture capacity of FRP plates A_pf_{FRP}, and the IC debonding resistance $(P_{IC})_{max}$ when fully anchored. The latter should be based on the IC debonding resistance in pull tests, as given by Eq. 2.1 and the α coefficients in Table 2.1. This is because a pull-test represents a plate with one intermediate crack which is equivalent to a single diagonal crack intercepting a plate. It is felt that for T and L-beams, P_{plate} should be only derived from those plates adhesively bonded close to the web of the beam.

4.5.3 Comparison with guidelines

In the European guidelines in Table 1.1, Blaschko (1997) in a seminar paper suggested that peeling off at shear cracks may be prevented by limiting the shear force to the shear resistance of RC members without shear reinforcement V_c, with the following modification of the shear capacity by treating the FRP as additional reinforcing bars.

$$\rho_{eq} = \frac{A_{sl} + A_p\dfrac{E_p}{E_s}}{b_c d} \qquad 4.37$$

where ρ_{eq} is an equivalent area of longitudinal reinforcing bars.

It can be seen in Eq. 4.37 that the cross-sectional area of plate has been transformed into an equivalent steel area of longitudinal reinforcement of the same axial stiffness but not axial strength. Hence unlike Eqs 4.20 and 4.23 which depend on the bond strength of the plate, Eq. 4.37 does not consider the maximum axial force

that the plate can resist. It should be used with care as by not recognising the IC debonding resistance of the plate, Eq. 4.37 does encourage the use of thick plates which it is felt might debond prematurely. As has been pointed out in Section 2.3.1.3 and Fig. 2.16, the bond or anchorage behaviour of externally bonded plates is totally different from that of the internal reinforcing bars encased in concrete. Hence, converting externally bonded FRP plates, that have a brittle bond characteristic and a brittle material characteristic, to embedded steel reinforcing bars, that have a ductile bond and ductile material characteristic, should be used with care.

Also in the European guidelines in Table 1.1, Jansze (1997) in his PhD thesis also computes an effective shear resistance of the beam V_c which does not appear to depend on the cross-section of the FRP plate but on the extent of plating and which suggests that if the plate is terminated at a support then the shear capacity is infinite. However, terminating a plate at a support as shown in Figs 1.19, 1.38 and 1.39 does not prevent shear failure nor debonding. As can be deduced from Section 4.4, plating does inhibit but does not prevent the formation of critical diagonal cracks within the plated region which depends on the properties of the plates such as their axial strengths.

In the Hong Kong approach in Table 1.1, Smith and Teng (2001) restrict the vertical shear to $1.4V_c$ which is reasonable as the addition of longitudinal plates can easily increase the concrete component of the shear capacity by 40%, as will be illustrated in Section 5.5.1, but it is felt that this is more of a rule of thumb guidance.

4.6 Results of CDC analyses

The following results were from an iterative CDC analysis as described in Section 4.4.1 and which used the hinge approach described in Section 4.4.2.1. Full and comprehensive worked examples are given in Chapter 7.

4.6.1 Hinge approach with FRP plates in hogging region of beam

The reinforced concrete beam in Section 3.5.2.1 and Fig. 3.41 has already been strengthened in the hogging region with a 1.2 mm thick carbon FRP tension face plate that is 600 mm wide. The plate increased the flexural capacity from 339 kNm to 450 kNm. The plate has been designed using the hinge approach, Section 2.5.2 and 4.4.2.1, so that it can be terminated short of the point of contraflexure. To maintain an elastic moment distribution, the sagging region of the beam must also be strengthened to increase the moment capacity from 173 kNm to 225 kNm. Hence, the new total static moment that is to be resisted is 675 kNm which equates to a 30% increase in the total applied load from 41 kN/m to 54 kN/m. The corresponding maximum shear force at the supports is 270 kN. The shear and moment distributions for the beam are shown in Fig. 4.23. As $V = 270$ kN is greater than $V_c = 134$ kN in the hogging region, calculated using the Australian concrete code AS3600, a CDC will occur in the unplated beam and hence, the plate is also required to increase the concrete component of the shear capacity V_c. The questions are: where to terminate the plate so that the critical diagonal crack falls within the plated region; and whether the increase in the concrete component of the shear capacity is sufficient to prevent CDC debonding within the hogging region.

For the elastic moment distribution shown in Fig. 4.23 the point of contraflexure is located 2113 mm from the support. Normally, the point of contraflexure is a convenient position to use as the datum point as the moment is zero.

However, to illustrate the use of the K_M factor in Eq. 4.12 the datum point will be taken at L_O = 1500 mm from the support as shown in Fig. 4.23 where it can be seen that V_{dat} = 270 – 54(1.5) = 189 kN and M_{dat} = 450 – 0.5(270+189)(1.5) = 106 kNm. Furthermore, there may not always be a point of contraflexure where the moment is zero as in vehicular bridges where there is an envelope of stress resultants. From Eq. 4.12, $K_M = 106x10^6/189x10^3$ = 561 mm and for a shear span in the hogging region subjected to a udl, $K_W = 2(1500 - x)/5774 = (0.52 - 0.346x10^{-3}x)$ from Eq. 4.17. The next step in the CDC design follows the procedure in Section 4.4.2.1 for the hinge approach where the load to cause cracking is given by Eq. 4.19 and the load to cause crack sliding by Eq. 4.25 using the *passive prestress approach* as we are using an FRP plate in this example.

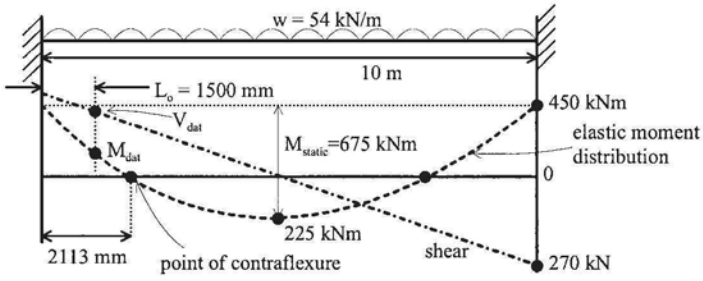

Figure 4.23 Shear and moment distributions for hogging analysis

The procedure begins by assuming that the beam is fully plated along the hogging region, that is the plate extends at least the effective length L_e (Eq. 2.3) beyond the root of any diagonal crack so that the maximum plate force P_{plate} can be assumed to be constant along the region and given by the IC debonding resistance. From Eq. 2.1 P_{plate} = 294 kN using α = 0.427 from Table 2.1 which is the mean debonding coefficient from pull tests, the same material properties as given in Section 3.5.2.1, and b_p/b_c = 0.3 but based on the suggested limit described in Section 2.4.3 was taken as 0.33. Using a spreadsheet analysis, the solid curves in Fig. 4.24 are produced for the fully plated beam where it can be seen that the critical diagonal crack in the plated region of beam intersects the tension face 1235 mm from the focal point (that is the support in this example) at a shear force $(V_{dat})_{c\text{-}plate}$ = 133 kN at the datum point. Hence, the *minimum* extent of plate required is 1235 mm plus L_e = 187 mm (Eq. 2.3) to achieve the maximum IC debonding resistance and an additional h/2 = 250 mm is recommended considering shear cracks are not linear as idealized in the analysis giving a total length of plate of 1672 mm measured from the internal support. Unfortunately in this example, $(V_{dat})_{c\text{-}plate}$ = 133 kN is less than V_{dat} = 189 kN due to the applied loads and hence CDC debonding would occur prior to achieving the increased applied load of 54 kN/m. To increase the CDC debonding resistance, an alternative plating arrangement could be investigated or the plates could be bolted.

Even though this plating arrangement did not work, the increase in the concrete component of the shear capacity after plating can be determined using Eq. 4.27 where K_W is taken as positive in the hogging region to give $\Delta V_{c\text{-}plate}$ = 28.4 kN. In Eq. 4.27, the shear force at the datum point to cause the CDC in the unplated beam $(V_{dat})_c$ = 107 kN and is given by the intersection point of the dashed lines shown in Fig. 4.24, which were calculated using Eqs 4.19 and 4.25 with t_{tfp} = 0. As $(V_c)_{code}$ = 134 kN for the hogging region as given previously, the concrete component of the

shear capacity of the plated beam is determined using Eq. 4.28 to give $V_{c\text{-plate}}$ = 162.4 kN, a 21% increase from the unplated beam strength.

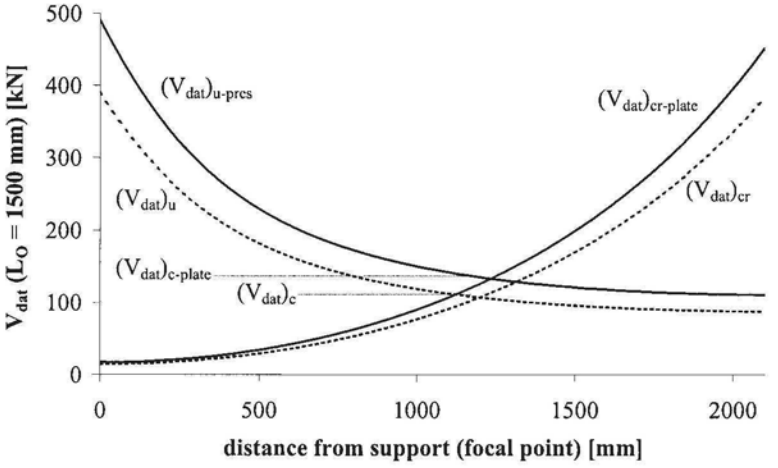

Figure 4.24 CDC analysis of FRP tension face plated beam in the hogging region

For comparison, the *simplified mean approach* described in Section 4.5.1 is also used to predict the increase in the concrete component of the shear capacity after plating. Using the simplifications given by Eqs 4.29-4.31 for an assumed crack inclination of 57°, Eq. 4.19 was used to calculate $(V_{dat})_{cr\text{-}plate}$ = 58.8 kN and Eq. 4.25 to calculate $(V_{dat})_{u\text{-}pres}$ = 176.2 kN so that from Eq. 4.32 $(V_{dat})_{c\text{-}plate\text{-}mean}$ = 117.5 kN. Using the same procedure but taking t_{fp} = 0, $(V_{dat})_{c\text{-}mean}$ = 95 kN for the unplated beam so that from Eq. 4.33 the increase in the concrete component of the shear capacity using the mean approach is $\Delta V_{c\text{-}plate}$ = 28.2 kN. In this example, the increase is only slightly less than that obtained using the rigorous iterative CDC analysis described above.

The increase in the concrete component of the shear capacity can also be determined using the *prestress code approach* described in Section 4.5.2 where the increase in shear capacity due to passive prestress is simply given by Eq. 4.36 so that $(V_{incr})_{pp}$ = 38.2 kN.

4.6.2 Anchorage approach with steel plates in sagging region of slab

The reinforced concrete slab shown in Fig. 3.38, with the specifications in Section 3.5.1.1, has been strengthened in the sagging region with 3 mm thick steel tension face plates of width 140 mm per meter width of slab. The plate increased the flexural capacity from 31 kNm/m to 47 kNm/m width of slab as shown in Fig. 4.25. The steps in the flexural analyses are given in Section 3.5.1.4 (for *unpropped* construction) and the complete analysis for the slab in Chapter 7. To summarise briefly, the 22% increase in the sagging flexural capacity is required to accommodate the maximum 30% moment redistribution from the hogging region. Consequently, the increase in applied load from 23 kN/m/m to 28 kN/m/m in Fig. 4.25 has increased the maximum shear force at the supports from 57.5 kN/m to 70 kN/m. The final shear and moment diagrams shown in Fig. 3.39 are repeated in Fig. 4.25. The plates are fully anchored beyond the points of contraflexure using the anchorage approach, Section 2.5.1 and

4.4.2.2, and it is now a question of determining whether the increase in the shear capacity is sufficient to prevent CDC debonding within the sagging region.

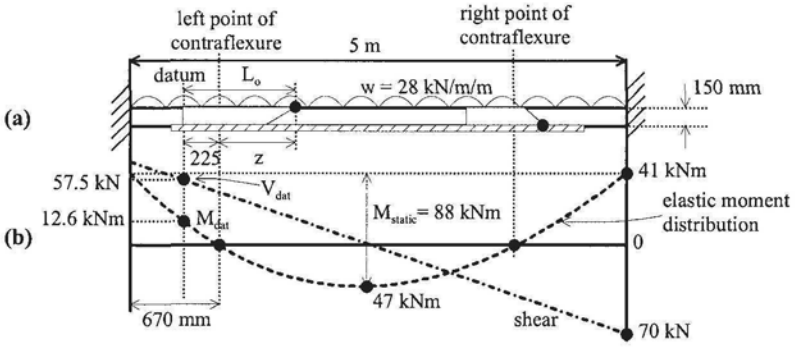

Figure 4.25 Shear and moment distributions for sagging analysis

As the absolute maximum shear force V = 70 kN/m is much less than the code concrete shear capacity 108 kN/m in the sagging region, a critical diagonal crack will *not* occur in the plated section. Hence, a CDC debonding analysis is obviously not necessary. However to illustrate the CDC debonding analysis, the example is continued to quantify the increase in V_c due to the addition of the plate. For the redistributed moment distribution in Fig. 4.25, the point of contraflexure is located 670 mm from the support as shown. In the following analyses, we will determine the shear capacity in the sagging region adjacent to the point of contraflexure. We will only consider focal points on the compression face of the sagging region as shown adjacent to the left point of contraflexure in Fig. 4.25(a). To complete the analyses, focal points in the hogging region as shown on the right point of contraflexure may have to be considered as these critical diagonal cracks may extend into the sagging region.

As discussed in Section 4.4.1.1, the position of the focal point, on the left hand side of Fig. 4.25(a), is not as clearly defined for sagging regions of beams with uniformly distributed loads as for concentrated loads. It would be expected to lie in the vicinity of the point of contraflexure where the applied shear is near its maximum but its exact position will have to be determined by trial and error. As it is theoretically possible for the CDC to pass through the point of contraflexure, it may be more convenient to choose a free body with a datum in the hogging region as shown adjacent to the left point of contraflexure in Fig. 4.25(a).

Examples of free bodies for use in the CDC analyses are shown Fig. 4.26. In Fig. 4.26(a), the focal point is at the point of contraflexure and the diagonal crack which is in the hogging region crosses both the top and bottom longitudinal reinforcing bars. It may be worth noting that Zhang's crack sliding approach in Section 4.3.3 and the indirect crack sliding CDC analyses described in Section 4.4 do not require the designer to distinguish between tension reinforcing bars and compression reinforcing bars as the cross-sectional area of the reinforcing bars A_s in Eq. 4.8 consists of all the fully anchored bars. Hence, there is not a sudden step change in the strength when moving from the sagging region to the hogging region. It will also be shown in Chapter 5, that compression, side and tension face plates can also be treated in the same way and all add to the shear capacity; this further

emphasises the versatility of this crack sliding approach. Figure 4.26(b) shows an example of a critical diagonal crack crossing the point of contraflexure and, hence, the reason for the datum being away from the point of contraflexure, and Fig. 4.26(c), shows an example of a CDC within the sagging region.

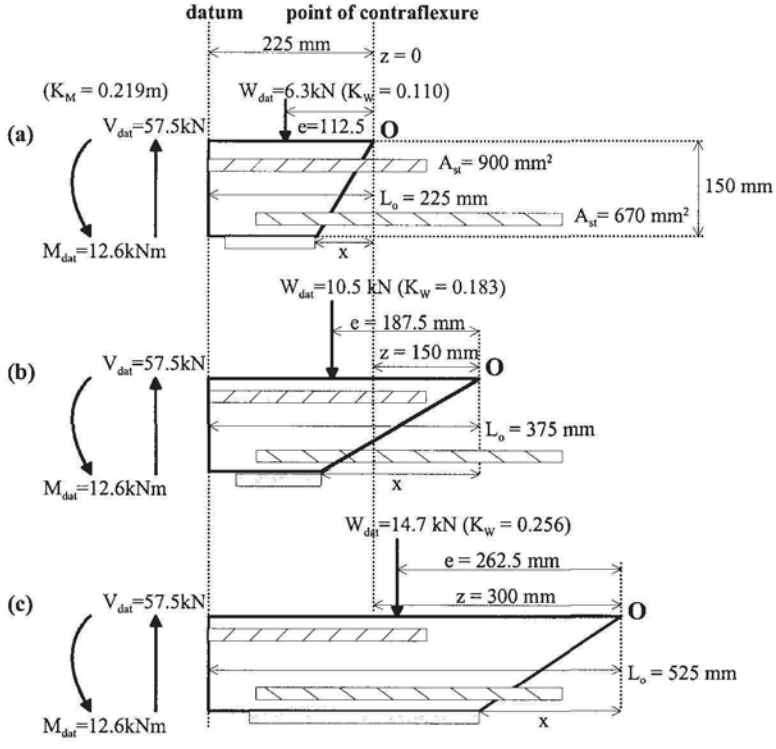

Figure 4.26 Free body diagrams for CDCs near point of contraflexure

The stress resultants at the datum in Fig. 4.26 are constant and hence K_M from Eq. 4.12 is fixed at 0.219 m as shown. However, the resultant force on the free body due to the uniformly distributed load varies as shown giving the variation in K_W from Eq. 4.13 as shown. From a comparison of the stress resultants in Fig. 4.26 with those in Fig. 4.12, it can be seen that the only difference is the direction of M_{dat} so that K_M in Eq. 4.18 changes from $+K_M$ to $-K_M$ as follows

$$\left(\left(V_{dat}\right)_{cr-plate}\right)_{sag} = \frac{\left(\left(x^2+h^2\right)\left(\frac{b_c f_{tef}}{2} + \frac{m_p f_t b_{ifp} t_{ifp}\left(h+0.5t_{ifp}\right)}{h^2}\right)\right) + \left(F_{ps} d_{ps}\right)}{L_O - K_M - K_W e} \qquad 4.38$$

The figure for the shear load to cause crack sliding in Fig. 4.14 remains unchanged so that the crack sliding resistance of Eq. 4.24 with Eq. 4.23 remains unchanged.

The next step in the CDC design follows the procedure in Section 4.4.2.2 for the anchorage approach where the load to cause cracking is given by Eq. 4.38 and the

load to cause crack sliding by Eq. 4.21 using the *longitudinal reinforcement approach*, which can be used in this example only because we are using a metal plate.

As we are using the anchorage approach in this example the slab must be fully plated in the sagging region and fully anchored so that the plate must extent at least the effective length L_e = 330 mm (Eq. 2.3) beyond the point of contraflexure. It is also suggested that the plate be extended an additional h/2 to allow for possible variations in the position of the point of contraflexure due to variations in the applied load so that the *minimum* length of plate required in this example is $L_{sag} + 2L_e + h$ = 4470 mm. If the CDC extends beyond the point of contraflexure into the hogging region as illustrated in Figs 4.26(a) and (b), then the plate must be extended $L_e + h/2$ beyond the end of the CDC. As discussed in Section 2.4.4, the 3 mm thick 300 MPa steel tension face plate will yield prior to IC debonding hence the maximum force in the plate is governed by the yielding giving P_{plate} = 126 kN/m width of slab. Using a spreadsheet analysis, the solid curve representing $(V_{dat})_{c\text{-}plate}$ in Fig. 4.27 is produced for the fully plated beam by equating Eqs 4.38 and 4.21 for increasing z from the point of contraflexure. From Eq. 4.26, the concrete shear capacity of the fully plated beam $V_{c-plate}$ is found where it can be seen that the capacity is greater than maximum applied shear force at the focal point given by $(V_{max})_{Lo}$. Hence, CDC debonding will not occur confirming the original observation.

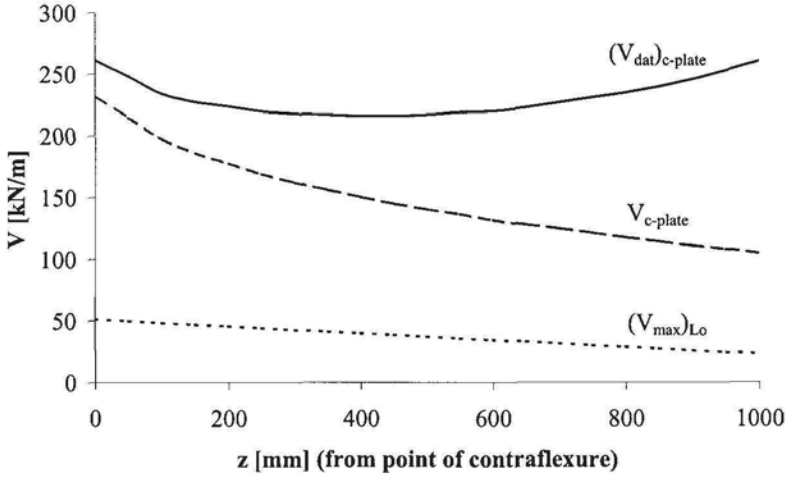

Figure 4.27 CDC analysis of steel tension face plated slab in the sagging region

It is interesting to note that $V_{c\text{-}plate}$ in Fig. 4.27 decreases as the focal point moves from the point of contraflexure to the midspan in the sagging region, that is as *z* increases in Fig. 4.26. This can be explained using the CDC analysis as the shear load to cause cracking, for example $(V_{dat})_{cr}$ in Fig. 4.24, reduces as the moment increases towards the midspan in the sagging region, hence, $(V_{dat})_c$ also reduces.

4.7 References

ACI 440.2R-02 (2002). Emerging Technology Series. "Guide for the Design and Construction of Externally Bonded FRP Systems for Strengthening Concrete Structures". Reported

by ACI Committee 440. American Concrete Institute, Farmington Hills, Michigan, USA.

Bay, B., Nguyen, T., Webster, A., and Wilkins, S. (2003). "Vertical shear strength of FRP plated reinforced concrete beams." 4th year research report, Dept. of Civil and Env., Engng, Adelaide University.

Blaschko, M. (1997), "Strengthening with CFRP". Munchner Massivbau Seminar, TU Munchen.

Eurocode 2: "Design of concrete structures Part 1: General rules and rules for buildings (1992)". BSI Standards.

Farrant, K., Kollevris, V., Modistach, A., and Young, T. (2002) "Study and application of retrofitting techniques." 4th year research project, Dept. of Civil and Environmental engineering, University of Adelaide.

Jansze, W. (1997), "Strengthening of reinforced concrete members in bending by externally bonded steel plates". PhD dissertation, TU Delft, The Netherlands

Oehlers, D.J., Liu, I., and Seracino, R., (2004a) "Passive prestress approach for CDC debonding of adhesively bonded steel and FRP plates." Submitted November 2003.

Oehlers, D.J., Liu, I., and Seracino, R., (2004b) "Prestress code approach for shear deformation debonding of adhesively bonded plates." Provisional acceptance Proceedings Structures and Buildings Journal, November 2003.

Smith, S.T. and Teng, J.G. (2002) "FRP strengthened RC beams – II: assessment of debonding strength models", *Engineering Structures.* 24(4): 397-417, April.

Zhang J.P. (1997) "Diagonal Cracking And Shear Strength Of Reinforced Concrete Beams." *Magazine of Concrete Research.* Vol.49, No.178, Mar., pp 55-65

Chapter 5: Generic Rules for CDC Debonding

5.1 Introduction

The generic design approach for CDC debonding developed in this chapter applies to all plating arrangements and plating combinations, some of which are shown in Fig. 5.1. The plates can be applied to the tension faces as shown at *A* which is probably the most common form of plating. The tension face plate at *B* can be extended into the compression face at *C*, which also inhibits the formation of the critical diagonal crack in this region. Tension face plates can also be positioned at the underside of the flange as at *D*, which encourages the tension reinforcing bars to yield before the plates debond. Plates can be adhesively bonded to the sides of the beam at *E*, which often allows a greater area of plate to be used, particularly on the sagging region of beams where the width of the web may severely restrict the amount of plate that can be bonded. The side plates can be placed at any level along the web, in the tension zone at *F* or in the compression zone at *G* and, wherever they are placed, tests have shown that they can substantially increase the concrete component of the shear capacity. Furthermore, angle or channel sections can be used such as at *H*. Any combination of these plates can be used and any type of material or combinations of materials can be used. All of these plates must be checked for IC debonding as described in Chapters 2 and 3 and for plate end debonding, as will be described in Chapter 6; although plate end debonding is never a problem as PE debonding can always be prevented by terminating the plate at the point of contraflexure.

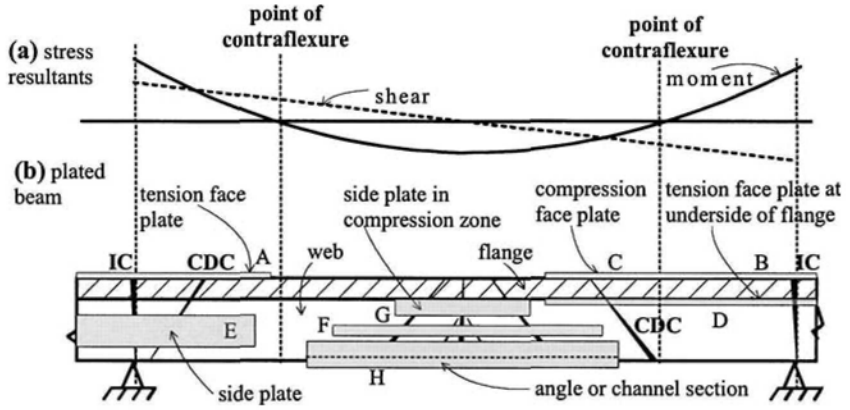

Figure 5.1 Plating arrangements

The design procedure, that has so far been dealt with in preceding chapters in this book, has consisted of first deciding what plates are required for a specific increase in the flexural strength at a section, and this has been based on the IC debonding resistance as described in Chapters 2 and 3. Having chosen the adhesively bonded plating system, the next step was to decide on how far to extend the plate along the beam and to ensure that the plate does not debond prematurely due to CDC debonding; this was covered in Chapter 4, specifically for tension face plates as these are covered in the guidelines in Table 1.1. Hence, the emphasis, so far, has been on

flexural strengthening, although it was shown in Chapter 4 that longitudinal tension face plates can enhance the shear capacity of slabs without stirrups.

In this chapter, we will place more emphasis on the increase in the shear capacity due to plating and, in particular, for all types of longitudinal plating such as the range shown in Fig. 5.1. Generic rules are developed for CDC debonding for all types of longitudinal plates and combinations of longitudinal plates. It will be shown how substantial increases in the shear capacity can be attained through longitudinal plating. Furthermore, the interaction between the shear enhancement due to longitudinal plating and that due to transverse plating, that is externally bonded stirrups, will be described. The generic CDC analysis is first explained in this chapter, this is then incorporated into a generic design procedure that covers both the hinge and anchorage design philosophies, unusual cases are then considered such as compression face plates or short side plates in the vicinity of the ends of tension face plates, followed by examples of the ability to enhance the shear capacity and then some typical analyses. As this generic approach is based on Zhang's work, it can be considered to give a characteristic or lower bound value suitable for design.

5.2 Generic CDC debonding analysis

The fundamental principles behind critical diagonal crack analyses have been explained in Chapter 4 in terms of unplated and tension face plated beams. The governing equations are now given in a generic form that can be applied to all plate materials, plate positions and combinations of plates. To allow this chapter to be self contained some of the equations in Chapter 4 have been repeated. Furthermore, some of the notation used in Chapter 4 will be changed to become more consistent and the terminology will be clarified.

The subscript *dat* will refer to the datum point. The subscript *crack* will refer to the formation of a diagonal crack at a specific position of the beam such as O-A in Fig. 5.2. The term *diagonal crack* will refer to cracks that can spread through the depth of the beam, such as those in Figs. 4.5 and 4.6, across which a rigid body sliding action can take place if their shear capacity is reached; the term diagonal crack does not refer to the flexural-shear cracks in Fig. 4.5. The subscript *slide* will refer to the rigid body displacement or crack sliding across a specific diagonal crack that already exists such as O-A in Fig. 5.2. Hence for beams or slabs without stirrups, the subscript *slide* infers both plate debonding and shear failure at a specific diagonal crack. Whereas for beams or slabs with stirrups, the subscript *slide* will refer to plate debonding only at a specific diagonal crack.

The subscript *crit* will refer to the weakest critical diagonal crack in a region, that is the weakest relative to the distribution of the applied shear. Hence for beams or slabs without stirrups, the subscript *crit* will refer to shear failure and to critical diagonal crack (CDC) plate debonding. However, for beams or slabs with stirrups, the subscript *crit* will refer to CDC debonding. The subscript *conc* will refer to the shear capacity at the weakest or critical diagonal crack, which is equivalent to the concrete shear capacity in unplated beams in national standards which will be referred to as $(V_c)_{code}$. However, the subscript *conc* will be used for both the shear capacity of plated and unplated structures. Where it is necessary to differentiate between plated and unplated structures, then the subscript *pl* will refer to plated and *un* to unplated.

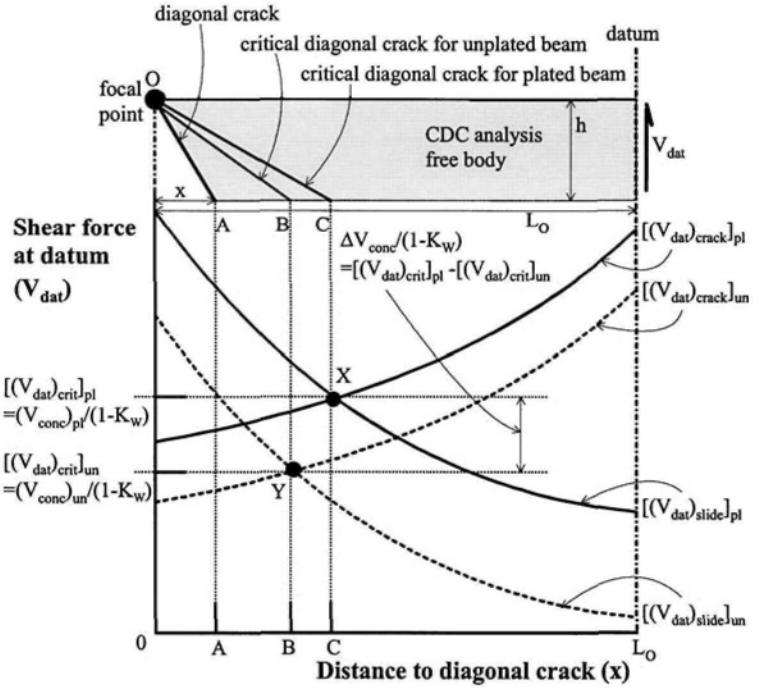

Figure 5.2 CDC analysis, notation and terminology

5.2.1 Iterative approach

Examples of free bodies that can be used in a CDC analysis are shown in Fig. 5.3 for the hogging and sagging regions of part of a span of a continuous beam from a support to the position of maximum moment. In Fig. 5.3(c) are examples of free bodies that are fully encompassed within a hogging region or sagging region, and in Figs 5.3(d) and (e) are examples of free bodies that lie within both regions, that is the free body straddles the point of contraflexure. The *focal points* O in Fig. 5.3 fixes one side of the free body and the *datum* the other side. The focal point must be on a compression face but it can be anywhere on the compression face. It is a question of finding the angle θ of the diagonal crack that emanates from the focal point that has the weakest resistance to the vertical shear forces for that particular position of the focal point. It is then a question of finding the position of the focal point that has the weakest of the weakest resistances to find the critical diagonal crack.

The datum, at a distance L_O from the focal point in Fig. 5.3(c), can be at any position. The beam is subjected to the applied loads shown in Fig. 5.3(b). These applied loads induce the moment M_{dat} and shear force V_{dat} distributions in Fig. 5.3(a). Furthermore, part of the applied load in Fig. 5.3(b), that is shown shaded and referred to as W_{dat}, is acting directly on the free bodies used in the CDC analyses in Fig. 5.3(c). Hence, it can be seen that M_{dat}, W_{dat} and V_{dat} are all related to the distribution of applied loads in Fig. 5.3(b). For analytical convenience, M_{dat} and W_{dat} are written in terms of V_{dat}, that is $M_{dat} = K_M V_{dat}$ in Fig. 5.3(a) and $W_{dat} = K_W V_{dat}$ in Fig. 5.3(b). It is worth bearing in mind that the factors K_M and K_W are not affected by the magnitude of the applied loads but by their distribution, so that if the distribution can be assumed to be constant then K_M and K_W remain constant in the analysis. A free

body in Fig. 5.3(c) is subjected to a shear force V_{dat}, moment $M_{dat} = K_M V_{dat}$ at the datum and the applied loads acting on the free body $W_{dat} = K_W V_{dat}$ as shown in Fig. 5.3(b). The applied load W_{dat} is the load acting on the free body due to dead and live load. For the hogging region it is shown as that part of the total applied load resisted by the length of the beam L_O-x and for the sagging region that part resisted by L_O.

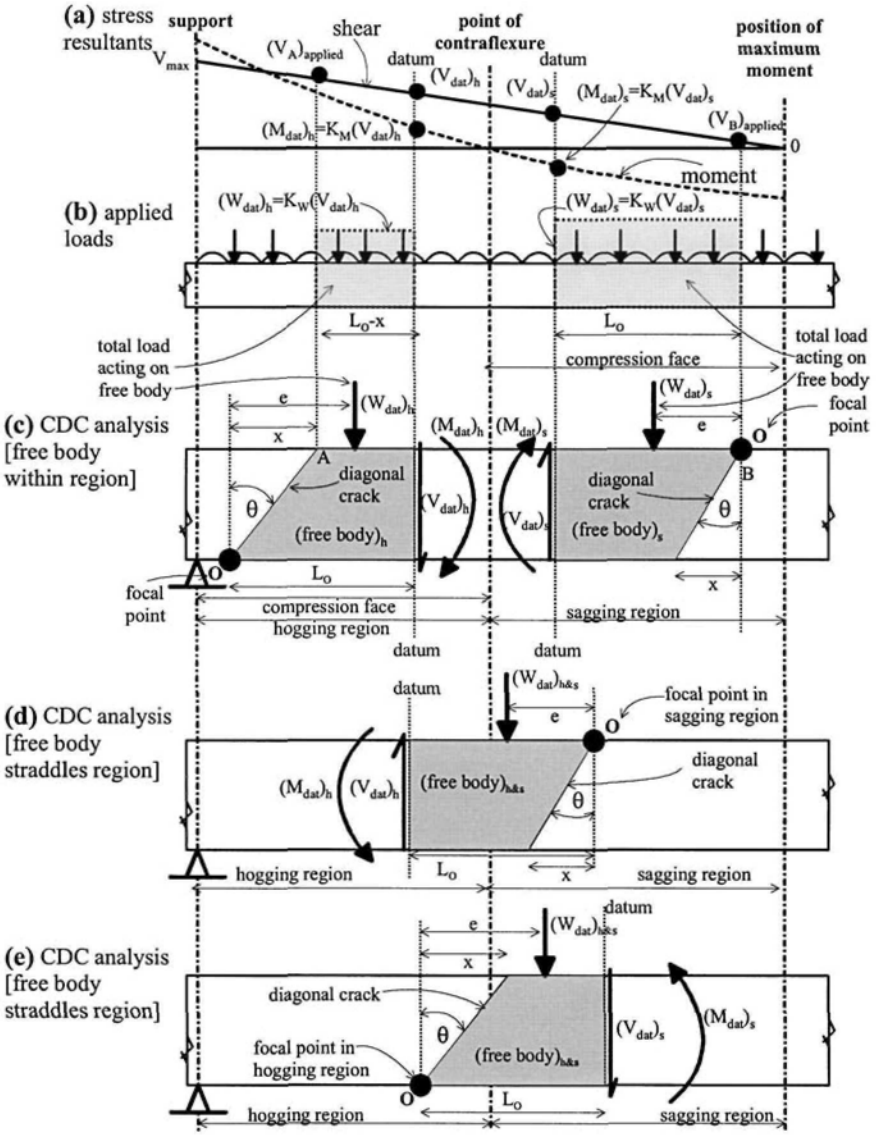

Figure 5.3 CDC analysis free bodies

5.2.1.1 Shear to cause cracking

The free body in the hogging region of Fig. 5.3(c) is shown in Fig. 5.4, and that for the sagging region in Fig. 5.5. For ease of analysis, each rectangular element of plate is considered independently. From rotational equilibrium, the shear load at the datum point V_{dat} to cause a diagonal crack at a position x from the focal point is given by

$$(V_{dat})_{crack} = \frac{\left(\left(x^2 + h^2\right)\left(\frac{b_c f_{tef}}{2} + \frac{f_t \sum\left(m_p A_{rect} L_{rect}\right)}{h^2}\right)\right) + \left(F_{ps} d_{ps}\right)}{L_O \pm K_M \pm K_W e} \qquad 5.1$$

where h is the total depth of the beam or slab; b_c is the width of the slab or the width of the web of a beam; f_{tef} is an effective tensile strength of the concrete; f_t is the actual tensile strength of the concrete which can be taken as $0.4\sqrt{f_c}$ (N and mm) when not measured directly; m_p is the modular ratio of the plate Young's modulus to that of the concrete E_p/E_c; A_{rect} is the area of a rectangular section of the plate; L_{rect} is the lever arm from the centroid of the rectangular section to the compression face, for example, for the tension face plate $A_{rect} = b_{tfp}t_{tfp}$ and $L_{rect} = h+0.5t_{tfp}$; the summation applies to each individual rectangle of plate; F_{ps} is the prestressing force; d_{ps} the lever arm of the prestressing force from the compression face; L_O is the length of the free body; the moment factor K_M is given by the stress resultants at the datum as follows

$$K_M = \frac{M_{dat}}{V_{dat}} \qquad 5.2$$

where K_M is positive when the free body is fully contained within a region as shown in Fig. 5.3(c) and where K_M is negative when the free body straddles a point of contraflexure as shown in Figs 5.3(d) and (e); the load factor K_W is given by

$$K_W = \frac{W_{dat}}{V_{dat}} \qquad 5.3$$

where $K_W e$ in Eq. 5.1 is negative when the focal point is in the sagging region and positive when the focal point is in the hogging region; the effective tensile strength of the concrete is given by the following equation in which the units are N and mm.

$$f_{tef} = 0.156 f_c^{2/3}\left(\frac{h}{100}\right)^{-0.3} \qquad 5.4$$

It can be seen in Figs 5.4 and 5.5 that, for analytical convenience, each rectangular portion of plate is treated individually and this would also apply to channel and angle sections that were adhesively bonded where the webs and flanges would be treated as individual rectangular sections. Because the longitudinal reinforcing bars are assumed not to affect the load to cause cracking, they have been omitted from the figures.

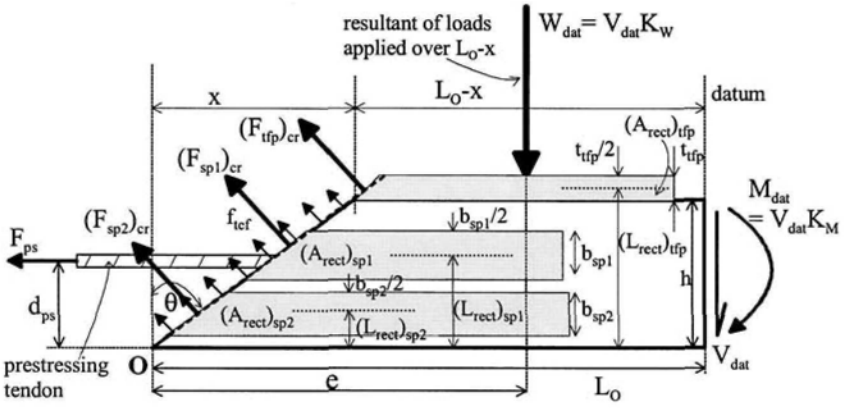

Figure 5.4 Hogging region – shear to cause cracking

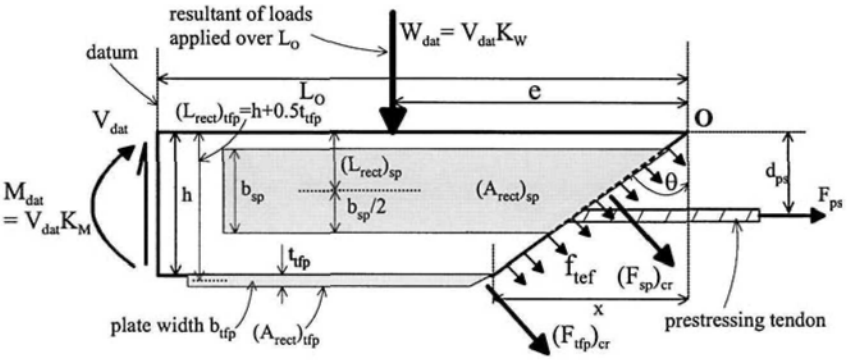

Figure 5.5 Sagging region – shear to cause cracking

5.2.1.2 Shear to cause crack sliding

The hogging region free body in Fig. 5.3(c) is shown in Fig. 5.6 and that for the sagging region in Fig. 5.7. The resistance to shear across the diagonal crack V_{conc} depends on the cross-sectional area of all the longitudinal reinforcing bars crossing the diagonal crack A_s; all the fully anchored longitudinal reinforcing bars at all levels of the beam or slab, are included in A_s. The shear resistance also depends on the sum of all the individual maximum axial forces in the plates P_{plate}. For a metal plate of yield capacity f_{yp}, P_{plate} is limited by $P_y = A_p f_{yp}$ where A_p is the cross-sectional area of the plate $b_p t_p$. For an FRP plate, P_{plate} is limited by its fracture capacity $P_u = A_p f_{FRP}$ where f_{FRP} is the fracture stress of the FRP plate. For both metal and FRP plates, P_{plate} is also limited by the intermediate crack debonding resistance $P_{IC} = A_p \sigma_{IC}$. The IC debonding resistance stress σ_{IC} is given by Eq. 2.1 which depends on the minimum of the anchor lengths on either side of the diagonal crack $(L_p)_{left}$ and $(L_p)_{right}$ in Fig. 5.6 and the effective length L_e as given by Eq. 2.3. For deep plates as in Fig. 5.7, it may be necessary to allow for the variation in the anchorage length from $(L_p)_{min}$ to $(L_p)_{max}$ by simply subdividing the plate width b_{sp} into narrow strips and treating each

individually and with a mean anchorage length as in Fig. 5.6 or just use $(L_p)_{min}$ as a lower bound. The shear capacity also depends on the prestressing force F_{ps}.

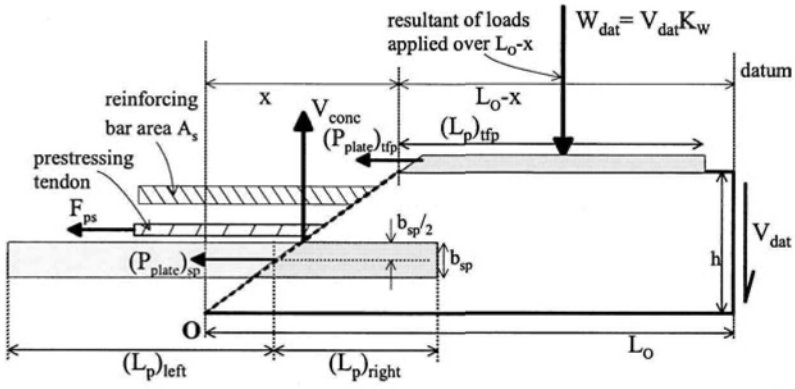

Figure 5.6 Hogging region – shear to cause crack sliding

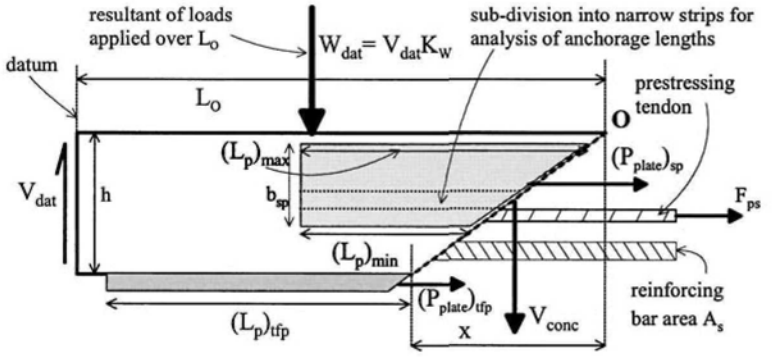

Figure 5.7 Sagging region – shear to cause crack sliding

The shear force at the datum point V_{dat}, in Figs 5.6 and 5.7, to cause crack sliding at a diagonal crack at a distance x from the focal point is given by the following equation which is based on the passive prestress approach described in Section 4.4.1.4; the passive *prestress approach* is used as it is a generic approach that can be applied to both metal and FRP plates as compared to the *longitudinal reinforcement approach* in Section 4.4.1.3 that can only be applied to metal plates.

$$(V_{dat})_{slide} = \frac{0.4 f_c b_c h \left(1 + \dfrac{2F_{ps} + 4\sum P_{plate}}{f_c b_c h}\right)\left(\sqrt{1+\left(\dfrac{x}{h}\right)^2} - \dfrac{x}{h}\right) f_1(f_c) f_2(h) f_3(\rho)}{1 \pm K_W} \qquad 5.5$$

where the summation is for all the axial forces in the plates crossing the diagonal crack and for each plate it is the lesser of P_y, P_u and P_{IC}; the load factor K_W is negative when the focal point is in a sagging region and positive when the focal point is in a

hogging region; and the remaining functions are defined below with the units required when the equation is dimensionally incorrect and also with the range of test data from which they were developed.

$$f_1(f_c) = \frac{3.5}{\sqrt{f_c}} \qquad \text{[N and mm]} \quad 5 < f_c < 60\,MPa \tag{5.6}$$

$$f_2(h) = 0.27\left(1 + \frac{31.6}{\sqrt{h}}\right) \qquad \text{[mm]} \quad 80 < h < 700 \tag{5.7}$$

$$f_3(\rho) = \frac{15A_s}{b_c h} + 0.58 \qquad \frac{A_s}{b_c h} \le 0.045 \tag{5.8}$$

5.2.1.3 Critical diagonal crack

Equation 5.1 can be used to plot the shear load at the datum point V_{dat} to cause the formation of a diagonal crack in the plated beam, which is shown as the line $[(V_{dat})_{crack}]_{pl}$ in Fig. 5.2, for every position x of the diagonal crack. Equation 5.5 can be used to plot the shear load at the datum point to cause crack sliding in the plated beam, $[(V_{dat})_{slide}]_{pl}$ in Fig. 5.2, for every position of the diagonal crack x. The intercept of these two lines at point X gives the shear load at the datum point to cause crack sliding in the critical or weakest diagonal crack $(V_{dat})_{crit}$ which is the shear load at the datum point to cause debonding.

The shear $(V_{dat})_{crit}$ is an indirect measure of the capacity of the plated beam as it is the shear load at the datum point to cause debonding and not the shear load at the critical diagonal crack. If the applied load or design load, such as in Fig. 5.3(b), induces a shear load at the datum point $(V_{dat})_{applied}$ which is greater than the capacity $(V_{dat})_{crit}$ then the plate will debond prior to the design load being reached and vice versa.

An alternative way of interpreting the CDC analysis is to consider the shear at the critical diagonal crack at which crack sliding occurs which is given by the following shear capacity

$$(V_{conc})_{pl} = [(V_{dat})_{crit}]_{pl}(1 \pm K_w) \tag{5.9}$$

where K_W is negative when the focal point is in a sagging region and positive when the focal point is in a hogging region. $(V_{conc})_{pl}$ is the shear capacity at a section through the focal point O in the sagging region in Fig. 5.3(c) shown as point B, or at point A in the hogging region which is through the root of the diagonal crack at the distance x from the focal point. It may be worth noting that the K_W factor in Eq. 5.9 simply allows for the difference in the vertical shear between the datum point, V_{dat} in Fig. 5.3(a) and the critical diagonal crack, $(V_A)_{applied}$ or $(V_B)_{applied}$. The shear capacity at the critical diagonal crack can then be compared with the applied shear at the critical diagonal crack, that is $(V_B)_{applied}$ or $(V_A)_{applied}$ in Fig. 5.3(a) to determine whether premature debonding occurs. A safe design would be to ensure that the applied shear did not exceed this shear capacity throughout the plated region.

It is suggested that a preferred approach is to determine the increase in the sliding resistance due to plating and to add this to the national code value for the concrete shear capacity $(V_c)_{code}$, to determine the shear to cause crack sliding and

hence debonding. This will help tie the design approach directly to the designers national code. If this approach is preferred, then a CDC analysis will have to be performed on the unplated section to give the shear load at the datum point to cause cracking, $[(V_{dat})_{crack}]_{un}$ in Fig. 5.2 and the shear load to cause crack sliding $[(V_{dat})_{slide}]_{un}$. The intercept of these two lines at Y will give shear load at the datum point to form the critical diagonal crack $[(V_{dat})_{crit}]_{un}$. Hence, the shear capacity at the critical diagonal crack is

$$(V_{conc})_{un} = [(V_{dat})_{crit}]_{un}(1 \pm K_w) \qquad 5.10$$

$(V_{conc})_{un}$ in Eq. 5.10 is the concrete shear capacity of the unplated beam which is also given in national codes $(V_c)_{code}$. $(V_{conc})_{un}$ and $(V_c)_{code}$ are bound to differ slightly, as does $(V_c)_{code}$ between codes, which would place the designer in a dilemma in deciding which to use. To overcome this dilemma, it is suggested that the following approach is used. The difference between Eqs 5.9 and 5.10 is the increase in the shear capacity due to plating given by

$$(\Delta V_{conc})_{pl} = \{[(V_{dat})_{crit}]_{pl} - [(V_{dat})_{crit}]_{un}\}(1 \pm K_w) \qquad 5.11$$

which can then be added to the national concrete code strength $(V_c)_{code}$ as follows.

$$(V_{conc})_{code} = (V_c)_{code} + (\Delta V_{conc})_{pl} \qquad 5.12$$

Hence it is suggested that the national code value $(V_c)_{code}$ be used and the CDC analysis procedure is only used to determine the increase in shear due to plating.

5.2.1.4 Simplifications

Examples of free bodies that can be used in CDC analyses are shown in Fig. 5.8 for both a hogging and sagging region. The applied stress resultants are shown in Fig. 5.8(a), the applied loads are in the diagrams with the subscript 1 such as (b_1) and the CDC analyses are in the diagrams with the subscript 2 such as (b_2).

The focal points O always occur on the compression face of the beam or slab. The focal point with the weakest, or critical diagonal crack, often occurs at a concentrated load P that is on the compression face, such as in Figs 5.8(b_2) and (d_2) where the concentrated load is the support reaction and in Fig. 5.8(c_2) where the concentrated load is applied to the beam. As the concentrated loads P in Figs 5.8(b_2), (c_2) and (d_2) are acting at the focal points, they do not contribute to the CDC analysis of Eq. 5.1. Furthermore, they are not included in W_{dat} in Fig. 5.8 in the vertical equilibrium in Eq. 5.5 as they reduce the shear force acting on the free body. By not including these concentrated forces on the free body, we are in effect comparing the shear capacity with the maximum applied shear just to the side of the concentrated load. The reader may wish to both include and not include the concentrated force P on the free body to confirm what has been said. When the region of the beam is subjected to predominantly uniformly distributed loads *w* as in Fig. 5.8(e_1), then the position of the focal point of the CDC in Fig. 5.8(e_1) has to be determined by trial. It is likely that the CDC is close to the point of contraflexure where the shear in the sagging region is at its maximum so that it may be convenient to choose a datum point away from the point of contraflexure as shown in Fig. 5.8(f_2) so that the CDC can pass through the

point of contraflexure. It may also be necessary to check for possible critical diagonal cracks with focal points in the hogging region as shown in Fig. 5.8(f_2)*.

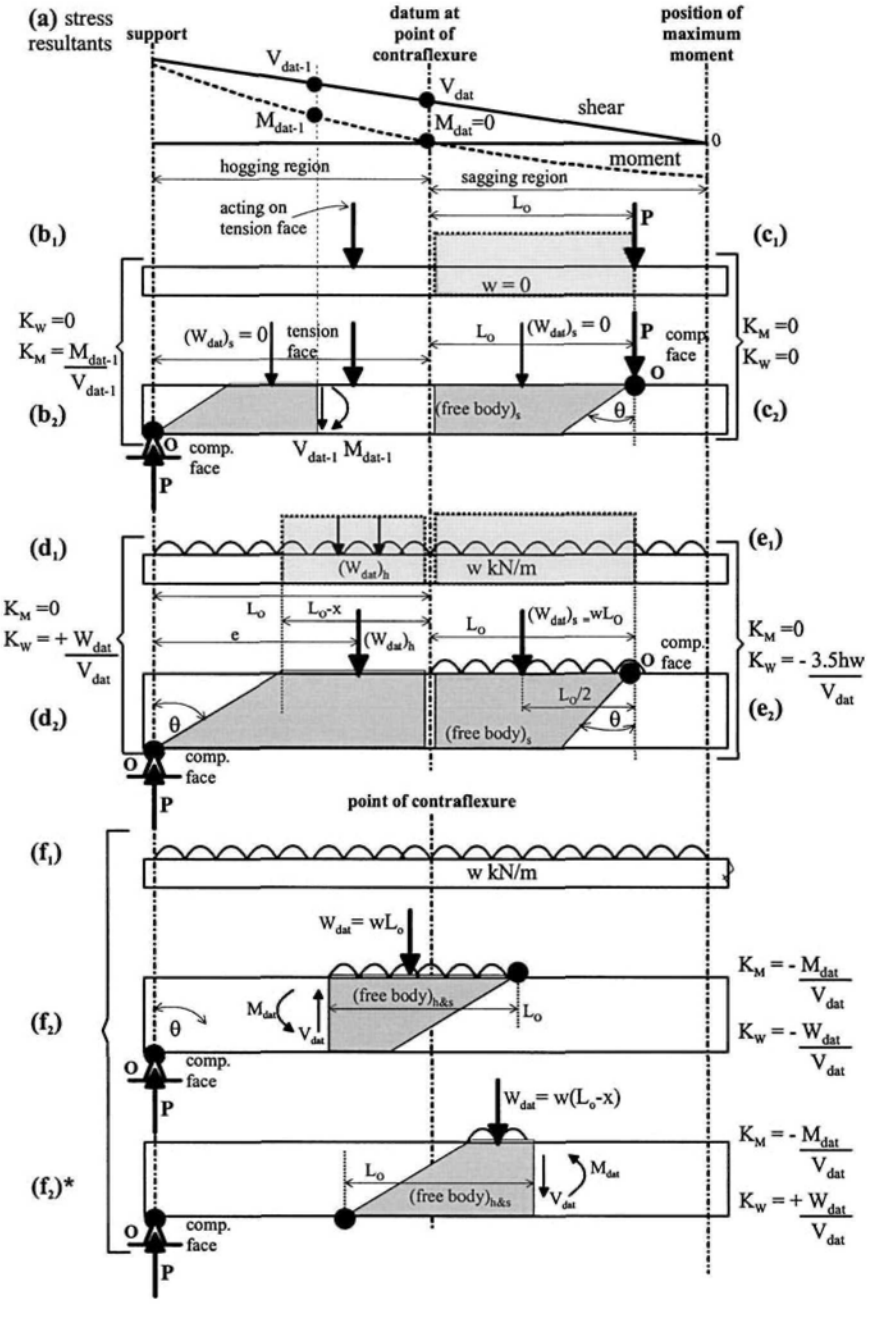

Figure 5.8 Simplification in CDC analysis

The most convenient position for the datum point is at the point of contraflexure as in Figs 5.8(c), (d) and (e) as this ensures that the moment factor K_M of Eq. 5.2 is zero in the CDC analysis of Eq. 5.1. When the applied load *w* is insignificant compared with the concentrated load P in Fig. 5.8(c_1), then the load factor K_W, from Eq. 5.3, can be considered to be zero in Eqs 5.1 and 5.5. When a concentrated load is acting on the tension face as in Fig. 5.8(b_1), then it may be more convenient to move the free body away from this concentrated load.

A further discussion and simplification of the K_M and K_W factors is given in Section 4.4.1.1. If it is unclear where the best position for the focal point is, then a few positions should be tried to find the critical diagonal crack.

5.2.1.5 Interpretation of CDC analysis results

Figure 5.2 can be used for the CDC analysis of fully plated and fully anchored beams as well as the CDC analysis of partially plated beams, and its interpretation is considered in Fig. 5.9. To help in the discussion of Fig. 5.9, it will be assumed that there are no applied loads, $W_{dat} = 0$, acting on the free body of the CDC analysis, such as in Fig. 5.8(c), in which case $K_W = 0$ in Eq. 5.9 so that the shear load at the datum point is also the shear load at the diagonal crack.

(a) Short plates

Let us first consider terminating the plate close to the supports at point A_2 in Fig. 5.9(a). As the effective length of the plate is L_e, point A_1 represents the position of the plate where the plate is fully anchored, that is plate O-A_2 is fully anchored over the length O-A_1. As position A_1 is fully anchored, the shear load at the datum point to cause a critical diagonal crack through A_1 is shown as point 1 in Fig. 5.9(b), that is $(V_{dat})_1$ which lies on the shear load to cause crack sliding in the plated beam $[(V_{dat})_{slide}]_{pl}$. Furthermore, just beyond the plate end at A_2, the beam is unplated so that the shear load at the datum point to induce a critical diagonal crack through this position is shown as point 2, that is $(V_{dat})_2$ which lies on the shear load to cause crack sliding in the unplated beam $[(V_{dat})_{slide}]_{un}$. It is also worth noting that $(V_{dat})_2$ is the shear load to cause the plate near to the plate end to debond. This is because adjacent to the plate end, the shear load to causing cracking is given by points P on the plated line and Q on the unplated line in Fig. 5.9(b) both of which are below $(V_{dat})_2$. Hence a crack will first form, and then it will fail at the end of the plated region at $(V_{dat})_2$ on $[(V_{dat})_{slide}]_{un}$ which is really $[(V_{dat})_{slide}]_{pl}$ with the anchorage length of the plate tending to zero.

If a critical diagonal crack is not to occur in plate O-A_2 in Fig. 5.9(a), then the shear load must not be greater than $(V_{dat})_2$. If it is greater than $(V_{dat})_2$, then part of the plate will debond, in effect moving A_2 to the left and consequently A_1 to the left, thereby, reducing the length of the fully anchored region O-A_1. As $(V_{dat})_2$ is greater than the shear to cause a *critical* diagonal crack in a fully plated beam $[(V_{dat})_{crit}]_{pl}$, it can be seen that it is possible for the shear load required to cause CDC debonding to be greater, in a very short partially plated beam, than that required to cause the fully plated beam to debond at $[(V_{dat})_{crit}]_{pl}$. However, the shear load to cause debonding can also be less as shown for the plate terminating at B_2; in which case the shear load to cause the plate end to debond is given by point 4 on $[(V_{dat})_{slide}]_{un}$ which is just weaker than $[(V_{dat})_{crit}]_{pl}$. It is also worth considering terminating the plate at C_2, in which case the plate debonds at point 6 which is on the $[(V_{dat})_{crack}]_{pl}$ line, as the crack within the plate forms and fails at this shear load as the shear capacity after cracking $[(V_{dat})_{slide}]_{un}$

is less. It can be seen that the shear load to cause plate debonding is given by the broken line U-V-X where V is at the intercept between $[(V_{dat})_{crack}]_{pl}$ and $[(V_{dat})_{slide}]_{un}$.

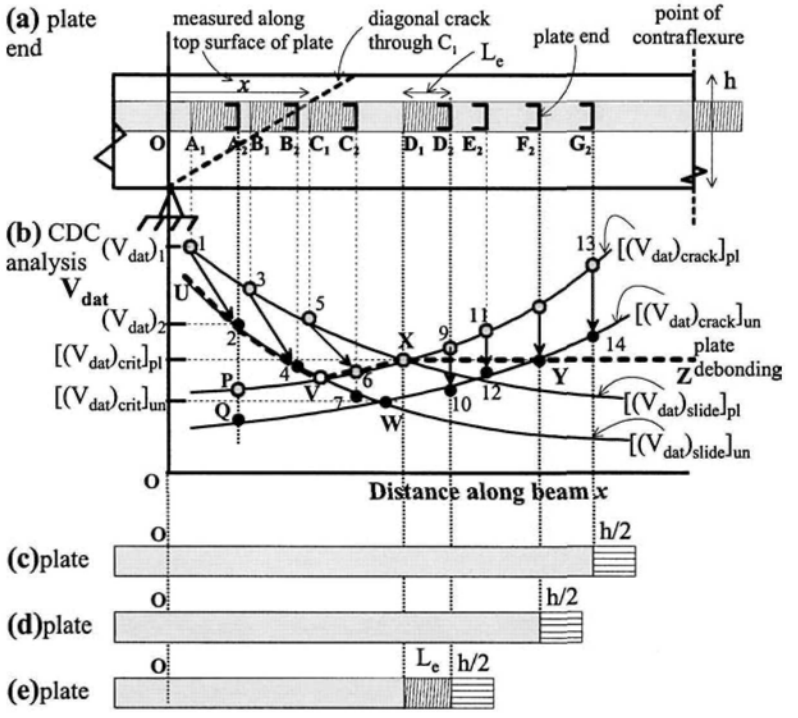

Figure 5.9 Shear capacity of partially plated members

When the plate is terminated at A_2, then the shear can be increased to $(V_{dat})_2$ which is greater than the shear capacity of the unplated beam $[(V_{dat})_{crit}]_{un}$ at point W. This is fine just as long as the total shear capacity of the unplated region V_c+V_s is greater than $(V_{dat})_2$. If not, then shear failure of the unplated beam will precede plate debonding. It is suggested that short plates by themselves should not be used in design as their strength is greatly influenced by the assumed position and shape of the diagonal crack. Instead medium or long plates should be used.

(b) Long plates

Let us now consider terminating the plate closer to the point of contraflexure such as plate O-G_2 in Fig. 5.9(a). The debonding resistance at G_2 is governed by the shear load to cause cracking $[(V_{dat})_{crack}]_{pl}$ at point 13 and not the shear load to cause crack sliding $[(V_{dat})_{slide}]_{pl}$ as the latter has a lower strength at position G_2. This means that the plate in this region does not need to be anchored as shown in Fig. 5.9(c) although it is suggested that the plate is extended a further distance h/2 to allow for the fact that the diagonal crack is usually curved and for variations in the distribution of the applied loads. As the plate is extended from D_1 to G_2 in Fig. 5.9(a), the shear load to cause cracking in this region and within the plated beam $[(V_{dat})_{crack}]_{pl}$ increases and is always greater than the shear to cause the critical diagonal crack $[(V_{dat})_{crit}]_{pl}$ at X, so that the shear load to cause debonding remains on the broken line X-Y-Z, that is

at $[(V_{dat})_{crit}]_{pl}$. Hence the failure envelope to cause plate debonding is given by the broken line U-V-X-Y-Z.

(c) Medium plates

When the plate is terminated at position G_2 in Fig. 5.9(a), a diagonal crack could form adjacent to the plate end in the unplated beam at the shear load 14. As this is greater than the shear load to cause the plate to debond $[(V_{dat})_{crit}]_{pl}$ at point X, the plate will debond at position D_1 prior to crack sliding at the plate end. Hence the shear capacity of the unplated region is of no consequence. Therefore, it can be concluded that it is only necessary to terminate the plate at F_2 where the shear load to cause cracking and subsequently crack sliding in the unplated region at Y is equal to the shear required to cause plate debonding at X. This maximum extent of plating is shown in Fig. 5.9(d) where it is recommended that the plate is extended a further distance h/2 to allow for vagaries in the distribution of the applied loads. Extending the plate any further is of no benefit.

To achieve $[(V_{dat})_{crit}]_{pl}$ at point X, the plate has to be fully anchored at D_1 so that the plate has to be extended by an effective length to position D_2 in Fig. 5.9(a). The shear to cause debonding in the anchorage length D_1-D_2 is greater than at X in Fig. 5.9(b) as it follows the path X-9 on $[(V_{dat})_{crack}]_{pl}$. So that plate debonding in this anchorage length will not precede plate debonding at X. This is in contrast to plate debonding for short plates such as that terminated at B_2 where the cracking shear is smaller than the sliding shear so the plate requires to be anchored.

The shear to cause failure in the unplated beam at D_2 is given by point 10 which is greater than that of the unplated beam at point W. However, in this case point 10 is smaller than that at point X to cause plate debonding. If the beam or slab has stirrups and just as long as the total shear capacity V_c+V_s in the unplated beam is greater than $[(V_{dat})_{crit}]_{pl}$, then crack sliding in the unplated region is of no consequence so that the plate can be terminated as shown in Fig. 5.9(e). However, if the beam or slab does not have stirrups, then shear failure within the unplated region will first occur which will probably be undesirable so that so the plate should be extended to that in Fig. 5.9(d).

To conclude, the failure envelope for the shear to cause CDC debonding in a partially plated beam is given by the broken line U-V-X-Y-Z in Fig. 5.9(b). If the shear to cause CDC debonding in the plated region is sufficient to cause a critical diagonal crack in an unplated region, then stirrups are required in the unplated region.

5.2.2 *Direct approaches*

The iterative approach outlined in Section 5.2.1 may be tedious for design purposes but it does quantify the position of the critical diagonal crack and, hence, does allow for partial plating. It is also worth noting, that the iterative approach automatically allows for the variation in the applied vertical shear and the variation in the vertical shear capacity along the length of the beam. Hence shear failure may occur at a section where the applied shear is not at its maximum. For example in the hogging region in Fig. 5.3(c), the minimum shear capacity $(V_{conc})_{pl}$ of the critical diagonal crack O-A should be compared with the applied shear $(V_A)_{applied}$ and not with the maximum applied shear of V_{max}; this can be done as the position of the critical diagonal crack is known. However, comparing the capacity $(V_{conc})_{pl}$ with V_{max} would give a safe conservative design.

The following approaches were developed to give directly safe estimates of the minimum shear capacity $(V_{conc})_{pl}$ but they do not give the position of the critical

diagonal crack. Hence these direct approaches require the whole region, either the hogging region or the sagging region, to be fully plated and fully anchored as shown in Fig. 4.20. These direct approaches also require the minimum shear capacity within a region $(V_{conc})_{pl}$ to be compared directly with the maximum applied shear V_{max} and hence will give a safe design.

5.2.2.1 Mean approach

The mean approach is described in Section 4.5.1.2. The shear load at the datum to cause crack sliding, Eq. 4.32, can be written with the following notation.

$$\left[\left(V_{dat}\right)_{crit}\right]_{mean} = \frac{\left[\left(V_{dat}\right)_{crack}\right]_{mean} + \left[\left(V_{dat}\right)_{slide}\right]_{mean}}{2} \tag{5.13}$$

where substituting the parameter in Eq. 4.30 into Eq. 5.1 gives

$$\left[\left(V_{dat}\right)_{crack}\right]_{mean} = \frac{\left(3.37h^2\left(\frac{b_c f_{tef}}{2} + \frac{f_t \sum\left(m_p A_{rect} L_{rect}\right)}{h^2}\right)\right) + \left(F_{ps} d_{ps}\right)}{L_O \pm K_M \pm K_W e} \tag{5.14}$$

where K_M is positive when the free body is contained within a region (that is a sagging region or a hogging region) and negative when the free body straddles a point of contraflexure, and where K_W is negative when the focal point is in the sagging region and positive when in the hogging region. Substituting the coefficient in Eq. 4.31 into Eq. 5.5 gives

$$\left[\left(V_{dat}\right)_{slide}\right]_{mean} = \frac{0.118 f_c b_c h\left(1 + \frac{2F_{ps} + 4\sum P_{plate}}{f_c b_c h}\right) f_1(f_c) f_2(h) f_3(\rho)}{1 \pm K_W} \tag{5.15}$$

Equation 5.13 can be used to determine the shear load at the datum to cause crack sliding in both the fully plated fully anchored beam $[[(V_{dat})_{crit}]_{mean}]_{pl}$ and the shear load at the datum to cause crack sliding in the unplated beam $[[(V_{dat})_{crit}]_{mean}]_{un}$. Hence, changing the notation in Eq. 5.11 gives the increase in the shear capacity due to plating as

$$\left(\Delta V_{conc}\right)_{pl} = \left\{\left(\left[\left(V_{dat}\right)_{crit}\right]_{mean}\right)_{pl} - \left(\left[\left(V_{dat}\right)_{crit}\right]_{mean}\right)_{un}\right\}\left(1 \pm K_w\right) \tag{5.16}$$

where K_W is positive when the focal point is in the hogging region and negative when in the sagging region. The shear capacity of the plated section $(V_{conc})_{code}$ is the sum of the code shear capacity of the unplated section $(V_c)_{code}$ plus the increase due to plating in Eq. 5.16 as in Eq. 5.12.

The whole region, hogging or sagging, needs to be plated and fully anchored by extending the plate beyond this region by at least an effective length L_e (Eq. 2.3). Furthermore, the applied shear force within the whole plate length must not exceed $(V_{conc})_{code}$.

5.2.2.2 Prestressed code approach

The passive prestress code approach is described in Section 4.5.2. It was shown that the increase in the concrete component of the shear capacity due to plating is given by

$$(V_{incr})_{pp} = 0.13\sum P_{plate} \qquad 5.17$$

where the summation applies to all the longitudinal plates, and the maximum axial force in a plate P_{plate} is the lesser of the yield capacity $A_p f_{yp}$ for metal plates, the fracture capacity $A_p f_{FRP}$ for FRP plates, and IC debonding resistance $A_p \sigma_{IC}$ for a fully anchored plate in a pull test which is given by Eq.2.1 with $\beta_L = 1$ and with α from the pull test results in Table 2.1. This increase can only be applied to fully plated and fully anchored regions as shown in Fig. 4.20.

The vertical shear load to cause CDC debonding is, therefore, given by

$$V_{c-plate} = (V_c)_{code} + 0.13\sum P_{plate} \qquad 5.18$$

where $(V_c)_{code}$ is the concrete shear capacity of the unplated RC section given by the national code. Equation 5.18 applies to both prestressed and unprestressed beams. For unprestressed beams, the national code value for $(V_c)_{code}$ can be used directly. However, care must be taken in deciding what value to use for prestressed beams as only code equations that are applicable to both prestressed and unprestressed beams, such as the Eurocode approach (1992) in Eq. 4.35, should be used.

5.3 Generic design approach for CDC debonding

The generic design procedure for CDC debonding is illustrated in Fig. 5.10, which uses the hogging region in Fig. 5.3 to illustrate the approach; although the same procedure applies to the other regions of the beam. The full sequence of design is given which includes IC, CDC and PE debonding and it covers the hinge approach in Section 2.5.2 and the anchorage approach in Section 2.5.1.

5.3.1 Basic analyses

The initial steps in the generic design procedure consist of the following.

- Determine the distribution of the design stress resultants in Fig. 5.10(a).
- Check for IC debonding at the position of maximum moment, M_{max} in Fig. 5.10(a) as described in Chapters 2 and 3. This may already have been done in determining the plates required for flexure. However, additional plates may have been added to increase the shear capacity.
- Perform a CDC analysis of the unplated beam to obtain $[(V_{dat})_{crack}]_{un}$ and $[(V_{dat})_{slide}]_{un}$ in Fig. 5.10(d) and the shear load at the datum point to cause the critical diagonal crack $[(V_{dat})_{crit}]_{un}$ at point N.
- Assume the plates extend over the whole region A-F in Fig.5.10(c) and beyond by at least the effective length L_e, so that the region is fully plated and the plates fully anchored throughout the region. Hence, the maximum force in each of the plates P_{plate} is constant along the region and depends on the minimum of: the maximum IC debonding resistance $P_{IC} = A_p \sigma_{IC}$; their fracture capacity, if an FRP plate, of $P_u = A_p f_{FRP}$; or their yield capacity, if a metal plate, of $P_y = A_p f_{yp}$.

- Analyse the fully plated and fully anchored plated beam for CDC debonding to obtain $[(V_{dat})_{crack}]_{pl}$ and $[(V_{dat})_{slide}]_{pl}$ in Fig.5.10(d) and the shear load at point L for critical diagonal crack debonding in the plated section $[(V_{dat})_{crit}]_{pl}$.

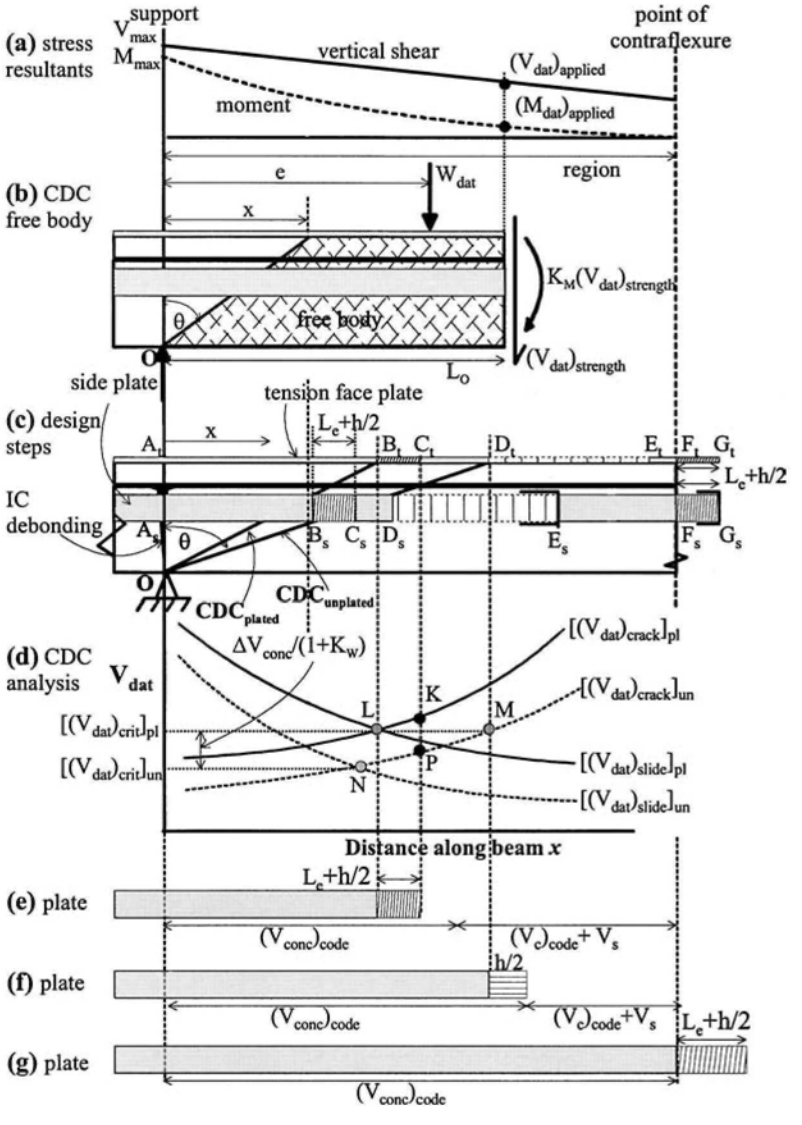

Figure 5.10 Generic CDC design approach

5.3.2 Shear load at datum point V_{dat} to cause CDC debonding

The CDC analysis procedure, depicted in Fig. 5.10(d), gives the shear load at some convenient datum point $V_{dat,}$ as shown in Fig. 5.10(b), to cause a diagonal crack to form at position x and also to cause that diagonal crack to fail. It may be worth noting

that position x in the CDC analysis is measured along the tension face of the beam as shown in Fig. 5.10(c). Therefore, this distance denotes the length of the tension face plate but the diagonal, such as O-B, denotes the extent of the upper edge of the side plate. The shear load V_{dat} is not necessarily the shear at the critical diagonal crack because of the applied loads acting on the CDC analysis free body W_{dat}. The design procedure can be based on the shear load at the datum point V_{dat} as will be described in this section. However, if it is necessary to relate the design to the national code value for the concrete shear capacity $(V_c)_{code}$, then this approach is described in Section 5.3.3.

The shear at the datum point V_{dat} in Fig. 5.10(d) is the shear required to cause cracking or crack sliding which depends on the capacity of the section. Hence V_{dat} in the CDC analyses represents the strength of the structure $(V_{dat})_{strength}$ as shown in Fig. 5.10(b). In contrast, from the loads applied to the structure in Fig. 5.10(a), the applied shear load at the datum point will be referred to as $(V_{dat})_{applied}$. When the capacity $(V_{dat})_{strength}$ is less than the applied $(V_{dat})_{applied}$, then CDC debonding occurs. Continuing with the design steps in Section 5.3.1.

- Consider the analysis, in Fig. 5.10(d), of the fully anchored fully plated beam, that is the lines $[(V_{dat})_{crack}]_{pl}$ and $[(V_{dat})_{slide}]_{pl}$ and the shear load at the datum point to cause debonding $[(V_{dat})_{crit}]_{pl}$. If the capacity $[(V_{dat})_{crit}]_{pl} = (V_{dat})_{strength}$ is smaller than the design shear load at the datum point $(V_{dat})_{applied}$ in Fig. 5.10(a), then the plate will debond before the design load is reached. In which case, another arrangement of adhesively bonded plates needs to be tried or another technique such as bolting.
- If the capacity $[(V_{dat})_{crit}]_{pl}$ is sufficient to resist the applied $(V_{dat})_{applied}$, then CDC debonding can be prevented. The plates will have to be extended beyond the point where they intercept the diagonal crack at positions B in Fig. 5.10(c) in order to fully anchor the plate to comply with the initial assumption in the analysis. The plates will have to be extended by at least an effective length L_e as in Fig. 5.10(e) and it is suggested that it is extended by a length $L_e + h/2$ to points C, to allow for the fact that the diagonal crack is not a straight line but tends to curve.
- The strength along the partially anchored region B-C in Fig. 5.10(c), follows the path of the shear load to cause cracking $[(V_{dat})_{crack}]_{pl}$ in Fig. 5.10(d), from point L to point K which is just before the plate end. The strength along the plate L-K is always greater than at L so the anchorage length will not debond prematurely.
- Just beyond the plate end, the strength reduces to that of the unplated beam at point P which will be less than the capacity of the plated beam at L. This means that a critical diagonal crack will first form in the unplated region.
- For beams and slabs with stirrups, the formation of a critical diagonal crack at P, prior to a critical diagonal crack forming within the plated region at the shear load $[(V_{dat})_{crit}]_{pl}$ at L, will not cause failure if the shear capacity of the unplated beam or slab, V_c+V_s, is not exceeded by $[(V_{dat})_{crit}]_{pl}$. Furthermore, a critical diagonal crack in the unplated region will not cause CDC debonding in the plated region.
- For slabs and beams without stirrups, the critical diagonal crack just beyond the plate end will cause failure at a shear $(V_{dat})_{strength\text{-}P}$ at P in Fig. 5.10(d). If the shear capacity $(V_{dat})_{strength\text{-}P}$ is not sufficient to resist the design shear load at the datum point $(V_{dat})_{applied}$, then it may be worth considering extending the plate to D in Fig. 5.10(f) such that the shear load at the datum point to cause cracking just beyond the plate end at M in Fig. 5.10(d) is the same as that required to cause crack sliding within the plated region at L. The extent of plating is given by Fig. 5.10(f)

where it is shown that there is no need for an anchorage length L_e as debonding from B to D is governed by the load to cause cracking $[(V_{dat})_{crack}]_{pl}$ although it is suggested to extend the plate by h/2.

5.3.3 Shear capacity V_{conc} to cause CDC debonding

The analyses in Sections 5.3.1 and 5.3.2 have dealt with the shear load at the datum point V_{dat} to cause failure at a position that is not at the datum point, and compared this with the design shear load at the datum point to see if failure would occur. It has not been necessary to determine directly the shear capacity of the structure nor relate this to the shear capacity from code requirements $(V_c)_{code}$. If this is the preferred approach, then the following design procedure continues from Section 5.3.1.

- The CDC analyses in Fig. 5.10(d) gives the shear load at the datum point to cause CDC debonding in the fully anchored plated section at point L, that is $[(V_{dat})_{crit}]_{pl}$, as well as the shear load at the datum point to cause crack sliding in the unplated beam at point N, that is $[(V_{dat})_{crit}]_{un}$.
- The increase in the concrete shear capacity due to plating is shown in Fig. 5.10(d) as $(\Delta V_{conc})_{pl}$ /$(1\pm K_W)$. Hence the increase in the concrete shear capacity due to plating $(\Delta V_{conc})_{pl}$ can be determined directly from the CDC analyses. The increase in the shear capacity $(\Delta V_{conc})_{pl}$ can than then be added to the national code value of the concrete shear capacity $(V_c)_{code}$ to get the concrete shear capacity of the plated region $(V_{conc})_{code}$. The concrete shear capacity $(V_{conc})_{code}$ is the shear load to cause CDC debonding in a plated beam.
- Let us consider terminating the plates at positions C in Fig. 5.10(c) so that it is fully anchored at the point B where the critical diagonal crack in the plated region will occur. This is shown in Fig. 5.10(e) where an additional length of plate h/2 has been added to allow for the fact that the diagonal cracks are not straight. In the plated region, the applied shear must be restricted to $(V_{conc})_{code}$. This even applies to the partially anchored region L_e+h/2 as the shear required to form a diagonal crack in this region lies on $[(V_{dat})_{crack}]_{pl}$ which has a higher capacity than at L and which does not require to be anchored as it is the shear load to cause cracking. The unplated region has a strength $V_s+(V_c)_{code}$.
- Let us now consider extending the plate to point M in Fig. 5.10(d), so that the shear load to cause crack sliding in the plated and unplated regions is the same. This is shown as the plate in Fig. 5.10(f). In this case there is no need for an anchorage length as the shear to cause cracking, $[(V_{dat})_{crack}]_{pl}$ in Fig.5.10(d), controls debonding at the plate end. The shear should be restricted $(V_{conc})_{code}$ in the plated region and $V_s+V_{c\text{-}code}$ in the unplated region.

5.3.4 Further extension of plate

So far the plate ends have been extended to positions D in Fig. 5.10(d) in Sections 5.3.2 and 5.3.3. This covers the hinge approach requirements for partially plated beams in Section 2.5.2. Continuing with the analysis in Sections 5.3.2 and 5.3.3.

- It may still be necessary to extend the plates further to position E in Fig. 5.10(c) in order to prevent plate end debonding and this is covered in Chapter 6.
- If the anchorage approach at Section 2.5.1 is being applied, the plate is automatically extended to a flexurally uncracked region, which can be assumed to be a point of contraflexure and then anchored by a length L_e+h/2 beyond the point of contraflexure as shown in Fig. 5.10(g).

- In which case, the shear force in the plated region which is the whole of the sagging region or hogging region must be restricted to $(V_{conc})_{code}$ from Section 5.3.3 or the shear load at the datum point $[(V_{dat})_{crit}]_{pl}$ from Section 5.3.2, depending on which analysis technique is being applied.
- In the hogging region shown in Fig. 5.1(b), the plate would be being extended into a reducing shear region and moment region as shown in Fig. 5.1(a). So that the plate end is being subject to less shear and curvature and therefore less likely to debond due to CDC or PE debonding. Hence the plate extension $L_e+h/2$ into the sagging region in Fig. 5.10(g) is unlikely to debond.
- However a plate in a sagging region in Fig. 5.1(a) would be being extended into a region of increasing shear so that it may not be possible to find an uncracked region to anchor the plates, that is the plate ends would be susceptible to CDC debonding. In which case a CDC analysis of the hogging region with the sagging plates extended into this region will have to be done to ensure that the plate ends do not debond. This is discussed further in Section 5.4.3.

5.4 Further plate combinations and positions

Plates can be attached to any surface of a beam or combinations of surfaces to enhance both the flexural and shear capacity of the beam. It will be shown that the generic CDC analyses described in Section 5.2 can cope with all combinations.

5.4.1 Angle and U-sections

Fibre reinforced polymer U-shaped plates, as in section A-A in Fig. 1.12, are often formed in the wet lay up process using bi-directional fibres in order to enhance both the flexural and shear capacities, as it is felt that the portion of the U-plate bonded to the tension face of the beam will be good at improving the flexural capacity whilst the portion of the U-plate bonded to the sides will be good at increasing the shear capacity as well as inhibiting the debonding of the tension face component.

As a further example of this form of construction, the beam in Fig. 5.11 was strengthened by adhesively bonding metal angle sections to both of the bottom corners. The angle plates were terminated close to the supports and eventually detached due to CDC debonding.

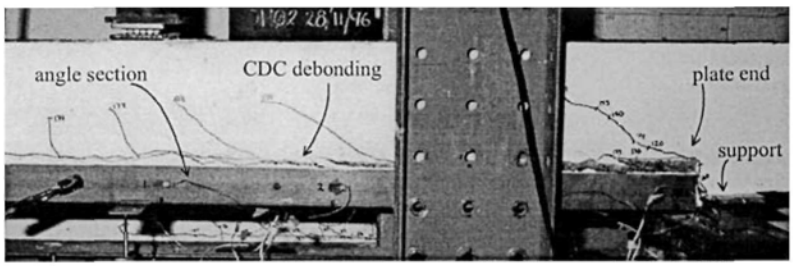

Figure 5.11 CDC debonding of angle section

The CDC analyses described in Section 5.2 can be applied directly to this form of construction by simply treating the portion of the plate bonded to the sides separately from those bonded to the tension face as illustrated in Figs 5.4 to 5.7.

5.4.2 Short side plates

Short longitudinal side plates can be adhesively bonded to the sides of beams above the plate end of a tension face plate as shown in Fig. 5.12. This combination of plates has been found to inhibit the debonding of the tension face plate due to plate end debonding, as the side plate reduces the curvature in the vicinity of the plate end of the tension face plate as will be explained in Chapter 6.

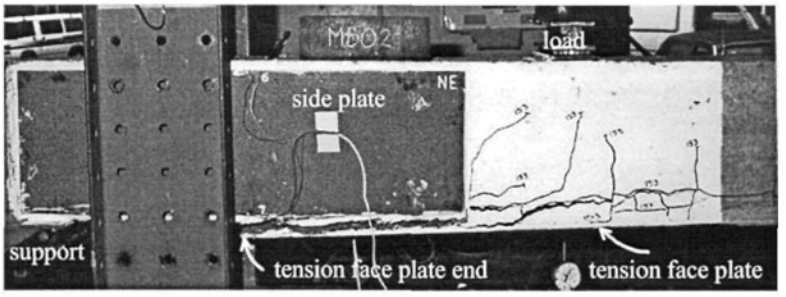

Figure 5.12 Short side plates with tension face plates

However, this combination of side plates and tension face plate also inhibits the CDC debonding in the vicinity of the tension face plate end as shown in Fig. 5.12. This may be useful in the anchorage approach for the design of longitudinal tension face plates, as the anchorage approach requires the tension face plate to be anchored in an uncracked region. As explained in Section 5.3.4, it may be difficult to find uncracked regions for sagging region plates, as extending the plates toward the points of contraflexure increases the vertical shear that the plate ends are subject to. Hence, it simply may not be possible to find an uncracked region as can be seen in Figs. 1.38 and 1.39. Plating the sides in the vicinity of the plate end may be sufficient to prevent diagonal cracks in this region and allow the tension face plate to be anchored in an uncracked region.

The CDC analyses described in Section 5.2 can also be applied directly to this form of construction. However care needs to be taken, particular in deriving the maximum axial force that the plate can resist P_{plate} in the crack sliding analysis in Section 5.2.1.2. Take for example the side and tension face plated CDC free body in Fig. 5.13 for a sagging region. The resultant axial force in the plate will be the smaller of the maximum axial force on the left of the diagonal crack $(P_{plate})_{left}$, which depends on the anchorage length to the right of the diagonal crack, and that to the right of the diagonal crack. A simple solution would be to slice the plate into narrow horizontal strips and sum the individual strengths which depend on their individual anchorage lengths based on the crack inclination. It may also be worth noting that the position of the plate relative to the diagonal crack is important; for example in Fig.5.13, the upper part of the plate does not intercept the diagonal crack and, therefore, this part of the plate is ineffective.

5.4.3 Compression face plates

Extending the tension face plate in the hogging region, such as in Fig. 4.17(b), into the compression face of the sagging region can increase the resistance to the formation of the critical diagonal crack. The free body for the CDC analysis is shown in Fig. 5.14. The shear load at the datum point to cause cracking $[(V_{dat})_{crack}]_{pl}$ is unaffected by the compression face plate as the plate intercepts the diagonal crack at the focal point.

However, the compression face plate does contribute to the shear load to cause crack sliding as the plate provides an additional force $(P_{plate})_{cfp}$ across the diagonal crack. Hence extending the tension face plate, in the hogging region in Fig. 4.17(b), into the compression face of the sagging region will help prevent CDC debonding of the tension face in the sagging region, which may be useful in applying the anchorage approach to the sagging region where the plate has to be terminated in an uncracked region.

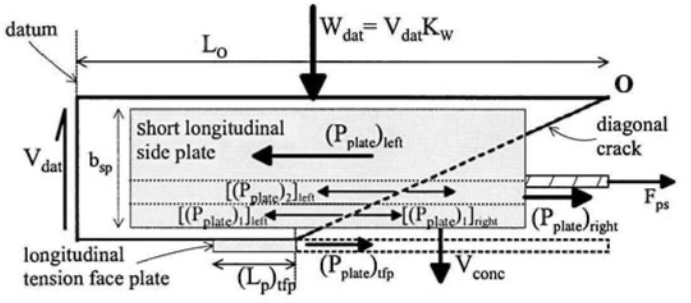

Figure 5.13 Short side plates with tension face plates in sagging region

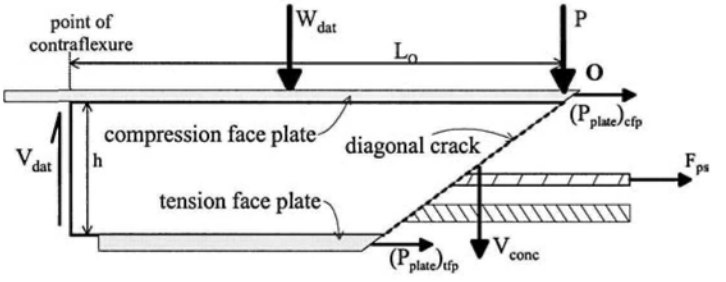

Figure 5.14 CDC analysis of compression face plate in sagging region

An example of a compression face plated beam test is shown in Fig. 5.15 where it can be seen that the compression face plate has debonded in the vicinity of the applied load but still remains intact over the support.

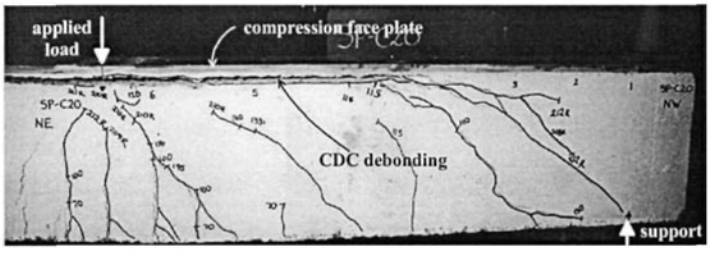

Figure 5.15 CDC of compression face plate

Extending the tension face plate in the sagging region in Fig. 4.17(b) into the compression face of the hogging region will have little effect on the CDC debonding of the tension face plate in the hogging region. This is because a compression face plate in the hogging region will not intercept a diagonal crack emanating from a support, unless of course the plate is placed over the support which is probably not possible in most cases.

5.5 Enhancement of shear capacity

This book is mainly concerned with the use of longitudinal plates to increase the flexural and shear capacities of reinforced concrete beams and slabs. The ability of longitudinal plates to increase the shear capacity as measured in tests is first illustrated in the following section, after which the interaction between the vertical shear enhancement of longitudinal plates and transverse plates is discussed.

5.5.1 Increase in shear capacity attained by longitudinal plating

Longitudinal plates can increase the concrete component of the shear capacity substantially. To illustrate the magnitude of the increase that can be obtained, a series of beams were cast with identical size, longitudinal reinforcement and concrete, and tested under identical loading conditions, so that any variations in strength were due to the externally bonded plates.

An unplated beam without stirrups was tested to determine the concrete shear capacity of the unplated beam, $(V_{conc})_{un}$, directly; this is the shear capacity given in codes $(V_c)_{code}$. The tested beam is shown in Fig. 5.16 and failed at a shear load of 81 kN due to crack sliding along the critical diagonal crack. This test will be used as our reference strength for comparison with the plated beams.

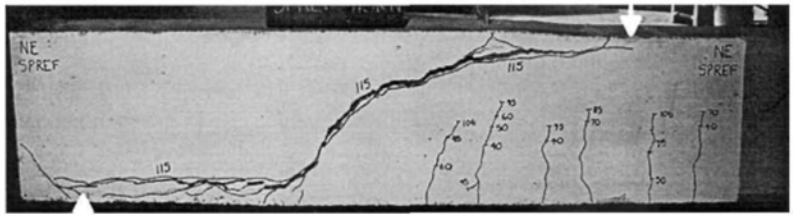

Figure 5.16 Reference beam unplated without stirrups: $(V_{conc})_{un}$ = 81 kN

The same beam as in Fig. 5.16 was fully plated along the tension face as in Fig. 5.17. The tension face plate was stopped just short of the supports and the beam failed in shear and debonded due to crack sliding at 140 kN, which is a 73% increase over that of the unplated beam. This is a very important finding as the increase in the shear capacity due to plating is normally associated with transverse or vertical plates which are often assumed to act like stirrups to increase the shear capacity. It can be seen that longitudinal adhesively bonded tension face plates can significantly increase the concrete component of the shear capacity.

Let us consider the implications of this increase in the concrete shear capacity. Most reinforced concrete slabs are designed without stirrups so that their shear capacity is limited by the concrete component of the shear capacity $(V_c)_{code}$. When the flexural capacity of an RC slab is increased using longitudinal tension face plates,

then the concrete shear capacity is also increased so that there is a good chance that the vertical shear capacity will not limit the flexural strengthening.

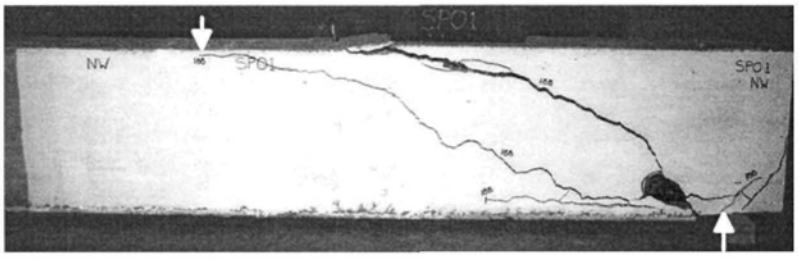

Figure 5.17 Tension face plate without stirrups: $(V_{conc})_{tfp}$ = 140 kN (73% increase)

The reinforced concrete beam in Fig. 5.18 is plated on both sides of the beam with side plates that extended from one support to the other, that is the beam is fully plated but not fully anchored. The beam did not have internal stirrups and failed by shear failure and CDC debonding due to crack sliding when a critical diagonal crack occurred at 156 kN which is a 93% increase in the shear capacity over that of the unplated beam. Hence longitudinal side plates can also substantially increase the concrete shear capacity.

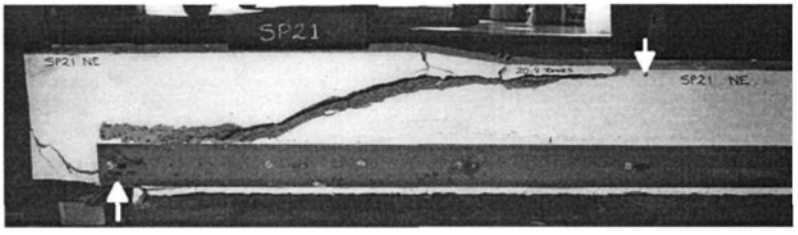

Figure 5.18 Side plates without stirrups: $(V_{conc})_{sp}$ = 156 kN (93% increase)

The plated beam in Fig. 5.19 is exactly the same as in Fig. 5.18, except that the beam has stirrups. In this test, CDC debonding occurred due to crack sliding at 162 kN but the beam did not fail in shear due to the stirrups. The shear load at crack sliding has increased by 100% over that of the unplated beam. But of much greater significance is the fact the shear load at crack sliding in the beam without stirrups in Fig. 5.18 is almost the same as that in the beam with stirrups in Fig. 5.19. This is just one of numerous tests that have shown that the presence of stirrups does not affect CDC debonding, as the plate debonds before the stirrups can be stretched to resist shear.

The findings from the tests in Figs. 5.18 and 5.19 have two important implications in the plating of continuous beams. Consider the continuous beam in Fig. 4.17. Prior to plating, let us assume that the maximum applied shear at the supports in Fig. 4.17(a) is significantly greater than the concrete shear capacity $(V_c)_{code}$ of the unplated beam, hence, stirrups are required to resist the vertical shear, that is the maximum applied shear in Fig. 4.17(a) requires a shear resistance of $(V_c)_{code}+V_s$. Even if the addition of longitudinal plates in the hogging region doubles the shear to cause crack sliding to $(V_{conc})_{pl}$, there is a good chance that $(V_{conc})_{pl} < (V_c)_{code}+V_s$ so that a critical diagonal crack will occur in the hogging region causing debonding

before the design shear is reached. Hence there is a good chance that CDC debonding will prevent the hogging regions of a beam from being plated using adhesively bonded plates, in which case bolting may have to be considered. In contrast, the sagging region in Fig. 4.17(a) is subjected to substantially less shear than in the hogging region, so that there is a good chance that $(V_{conc})_{pl}$ will be greater than the applied shear in this region so that adhesively bonded plates could be used in the sagging region. It can be seen that CDC debonding may restrict the use of adhesively bonded plates in some regions of a beam.

Figure 5.19 Side plates with stirrups: $(V_{conc})_{sp}$ = 162 kN (100% increase)

In the plated beam in Fig. 5.18, the side plate is placed as close to the tension face as possible and this increased the shear capacity by 93%. The same beam was tested with the plate at mid-depth as shown in Fig. 5.20, and shear failure and CDC debonding occurred at an increase of 97%, that is at virtually the same load.

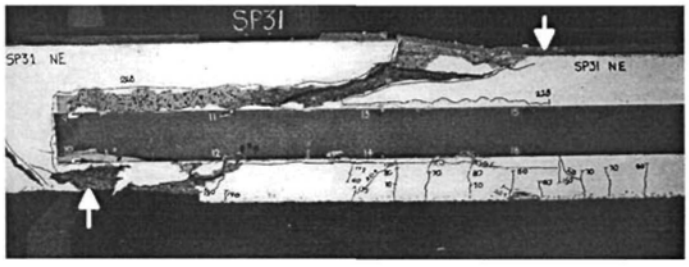

Figure 5.20 Side plates without stirrups: $(V_{conc})_{sp}$ = 160 kN (97% increase)

Placing the side plate next to the compression face in Fig. 5.21 increased the shear capacity and the resistance to crack sliding by 55% when the beam had nominal stirrups but by only 13% when there were no stirrups present. So it is recommended that side plates in the compression region of a beam be used only for beams with nominal stirrups which will rarely be a restriction as most beams have nominal stirrups. It can be seen that side plates at any level of the beam can substantially inhibit the formation of the critical diagonal crack and, hence, inhibit debonding.

5.5.2 Shear enhancement design philosophy

As described in Section 2.2.3, wherever a plate traverses an intermediate crack, as in Fig. 5.22, axial forces P_{plate} are induced in the plate which have an upper limit of the IC debonding resistance; this plate force may be reduced if the plate yields or fractures. These axial forces exist in longitudinal plates, shown in Fig. 5.22(a), whether the intermediate crack is induced by flexure or shear. These axial forces also exist in transverse plates, shown in Fig. 5.22(b), when the plates traverse a diagonal

crack. Hence the axial forces in both the longitudinal plates and transverse plates are induced by the IC debonding resistance as described in Chapter 2.

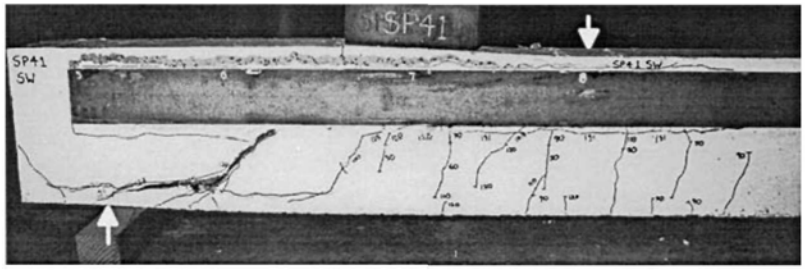

Figure 5.21 Side plates with nominal stirrups: $(V_{conc})_{sp}$ = 126 kN (55% increase)

The axial forces in the longitudinal and transverse plates in Fig. 5.22 help to increase the shear capacity of the beam, but they are considered to do so in different ways.

(a) Longitudinal plates – concrete component

As has been described in Sections 4.4.1.3 and 4.4.1.4, the longitudinal plates, as in Fig. 5.22(a), can be considered to solely increase the concrete shear capacity $(V_c)_{code}$ by acting as additional longitudinal reinforcing bars or as an additional prestressing force. Hence the longitudinal plates can be considered to enhance the concrete shear capacity as in the following equation.

$$(V_{conc})_{pl} = (V_c)_{code} + (\Delta V_{conc})_{pl} \qquad 5.19$$

Furthermore, tests have clearly shown that the concrete component $(V_{conc})_{pl}$ is not affected by internal steel stirrups as the plates debond as soon as $(V_{conc})_{pl}$ is achieved.

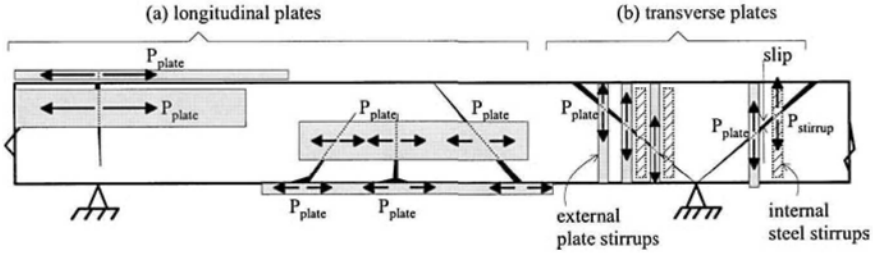

Figure 5.22 Axial forces in longitudinal and transverse plates

(b) Transverse plates – stirrup component

Transverse plates which can be referred to as externally bonded stirrups, in Fig. 5.22(b), are often treated in the same way as internal steel stirrups. Their contribution to the vertical shear resistance $(V_{stirrup})_{transverse}$ is assumed to be simply the sum of the plate forces P_{plate} traversing the diagonal crack. Hence the maximum shear force that can be resisted by the internal stirrups V_s and the external bonded stirrups $(V_{stirrup})_{transverse}$ is given by

$$\left(V_{stirrups}\right)_{pl} = V_s + \left(V_{stirrup}\right)_{transverse} \qquad 5.20$$

However it is extremely important to realise that Eq. 5.20 is an upper bound to the strength. As shown in Fig. 2.16, the slip required for a reinforcing bar to achieve its maximum bond stress, and hence the maximum force in the bar, is an order of magnitude greater than the slip required for the externally bonded plates to reach their maximum bond stress, and hence the maximum force in the plate. Therefore, as the diagonal crack in Fig. 5.22(b) starts to open up, the crack width being half the slip, the plates will reach their maximum force P_{IC} well before the internal stirrups yield. This applies in particular to transverse plates that are not anchored. Whereas, anchored and thin wet lay up plates may fail by rupture having allowed the steel stirrups to yield. As can be seen in Fig. 2.16, beyond the slip at which the plates achieve their maximum strength, the bond capacity of the plate reduces very rapidly. Hence, it is very unlikely that the maximum force in the external plate will be achieved at the same time or displacement as the maximum force in the steel stirrups. Consequently, it is not recommended to use Eq. 5.20 which should be viewed with extreme caution. A safe design would be to rely solely on $(V_{stirrup})_{transverse}$.

5.6 Analysis

The following results were from an iterative CDC analysis as described in Section 5.2 and which used the hinge approach described in Section 5.3. Full and comprehensive worked examples are given in Chapter 7.

5.6.1 Hinge approach with full depth steel plates in sagging region of beam

The reinforced concrete beam in Section 3.5.2.1 and Fig. 3.41 has already been strengthened in the sagging region with 3 mm thick steel plates over the full depth of the web. The plate increased the flexural capacity from 173 kNm to 277 kNm. The plate has been designed using the hinge approach, Section 5.2, so that it can be terminated short of the point of contraflexure. To maintain an elastic moment distribution, the hogging region was also strengthened as described in Section 4.6.1 and the total applied load can increase by 30% to 54 kN/m. The shear and moment distributions for the beam are the same as those shown in Fig. 4.23 where it can be determined that the applied shear force $V_{applied}$ = 156 kN at the point of contraflexure. From the Australian concrete code AS3600 (1994), $(V_c)_{code}$ = 104 kN in the sagging region, which is less than $V_{applied}$ hence, a CDC will occur in the unplated beam and therefore the plates are also required to increase the concrete component of the shear capacity V_c. The questions are: where to terminate the plate so that the critical diagonal crack falls within the plated region; and whether the increase in the concrete component of the shear capacity is sufficient to prevent CDC debonding within the sagging region.

The free body shown in Fig. 5.8(f_2) will be used in the CDC analysis to allow for the possibility that the CDC may straddle the point of contraflexure because we are dealing with a uniformly distributed load (udl) in the sagging region and hence, the position of the focal point O to give the *minimum* CDC is not known. The datum point was chosen 1000 mm from the point of contraflexure so that it is within the hogging region of the beam. Therefore M_{dat} = 183 kNm and V_{dat} = 210 kN so that the

factor K_M = 871 mm and, as in the example in Section 4.6.2 and Fig. 4.26, K_W varies with L_O.

The CDC analysis using the hinge approach begins by assuming that the beam is fully plated and fully anchored along the sagging region, that is the plate extends at least the effective length L_e (Eq. 2.3) beyond the root of any diagonal crack so that the maximum plate force P_{plate} can be assumed to be constant along the region. As discussed in Section 2.4.4, a 3 mm thick 300 MPa steel plate will yield prior to IC debonding hence the maximum force in the plate is governed by yielding so that P_{plate} = 666 kN. Using a spreadsheet analysis, the curve $(V_{dat})_{c\text{-}plate}$ in Fig. 5.23 is produced for the fully plated beam by equating the load to cause cracking (Eq. 5.1) and the load to cause crack sliding (Eq. 5.5) for increasing z from the point of contraflexure, using the procedure illustrated in Fig. 4.26 and where z is also defined. $(V_{dat})_{c\text{-}plate}$ in Fig. 5.23 is compared with V_{dat} = 210 kN, where it can be seen that the shear force at the datum point required to cause CDC debonding anywhere within the sagging region is greater than the applied shear force at the datum point. Hence, CDC debonding will not occur. This is further illustrated in Fig. 5.23 by comparing the concrete shear capacity of the plated beam $(V_{conc})_{pl}$, determined from Eq. 5.9, which always exceeds the maximum applied shear force at the focal point given by $(V_{max})_{Lo}$.

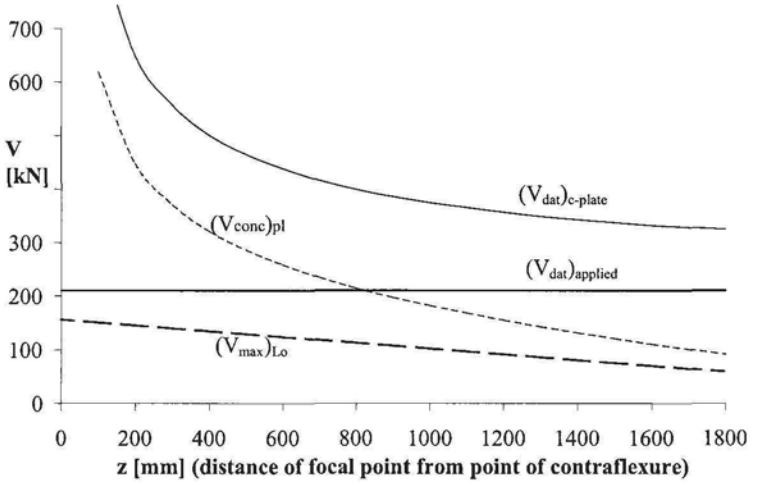

Figure 5.23 CDC analysis of steel side plated beam

Figure 5.24 shows $(V_{conc})_{pl}$ from Fig. 5.23 and the concrete shear capacity of the original unplated beam $(V_{conc})_{un}$, which was determined using the same iterative CDC analysis procedure. It is interesting to note that $(V_{conc})_{un}$ exceeds $(V_{max})_{Lo}$ everywhere along the sagging region suggesting that a CDC will not occur in the unplated beam and therefore the plates are not required to increase the concrete component of the shear capacity V_c as originally indicated when compared with $(V_c)_{code}$. The difference between $(V_{conc})_{pl}$ and $(V_{conc})_{un}$ is shown as $(\Delta V_{conc})_{pl}$ in Fig. 5.24 and represents the increase in shear capacity due to plating using the CDC analysis as defined in Eq. 5.11. From Eq. 5.12, adding the AS3600 concrete code strength $(V_c)_{code}$ to $(\Delta V_{conc})_{pl}$ gives the concrete component of the shear capacity of the plated beam $(V_{conc})_{code}$ in Fig. 5.24, which as already concluded, demonstrates that CDC debonding will not occur in the plated section as it exceeds $(V_{max})_{Lo}$ everywhere.

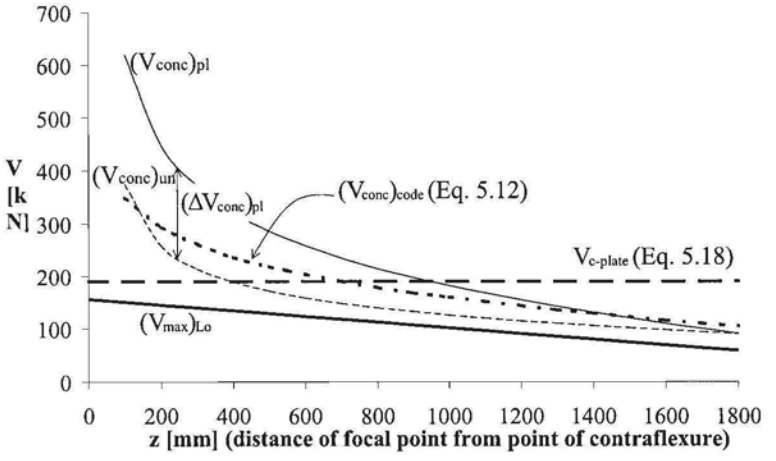

Figure 5.24 Comparison with prestress code approach

The analysis using the direct *passive prestress approach* is also shown in Fig. 5.24. Using P_{plate} = 666 kN, the increase in the concrete component of the shear capacity due to plating is 86 kN from Eq. 5.17, which is an 82% increase and from Eq. 5.18, the shear load to cause CDC debonding $V_{c\text{-}plate}$ = 190 kN. As $V_{c\text{-}plate}$ is greater than the applied shear force at the point of contraflexure, that is $(V_{max})_{Lo}$ = 156 kN at z = 0, this analysis confirms once again that CDC debonding will not occur.

5.7 References

Please note that as the generic design equations developed in this chapter are based on the fundamental principles described in Chapter 4; the references in Chapter 4 are also directly applicable to this chapter.

Eurocode 2: "Design of concrete structures Part 1: General rules and rules for buildings (1992)". BSI Standards.

AS 3600 – 1994. "Australian Standard Concrete Structures.". Standards Australia.

Chapter 6: Plate End (PE) Debonding

6.1 Introduction

The plate was first designed, in Chapters 2 and 3, for IC debonding due to the axial strains induced in the plate by flexure at the position of maximum moment. The plate was then extended, in Chapters 4 and 5, beyond the position of maximum moment to encompass the rigid body shear deformation that induces CDC debonding. It is now necessary to ensure that the end of the plate does not debond prematurely due to the curvature in the vicinity of the plate end, which is referred to as plate end (PE) debonding. This is the final stage of the design procedure for plating. Unlike IC debonding and CDC debonding, PE debonding will rarely, if ever, prevent plating, as this form of debonding can be easily prevented by terminating the plate at a point of contraflexure. After completion of the check for PE debonding, the three major debonding mechanisms due to axial strains in the plate, due to shear deformations in the beam and due to curvature in the beam have been designed for. Theoretically, it should now be necessary to check for interface shear stress ((VAy)Ib) debonding as described in Section 1.3.4, which tests have shown rarely occurs.

The plate end debonding mechanism is first described in this chapter, followed by generic analysis procedures that cover all forms of plating and combinations of plates. The PE debonding analysis is then placed in context with the CDC and IC debonding analyses in a design procedure where the interaction between these debonding mechanisms is also discussed. The chapter is completed with design examples to illustrate the circumstances in which PE debonding may affect the extent of plating.

6.2 PE debonding mechanism

6.2.1 PE debonding mechanism

The plate end (PE) debonding mechanism was explained in Section 1.3.3. As can be seen in Fig. 1.20, when curvature is applied to the beam, the plate tries to stay straight which can cause debonding from the plate end inwards. The PE debonding crack propagation is in the opposite direction to IC debonding where the debonding cracks propagate outwards towards the plate ends, as can be seen in Figs. 1.14 and 2.20, and it is also in the opposite direction to CDC debonding where the debonding cracks propagate outwards to the plate ends but spread inwards as in Fig. 4.4. It is also worth noting that the IC and CDC debonding resistances are associated with regions of the beam that are subjected to ultimate failure of the beam, that is flexural and shear failure, which require the sections to behave in a non-linear fashion. In contrast, PE debonding is associated with those regions of the beam where the flexural forces are small and where a critical diagonal crack has not occurred, so that the section at which PE debonding occurs can be assumed to behave in a linear fashion, that is linear elastic sectional analyses can be used albeit that the concrete has cracked in tension.

Whether the plate is on the side of the beam, as in Fig. 6.1(a), or on the tension face of the beam, the mechanism of debonding is the same. The beam in Fig. 6.1(a) is subject to a constant moment, M_{beam}, and the plate is terminated within the constant moment region.

6.2.1.1 Tension face plates

Let us first consider the tension face plate of the beam in Fig. 6.1(a). The curvature in the composite plated beam χ induces the same curvature in the plate χ and an axial strain in the plate $\varepsilon_{tfp} = \chi d_{tfp}$, where d_{tfp} is the distance between the neutral axis of the composite plated section and the centroid of the plate, as shown in Fig. 6.1(a). Hence, the tension face plate is subject to an axial force P_{tfp} due ε_{tfp} and a moment M_{tfp} due to χ. Another way of visualising the problem is that the stress resultants P_{tfp} and M_{tfp} have to be applied to the ends of the initially straight tension face plate, in Fig. 6.1(b), to achieve the same deformation as in the tension face plate in Fig. 6.1(a). These stress resultants, P_{tfp} and M_{tfp}, have to be transferred across the plate-beam interface, and this is done through the interface shear stresses τ and normal stresses σ_n, that is perpendicular to the plate/concrete interface, which are shown at position *C* in Fig. 6.1(a) and also shown enlarged in Fig. 6.1(d).

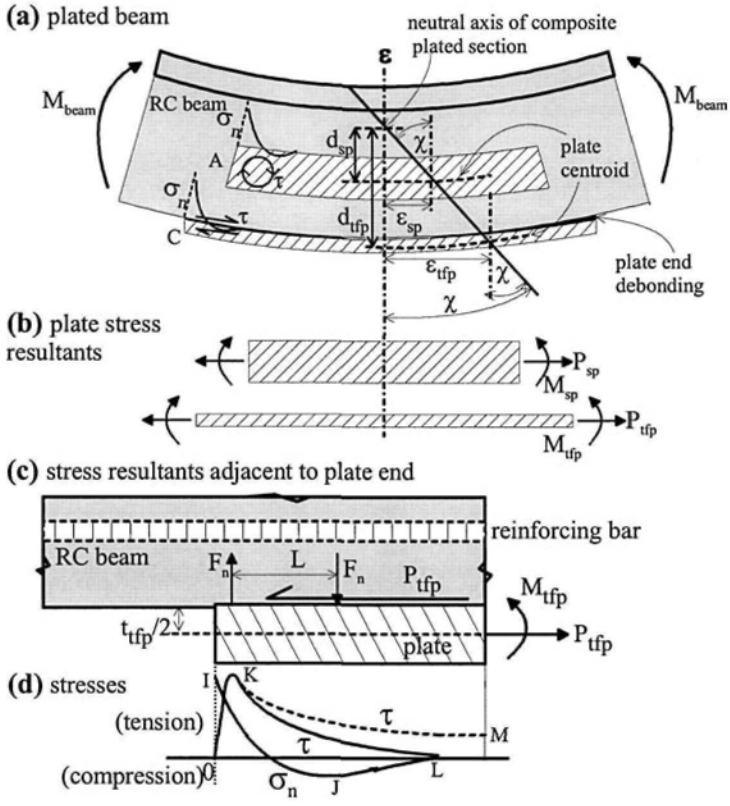

Figure 6.1 Plate end debonding mechanism

The forces acting on a free body of the plate that is near the plate end are shown in Fig. 6.1(c). The axial force in the plate P_{tfp} requires an interface shear force of the same magnitude to maintain equilibrium, as shown. Furthermore, the moment acting on the plate $M_{tfp} + P_{tfp}t_{tfp}/2$ requires a counter moment due to the normal

interface forces F_n of F_nL, as shown. The shear force P_{tfp} on the interface induces the shear stress τ distribution O-K-L in Fig. 6.1(d) which must be zero at the plate end, due to the free surface, and zero at L, because the plate is in a constant moment region. If the plated beam was in a region of varying moment, then the shear stress distribution would be O-K-M, where M is given by the interface shear stress VAy/Ib discussed in Section 1.3.4. The moment $F_nL = M_{tfp} + P_{tfp}t_{tfp}/2$, in Fig. 6.1(c), induces the normal stress distribution σ_n of I-J-L in Fig. 6.1(d), where the peak normal stress occurs at the plate end at I and which has a greater magnitude than the compressive normal stress at J. Finite element analyses of the constant moment region in Fig. 6.1(a) show that the interface stresses σ_n and τ in Fig. 6.1(d) are concentrated towards the plate ends and that the spread of the interface stresses O-L is a function of the plate thickness, for plated beams in which the plate thickness is much less than the beam depth, which is the usual case for tension face plates. It is the stresses at the plate end in Fig. 6.1(d) that induce PE debonding.

6.2.1.2 Compression face plates

For compression face plates, the stress distribution of the interface stresses for tension face plates in Fig. 6.1(d) applies, except that the signs of the stresses are reversed. In which case for compression face plates, the maximum normal tensile stress now occurs away from the plate end at J which is much smaller than the maximum normal compressive stress now at the plate end at I. Hence compression face plates are less likely to debond than tension face plates, but they can and do debond because tensile stresses do exist at J. It is also worth noting that analysing a compression face plate as if it were a tension face plate would give a safe design, although design rules are available for compression face plates.

6.2.1.3 Side plate with centroid in tensile zone

The same logic, as for tension face plates, can be applied to the side plate in Fig. 6.1(a). The curvature χ induces an axial force in the plate P_{sp} and a moment M_{sp}. The moment component M_{sp} is now resisted by interface shear stresses τ, as shown at position *A* in Fig. 6.1(a); this is in contrast to the moment component in the tension face plate which is resisted by normal stresses as shown at position *C*. The axial force in the side plate P_{sp} is resisted by interface normal stresses σ_n (that is in a direction perpendicular to the side-plate/concrete interface), at position *A* in Fig. 6.1(a), in the same way as the axial force in the tension face plate at position *C*, which is shown enlarged as I-J-L in Fig. 6.1(d). The interaction between the shear stress τ and the peak of the tensile normal stress σ_n near the plate end at position A determines when debonding occurs.

6.2.1.4 Side plate with centroid in compression zone

Let us consider what happens when the position of the side plate centroid, d_{sp} in Fig. 6.1(a), lies above the neutral axis of the composite plated member, that is in the compression zone. As the curvature is the same at all levels of the beam, the moment component is unchanged so the interface shear τ at position *A* in Fig. 6.1(a) remains unchanged. However, moving the plate centroid above the neutral axis of the composite plated beam causes the resultant axial force in the plate P_{sp} to change from being tensile to compressive, so that the peak stress at the plate end at I in Fig. 6.1(d) is now compressive but the relatively smaller stress at J is now tensile. This reduction

in the magnitude of the peak tensile stress is beneficial and will delay, that is inhibit, debonding but it may not prevent debonding.

It can be seen that a safe design would be to treat side plates with centroids in the compression zone as if they were in the tension zone. This is the recommendation in the following analyses for sections that are bonded to the sides of the beam, because the beneficial effect of having a plate with the centroid in the compression zone has as yet not been quantified. Under no circumstance can the sign of d_{sp} be made negative as this ignores the fact that there are tensile stresses at J which will reduce the resistance to plate end debonding.

6.2.2 Examples of PE debonding

In order to illustrate plate end (PE) debonding, the reinforced concrete beams in the following tests were plated within a constant moment region; the plate ends were terminated well within this constant moment region as shown in Fig. 6.2 for a tension face plated beam. This set up ensured that CDC debonding, Section 1.3.2, and interface shear stress (VAy/Ib) debonding, Section 1.3.4, did not occur, as the vertical shear was zero. Furthermore, IC debonding as in Section 1.3.1, did not occur as all the specimens debonded from the plate end inwards which is characteristic of PE debonding and in the opposite direction to that associated with IC debonding.

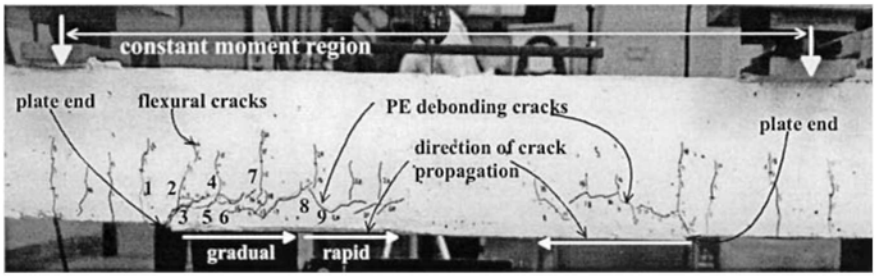

Figure 6.2 PE debonding of a tension face plate

6.2.2.1 Plates bonded to horizontal surfaces

In the tension face plated beam in Fig. 6.2, flexural cracks first formed adjacent to the plate ends such as that marked 1. These flexural cracks increased the local curvature near the plate ends and simultaneously induced the flexural crack marked 2 and a short horizontal crack marked 3. The horizontal debonding crack 3 is at the level of the tension reinforcing bars, and slowly propagated inwards as the applied load was increased. The horizontal debonding crack, or peeling crack, was preceded by flexural cracks. For example, when the debonding crack reached position 3, the flexural crack at 4 formed which increased the curvature locally and allowed the horizontal crack to propagate to 5 and 6, after which the flexural crack at 7 formed. The crack gradually propagated to position marked 8. After which from position 9 onwards, there was a very rapid crack propagation at the same load which caused the strains in the plate at mid-span to reduce even under increasing applied load. Plate end debonding is characteristically a gradual failure; the moment to cause the first horizontal crack at 3 to form being about half of that to cause the rapid crack propagation at 9, so that there is plenty of prior warning.

For tension face plated beams, the PE debonding crack invariably occurs at the level of the longitudinal tension reinforcing bars which is at the same level as in CDC

debonding in Fig. 4.4. This is in contrast to IC debonding which occurs in the concrete adjacent to the plate as in Fig. 2.3. Research on PE debonding has found that the scatter of results for tension face plates is much greater than that associated with side plates, and it is felt that it is the influence of the tension reinforcing bars which is causing this increase in scatter.

Extending the tension face plate, as in the left hogging region in Fig. 4.17(b), into the compression face does not necessarily prevent PE debonding, as can be seen in Fig. 6.3 where the compression face plate has debonded. In contrast to the tension face plate in Fig. 6.2 where the debonding crack starts at the plate end, the debonding crack in the compression face plate started away from the plate end as shown in Fig. 6.3. This was to be expected, as discussed in Section 6.2.1.2 for compression face plates, as the peak tensile normal stress, that is the stress perpendicular to the plate/concrete interface, now occurs at J in Fig. 6.1(d). The debonding crack also occurred at a level adjacent to the plate as can be seen in Fig. 6.3 which can be compared to that of the tension face plate in Fig. 6.2 which shows that it is not influenced by any longitudinal compression reinforcement.

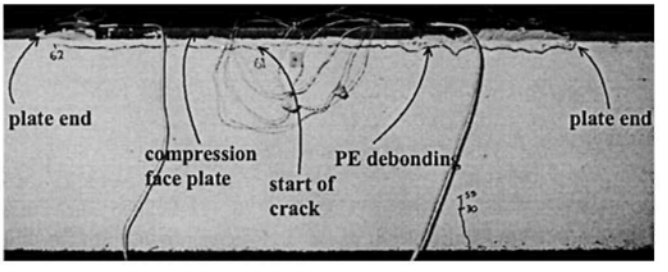

Figure 6.3 PE debonding of a compression face plate

The compression face plate in Fig. 6.3 has been removed in Fig. 6.4 to show the debonding failure surface in the concrete which is adjacent to the plate. This is typical of PE debonding failure surfaces in compression face plates as well as in side plates and in angle plates adhesively bonded to the sides, where it has been found that the scatter of results is much less than those associated with tension face plated specimens.

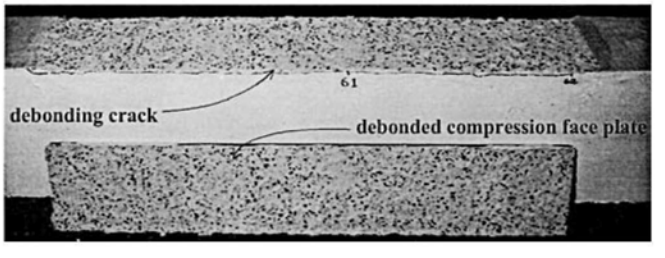

Figure 6.4 PE debonding adjacent to plate

6.2.2.2 Plates bonded to vertical surfaces

An example of plate end debonding in a side plated beam is shown in Fig. 1.21. In this beam, the depth of the plate was quite small compared to the depth of the beam, so that the plated beam can be considered to be a shallow plated beam with the side

plate in the tension zone. Even though the plates are on the sides, the sequence of crack propagation is the same as that described for the tension face plated beam in Fig. 6.2: the flexural crack marked 1 first formed which increased the local curvature; inducing the debonding crack at the plate end which gradually propagated along both the top and bottom edges of the plate; being preceded by the flexural cracks; until there was rapid crack propagation at which the plate strains at mid-span, on the left strain gauge, reduced even with increasing applied load. It can be seen that some of the flexural cracks traverse the plate confirming that the side plate was bonded to the tension zone of the beam.

In contrast to the shallow side plated beam in Fig. 1.21, Fig. 6.5 shows a deep side plated beam. It can be seen in Fig. 6.5, that the flexural cracks do not extend above the plate, in fact the flexural cracks to the side of the plate stop short of the top level of the plate, so that the top of the plate is in the compression zone of the plated beam. However, the same PE debonding sequence of crack propagation has occurred, with the flexural cracks first forming adjacent to the plate end, followed by the debonding cracks around the edges of the plate. The debonding failure plane in both the shallow side plated beam in Fig. 1.21 and the deep plated beam in Fig. 6.5 was the same as that in the compression face plate in Fig. 6.4, that is in the concrete adjacent to the plate.

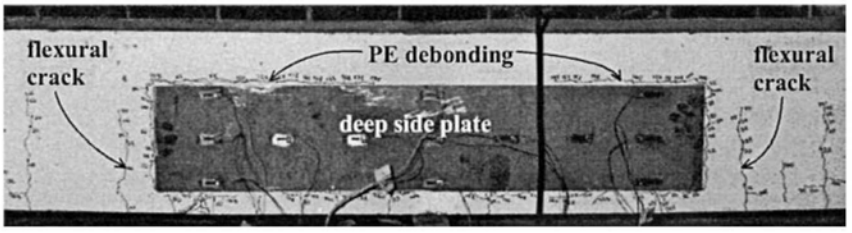

Figure 6.5 PE debonding in deep side plated beam

Finally in Fig. 6.6 is an example of an angle section in which the web has been adhesively bonded to the side of the beam and the flange has been adhesively bonded to the tension face of the beam. Once again, the sequence of PE debonding crack propagation was the same as previously described. However, the analysis of the test results showed that the flange first debonded from the tension face at an early stage of loading after which the web remained bonded to the side and hence the angle section acted as a side plate.

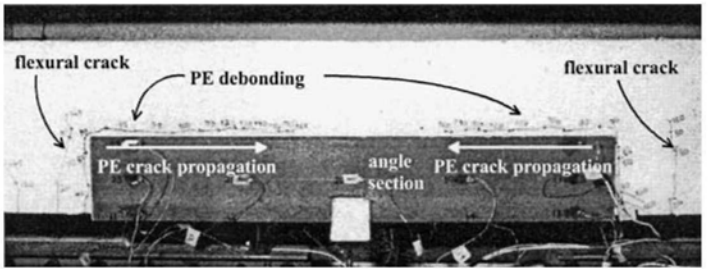

Figure 6.6 PE debonding in angle plated beam

6.3 Generic PE debonding analysis

6.3.1 PE debonding curvature capacity

It was explained in Section 6.2.1 and illustrated in Fig. 6.1 that plate end debonding is a function of the curvature χ in the composite plated section. It is this curvature, which induces a moment in an individual plate M_p and an axial force in the plate P_p that have to be resisted by the interface plate stresses, which can lead to PE debonding. The mathematical model for the curvature in a composite plated beam to cause plate end debonding in an individual plate χ_{PE} (Nguyen et al 1998) is given in the following generic form

$$\chi_{PE} = \frac{f_{cb}}{f(M_p) + f(P_p)} = \chi_{cap} \qquad 6.1$$

where: f_{cb} is the concrete splitting tensile strength, sometimes referred to as the Brazilian or indirect tensile strength, which can be assumed to be $0.53\sqrt{f_c}$ (N and mm) if not measured directly; the function $f(M_p)$ allows for the moment in the plate; and the function $f(P_p)$ for the axial force in the plate. It must be stressed that Eq. 6.1 applies to an individual plate at a cross-section, so that if there are multiple plates, as in Fig. 5.1, then each plate must be checked individually for PE debonding. Equation 6.1 is the curvature capacity χ_{cap} and it is derived from the geometric and material properties of the plated cross-section. For example, $f(M_p)$ depends on the flexural rigidity of the plate $(EI)_p$, and $f(P_p)$ depends on the axial rigidity $(EA)_p$ as well as the distance of the plate centroid from the neutral axis of the composite plated member d_p, such as d_{sp} and d_{tfp} in Fig. 6.1(a).

6.3.2 Plate end applied curvature

It is the applied curvature at the plate end and, hence, the moment at the plate end that determines whether plate end debonding occurs. Furthermore, it is the additional curvature applied after plating at the plate end, χ_{add}, that induces PE debonding. The curvature that is applied after a beam has been plated can be considered to consist of the following components.

$$\chi_{short} + \chi_{creep} + \chi_{shrink} = \chi_{add} \qquad 6.2$$

where χ_{short}, χ_{creep} and χ_{shrink} are the curvatures applied at the plate end after plating due to short term loads, concrete creep due to long term loads and concrete shrinkage. It must be emphasised that tests have shown that it is the additional curvature at the plate end after plating that induces PE debonding, and any existing curvature prior to plating does not affect PE debonding. This is because plates tend to stay straight when adhesively bonded to a curved surface with the glue thickness allowing for the difference in shape, so that M_{sp} and M_{tfp} in Fig 6.1(b) tend to zero. Furthermore, the axial component P_{sp} and P_{tfp} in Fig. 6.1(b) will certainly be zero on adhesive bonding the plate to a beam already loaded, as the plate is not stretched longitudinally prior to adhesive bonding so that P_{sp} and P_{tfp} are zero on adhesive bonding. Hence it is the additional curvature after plating that induces PE debonding.

The procedures in national standards for determining the shrinkage curvature for deriving the shrinkage deflection can be used to determine χ_{shrink} in Eq. 6.2. The

following equation is typical of equations available in national standards for determining the shrinkage curvature.

$$(\chi_{shrink})_{code} = \frac{1.15\varepsilon_{sh}}{d}\left(1 - \frac{A_{sc}}{A_{st}}\right) \qquad 6.3$$

where: ε_{sh} is the shrinkage strain in the concrete which for the PE debonding analysis would be the increase in the concrete shrinkage strain after plating; d is the effective depth of the RC member; A_{sc} is the cross-sectional area of the compression reinforcing bars which for the PE analysis would include the area of any plates in the compression zone of equivalent stiffness, that is A_pE_p/E_s, as the A_{sc} term in Eq. 6.3 provides a stiffness restraint against the shrinkage deformations; and where A_{st} is the cross-sectional area of the tension reinforcing bars plus an equivalent area for plates in the tension zone for the PE debonding analysis. Often, structures are retrofitted by plating well after the concrete has stopped shrinking in which case this term tends to zero.

The short term curvature χ_{short} is simply given by $\chi_{short} = M_{short}/(EI)_{short}$, where M_{short} is the moment at the plate end due to short term loadings such as live loads. The flexural rigidity $(EI)_{short}$ is the short term flexural rigidity of the cracked plated section which is derived using the short term modulus of elasticity of the concrete for $(E_c)_{short}$ and assuming in the derivation that the tensile strength of the concrete is zero. Similarly, the curvature due to creep is given by $\chi_{creep} = M_{crcep}/(EI)_{creep}$, where M_{creep} is usually the moment due to long term loads such as dead loads and sustained live loads, and $(EI)_{creep}$ is the long term flexural rigidity of the cracked plated section where the long term Young's modulus of the concrete $(E_c)_{long}$ should be used. It needs to be noted that only the creep expected after the beam is plated needs to be considered. Furthermore, as plating is required to strengthen/stiffen the structure, most likely the dead load or sustained live load would have increased which will result in additional creep.

The standard elementary analysis to determine the flexural rigidity of a cracked plated section is illustrated in Fig. 6.7, just to emphasise to the reader the importance of using the cracked sectional flexural rigidity in determining the curvatures. The plated cross-section in Fig. 6.7(a) has been transformed into a cracked concrete section in Fig. 6.7(b) in which the tensile strength of the concrete in flexure is assumed to be zero, where $m_{p1} = E_{p1}/E_c$, $m_{p2} = E_{p2}/E_c$, and $m_s = E_s/E_c$, and where the Young's modulus of the concrete E_c is either the short term material stiffness or the long term material stiffness that allows for creep. The depth of the neutral axis d_{na} in Fig. 6.7(b) can be found by equating the first moment of area about the neutral axis for elements on either side of the neutral axis, and then the second moment of area about the neutral axis I can be obtained from the parallel axis theorem.

6.3.3 Plate end debonding design

6.3.3.1 PE curvature capacity and applied curvature

The aim of the design is to ensure that the additional curvature, χ_{add} in Eq. 6.2, is always less than curvature capacity, χ_{cap} in Eq. 6.1, that is

$$\chi_{short} + \chi_{creep} + \chi_{shrink} \le \frac{f_{cb}}{f(M_p) + f(P_p)} \qquad 6.4$$

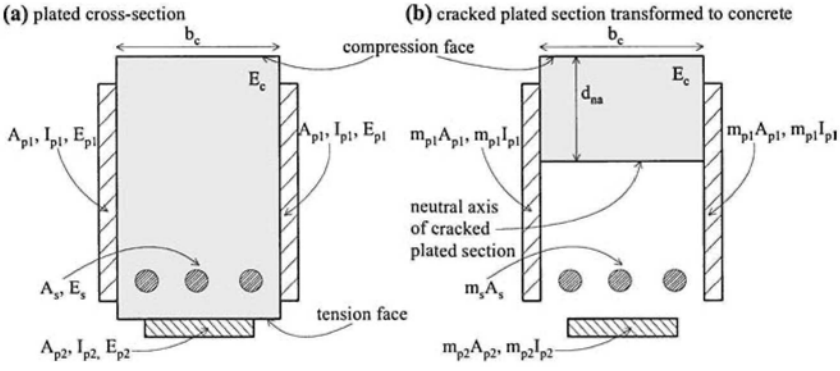

Figure 6.7 Cracked plated section

If an RC structure is plated soon after it has been built so that creep and shrinkage will be significant after plating, then it will be necessary to ensure that at the plate end

$$\frac{M_{short}}{(EI)_{short}} + \frac{M_{creep}}{(EI)_{creep}} \leq \frac{f_{cb}}{f(M_p) + f(P_p)} - \chi_{shrink} \qquad 6.5$$

It is then a question of terminating the plate at a position along the beam where the increase in the moment due to the live load M_{short} plus that due to dead load and sustained live load if applicable M_{creep} is less than the curvature capacity reduced by shrinkage.

6.3.3.2 PE debonding design for short term loads

Let us consider an RC structure that is plated many years after it has been built so that any additional creep and shrinkage after plating can be assumed to be negligible. Let us also consider the case when the beam or slab is not propped prior to plating so that the unplated beam is resisting its dead load prior to plating, in which case the plated structure will only be resisting the live load. Under these circumstances, which are probably common, Eq. 6.5 becomes

$$\frac{M_{short}}{(EI)_{short}} \leq \frac{f_{cb}}{f(M_p) + f(P_p)} \qquad 6.6$$

It may be worth emphasising that the left had side of Eq. 6.6 deals with the cross-sectional properties of the whole plated beam whilst the right hand side deals with those of an individual plate. If the beam is propped prior to plating, which may be required if the structure is plated to reduce deflections or crack widths, then M_{short} in Eq. 6.6 will have to include the dead load as well as the live load or $M_{creep}/(EI)_{creep}$ included on the left hand side for the dead load if creep can still occur as in the following section. Either way this would mean extending the plate further. It is interesting to note that it was shown in Sections 3.4.1 and 3.4.2 that with regard to IC debonding it is better to plate an unpropped beam. The same conclusion has been

drawn for PE debonding. Hence wherever possible, unpropped beams or slabs should be plated.

For design purposes, Eq. 6.6 can be written in the following form which is applicable to structures in which creep and shrinkage do not occur after plating

$$M_{short} \le \frac{(EI)_{short} f_{cb}}{f(M_p) + f(P_p)} \qquad 6.7$$

so that the plate end is terminated in a region where the moment is less than that on the right hand side of Eq. 6.7. As an example, the design consists simply of extending the plate in Fig. 5.10(c) to a position where the applied moment in Fig. 5.10(a) is less than M_{short}, assuming that the moment in Fig. 5.10 is due to the live loads.

6.3.3.3 PE debonding design for long term effects

For structures in which creep and shrinkage occur after plating, Eq. 6.5 can be written in the following form for design

$$M_{short} \le (EI)_{short} \left(\frac{f_{cb}}{f(M_p) + f(P_p)} - \chi_{shrink} - \frac{M_{creep}}{(EI)_{creep}} \right) \qquad 6.8$$

Equations 6.7 and 6.8 should be applied to each individual plate to check for their individual resistance to debonding. It may be worth noting that the flexural rigidities $(EI)_{short}$ and $(EI)_{creep}$ are the flexural rigidities of the whole section as shown in Fig. 6.7(b) and, hence, in its calculation they should include all the plates at that section. However the remaining variables in Eqs. 6.7 and 6.8 relate to a single plate; even the tensile strength of the concrete f_{cb} is the tensile strength of the concrete adjacent to the plate being analysed and, hence, could be varied to allow for deterioration of the concrete in parts of the structure if so required. We are determining the moment at a section that will cause a specific plate to debond. Eventually, all plates will have to be checked for PE debonding.

6.4 PE analysis for bonded interface perpendicular to bending axis

Let us first consider plates that are adhesively bonded to a surface that is perpendicular to the axis of bending, such as the side plate at position A in Fig. 6.8. Tests on adhesively bonded angle sections, described in Section 6.2.2.2, have shown that the flange of the angle section that is bonded to the tension face debonds first leaving the angle attached to the beam through the web adhesively bonded to the side. Hence the angle section at position B in Fig. 6.8 is also an example of a plate bonded to an interface perpendicular to the bending axis.

The following PE debonding design rules are given in the form of Eq. 6.7. However if shrinkage and creep occur after plating, the following design rules will have to be adapted to the form shown in Eq. 6.8, where the curvature capacity is reduced by the shrinkage and creep curvature.

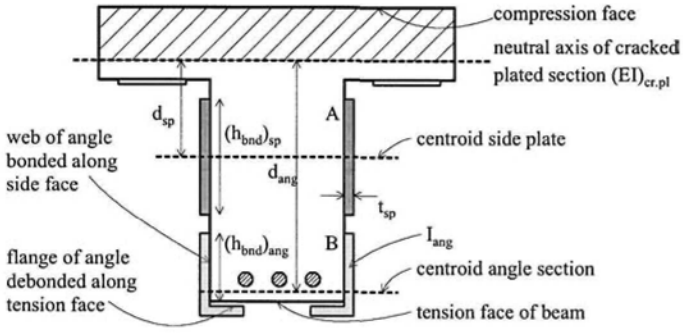

Figure 6.8 Plates bonded to the sides of beam in sagging region

6.4.1 Angle plates

The plate must be terminated at a section where the moment at the plate end is less than the PE debonding moment capacity $(M_{PE})_{ang.sp}$ (Nguyen et al 1998)given by the right hand side of Eq. 6.9

$$(M_{PE})_{ang.sp} = \frac{K(EI)_{cr.pl} f_{cb} (h_{bnd})_{ang}^3}{E_p \left(2.22 I_{ang} + 0.0185 |d_{ang}| (h_{bnd})_{ang}^3\right)} \qquad 6.9$$

where: K = 0.88 for the mean capacity and 0.40 for the 5% characteristic capacity which can be used for design; $(h_{bnd})_{ang}$ is the depth of the portion of the web of the angle adhesively bonded to the side of the beam as shown in Fig. 6.8; E_p is the Young's modulus of the plate and if it is an FRP plate, it is the Young's modulus in the longitudinal direction of the beam; I_{ang} is the second moment of area of the angle about the centroid of the angle and about an axis parallel to the axis of bending, as shown in Fig. 6.8; and d_{ang} is the distance between the angle centroid and the neutral axis of the cracked plated section. The coefficients 2.22 and 0.0185 in Eq. 6.9 were calibrated from test results in which the flexural rigidity of the cracked plated section $(EI)_{cr.pl}$ was used in this calibration and, hence, this form of the flexural rigidity has to be used in the design. It should be noted that $(EI)_{cr.pl}$ in Eq. 6.9 is the flexural rigidity of the whole cross-section as in Fig. 6.8 which includes all the plates at that section, whereas, the remaining parameters on the right hand side of Eq. 6.9 relate to a single plate.

6.4.2 Side plates

Equation 6.9 is a generic equation as it applies to all plates that are attached to the sides of the beam. Inserting the properties of a flat side plate into Eq. 6.9 gives the following resistance to PE debonding of a side plate (Oehlers et al 2000).

$$(M_{PE})_{sp} = \frac{K(EI)_{cr.pl} f_{cb}}{E_p \left(0.185 t_{sp} + 0.0185 |d_{sp}|\right)} \qquad 6.10$$

where K = 1 for the mean capacity and 0.81 for the 5% characteristic capacity for design. The distance d_{sp} is the distance between the centroid of the side plate and the neutral axis of the cracked plated section, as in Fig. 6.8. This distance remains

positive even when the plate centroid is in the compression zone as in Fig. 6.9 as explained in Section 6.2.1.4. It is interesting to note how Eq. 6.9 has simplified to Eq. 6.10 because the bonded length $(h_{bnd})_{sp}$ is also equal to the width of the plate.

6.5 PE analysis for bonded interface parallel to bending axis

As with plates bonded to surfaces perpendicular to the bending axis, generic design rules have also been developed for plates bonded to surfaces parallel to the axis of bending. These rules apply to angle sections as in Fig. 6.10, channel sections, tension face plates and compression face plates. The following debonding capacities have been given in the form of Eq. 6.7, but if the beam is affected after plating by long term material variations then Eq. 6.8 should be used.

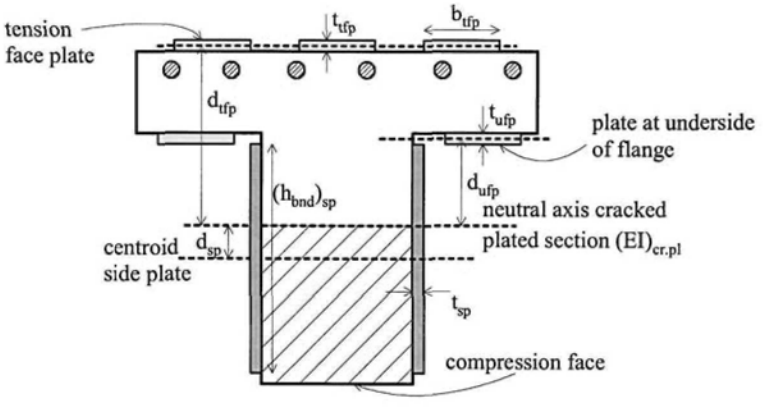

Figure 6.9 Plates bonded to a beam in the hogging region

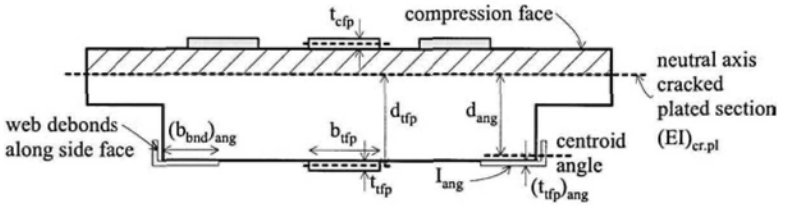

Figure 6.10 Plates bonded to horizontal surfaces in the sagging region

6.5.1 Angle plates

Tests have shown that angle sections tend to first debond at the tension face, as in Fig. 6.8, after which they behave as side plated beams. The following equation (Nguyen et al 1998) was derived for the case where the angle section first debonds from the side, as in Fig. 6.10, so that the plate remains attached to the tension face. None of the tests failed in this way so the scatter has not been determined directly, instead it will be assumed that the scatter is the same as for tension face plates which are just one form of this generic model. The moment at the plate end at which PE debonding occurs is given by

$$(M_{PE})_{ang.tfp} = \frac{K(EI)_{cr.pl} f_{cb} (t_{tfp})^2_{ang} (b_{bnd})_{ang}}{5.69 E_p I_{ang}} \qquad 6.11$$

where: K = 1 for the mean capacity and 0.53 for the 5% characteristic capacity; $(t_{tfp})_{ang}$ is the thickness of the plate in the angle attached to the tension face of the beam as shown in Fig. 6.10; $(b_{bnd})_{ang}$ is the width of the bonded region in Fig. 6.10; I_{ang} is the second moment of area of the angle about the angle centroid about an axis parallel to the axis of bending; and d_{ang} is the distance between the centroid of the angle and that of the cracked plated section. In summary, an angle section or channel section should be checked for initial debonding on the tension face and eventual debonding on the side face using Eq. 6.10 and also for initial debonding on the side face and eventual debonding on the tension face using Eq. 6.11 so that the debonding resistance is the lesser of these two possible modes.

6.5.2 Tension face plates

6.5.2.1 Basic analysis

Equation 6.11 can be used to develop the following mathematical model for tension face plates, although the coefficients in Eq. 6.12 vary slightly from those which would be derived from Eq. 6.11 as they were calibrated using different populations of test results (Oehlers and Moran 1990).

$$(M_{PE})_{tfp} = \frac{K(EI)_{cr.pl} f_{cb}}{0.474 E_p t_{tfp}} \qquad 6.12$$

where: K = 1 for the mean capacity and 0.53 for the 5% characteristic capacity; t_{tfp} is the thickness of the tension face plate as in Fig. 6.10; and d_{tfp} is the distance between the centroid of the tension face plate and that of the cracked plated section.

Equation 6.12 can also be applied to the plate at the underside of the flange in the hogging region in Fig. 6.9 of plate thickness t_{ufp} and at a distance from the neutral axis of d_{ufp}. The stress resultants in a tension face plate are shown in Fig. 6.1(c) where the couple $P_{tfp}t_{tfp}/2$ acts in the same direction as M_{tfp}. The difference between the tension face plate and underside of flange plate in Fig. 6.9 is that the couple $P_{tfp}t_{tfp}/2$ now acts in the opposite direction to M_{tfp} for the underside plate; this reduces the overall moment and, hence, reduces the interface normal debonding stresses in Fig. 6.1(d), leading to a safe design. Hence for underside of flange plates, the plate end moment capacity is given by

$$(M_{PE})_{ufp} = \frac{K(EI)_{cr.pl} f_{cb}}{0.474 E_p t_{ufp}} \qquad 6.13$$

where it can be assumed that the mean and scatter are the same as for the tension face plates, that is K = 1 for the mean capacity and 0.53 for the 5% characteristic capacity. Although it is felt that the scatter may be less as the underside of the flange is probably not influenced as much by the tension reinforcement.

6.5.2.2 Comparison of PE debonding rules for tension face plates

The plate end debonding rules in the design guidelines in Table 1.1 have been briefly discussed and compared in Section 1.6.3 and Fig. 1.36.

The European approach refers to plate end debonding as *concrete rip-off* but does not give any rules to prevent this form of failure. As the European approach requires the plate end to be anchored in an uncracked section, there will be a good chance the plate ends will be terminated near points of contraflexure where the applied curvature is low. Furthermore, the European approach only deals with thin FRP plates so that the curvature capacity from Eq. 6.12 will be high, as the plate thickness is in the denominator. As the European approach requires plated sections of high curvature capacity to be terminated in regions of low applied curvature, it is unlikely that PE debonding will occur using the European design approach. Should it be necessary to terminate the plate beyond the points of contraflexure in the compression face regions as in the left hand hogging region in Fig. 4.17(b), then the PE debonding capacity increases as will be shown in Eq. 6.15. Hence, it is understandable that plate end debonding is not considered in the European approach as quite simply it is not necessary for the anchorage design approach.

The British approach refers to PE debonding as *peeling failure* and uses the interface shear stress $\tau = VAY/Ib$, as described in Section 1.3.4, to prevent plate end debonding. This approach should be used with great caution as plate end debonding occurs in plates in constant moment regions ($V = 0$) as described in Section 6.2.2 and as can be seen in Figs. 1.21, 6.2 to 6.6. Furthermore because of the dependence on the vertical shear force V, this approach may encourage terminating the plate in a high moment, low shear region. For example, in a simply supported beam or in the sagging region of a continuous beam with uniformly distributed loads, this approach encourages the termination of the plate away from the supports or the points of contraflexure, that is closer to the mid-span where the curvatures are greater. The European, Australian and Hong Kong approaches discourage this and it is felt quite rightly.

The Hong Kong approach uses the term *concrete cover separation* for plate end debonding and restricts the moment at the plate end to two-thirds the ultimate moment capacity. Hence, they do restrict the curvature at the plate end. The combination of restricting the curvature at the plate end and the use of only thin FRP plates may be sufficient to prevent PE debonding, but it is felt that this is a rule of thumb approach which may be useful as an initial guideline.

6.5.3 Compression face plates

Tests that directly compared plate end debonding of compression face plates, such as those in Fig. 6.3, with tension face plates found that compression face plates were much less likely to debond, and this was attributed to the reversal of sign of the interface normal stresses I-J-L in Fig. 6.1 as explained in Section 6.2.1.2. To allow for this increase in capacity, Eq. 6.12 was adapted as follows

$$\left(M_{PE}\right)_{cfp} = \frac{K\left(EI\right)_{cr.pl} f_{cb}}{0.208 E_p t_{cfp}} \qquad 6.14$$

where t_{cfp} is the thickness of the compression face plate as in Fig. 6.10. As there were a limited number of tests, the scatter was assumed to be the same as in tension face plates so that $K = 1$ for mean capacity and 0.53 for the 5% characteristic capacity, although it is felt that the scatter for compression face plates will be less as they will not be affected by stress concentrations from the tension reinforcing bars.

6.6 Design for PE debonding

6.6.1 Generic design approach

The full sequence of design that encompasses all forms of debonding is outlined in Section 5.3 and illustrated in Fig. 5.10. In summary, the plate is first designed for its flexural strength for IC debonding at the position of maximum moment, as shown in Fig. 5.10(c). The length of the plate is governed by the region where the flexural strength has to be increased. The plate is then extended, if necessary, to encompass the position of the critical diagonal crack such as position C in Fig. 5.10(c). Extended if necessary to D to ensure a critical diagonal crack does not occur in the unplated region. The plate is then extended further if required, such as to position E, to ensure that the curvature at the plate end does not allow PE debonding. Then if the design is based on the anchorage approach, the plate is extended into a region that is uncracked in flexure and shear.

The design procedure is further illustrated in Fig. 6.11 for a continuous beam with a uniformly distributed dead and live load as well as uniformly distributed concrete shrinkage. The distribution of curvature along the beam is shown in Fig. 6.11(b). This consists of the shrinkage curvature $(\chi_{shrink})_{plate}$ that occurs after plating and which can be obtain from national standards using equations similar to Eq. 6.3. The curvature due to the live load $(\chi_{short})_{plate}$ which depends on the live load distribution as well as the short term Young's modulus of the concrete. And the curvature due to the dead load $(\chi_{creep})_{plate}$ which depends on the dead load distribution as well as the long term Young's modulus for the concrete. The subscript *plate* used in the notation for the curvatures is to remind the reader that it is the curvature after plating that can cause debonding. Also shown is the *anchorage* approach to design in Fig. 6.11(c) and the *hinge* approach in Fig. 6.11(d). The sequence of design from IC, to CDC and then to PE can be seen in Figs. 6.11(c) and (d). The three curvatures at each plate end in Figs. 6.11(c) and (d) are shown as groups of three dots in Fig. 6.11(b) and it is these curvatures that induce PE debonding.

Let us consider the hinge approach in Fig. 6.11(d) and its application to the hogging region over the left support. After the IC and CDC analyses, the plate end is then checked for PE debonding such as at section B-B. It is necessary to ensure that the sum of the three possibly induced curvatures at the plate end, shown as the three dots on the line B-B in Fig. 6.11(b), is less than the curvature capacity which is given by Eqs. 6.9 to 6.15 less the flexural rigidity term $(EI)_{cr,pl}$. It is simply a question of extending the plate towards the point of contraflexure until the applied curvature is low enough. There will always be a solution at the point of contraflexure. The same approach can be applied to the sagging region in Fig. 6.11(d), such as at Section D-D, where once again there will always be a solution at the point of contraflexure.

Let us now consider the left hand hogging region in the anchorage approach in Fig. 6.11(c). The anchorage approach requires that the plate is terminated in an uncracked region which is not cracked through either flexure or shear. Extending the plate to the point of contraflexure will ensure that flexural cracking will not occur at the plate end. It is also unlikely that a critical diagonal crack will occur at the plate end before a critical diagonal crack occurs in the vicinity of the support where the shear is greater, so that cracking due to shear at the plate end is unlikely. The plate end will have to be taken past the point of contraflexure, such as at C-C, in order to fully anchor the plate. In which case, the plate end may be subjected to curvature and subsequently PE debonding, but as it is on the compression face PE debonding is less likely to occur. The same procedure can be applied to the sagging plate in Fig.

6.11(c). However in this case, the plate is being extended into a region where the shear is increasing so that it may be difficult to find an uncracked region in which to anchor the plate.

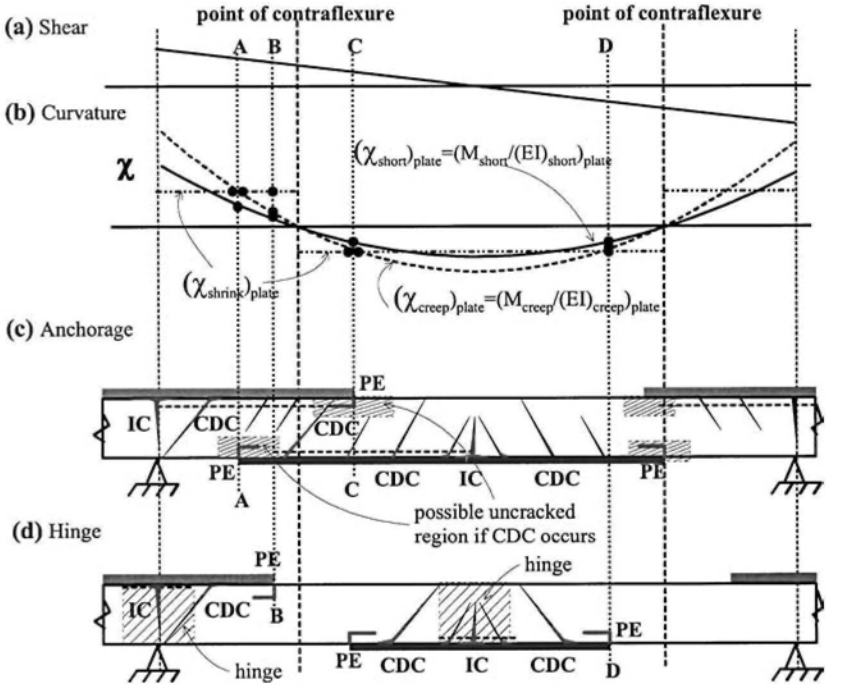

Figure 6.11 Summary of generic design procedure

6.6.2 Interaction between PE, IC and CDC debonding

It is essential, in whichever design approach is being used, to ensure that IC debonding and PE debonding do not coincide as existing design rules do not cover this scenario. In the hinge approach in Fig. 6.11(d), this is achieved by restricting the IC interface cracks to a small region around the position of maximum moment so that the IC interface cracks do not extend to the plate end where PE debonding may occur. In the anchorage approach in Fig. 6.11(c), this is achieved by terminating the plate in an uncracked region where the curvature is low so that PE debonding will not occur in the anchorage length which is required to resist IC debonding.

It can be seen in Fig. 6.11(d) for the hinge approach for partially plated beams that CDC and PE debonding can occur in the same region in the vicinity of the plate end. Research in the early nineties did appear to suggest that there was an interaction between PE and CDC for tension face plates. However, recent advances in the analysis and understanding of CDC debonding that was applied to these original partially tension face plated tests suggested that most of the beams failed by shear failure beyond the plated region, so that CDC debonding was not being measured. Recent tests on partially plated beams with compression face plates and sides plates showed that there was no direct interaction or at least no detrimental interaction between PE and CDC debonding. It is interesting to note that what interaction there was was found to be beneficial. Take for example the situation of extending the

hogging region plate in Fig. 6.11(c) past the point of contraflexure into the compressive face of the sagging region. This is simulated in the test in Fig. 6.12 where the compression face plate is placed over the supports. In this test, the formation of the diagonal crack under the plate end relieved the curvature in the compression face plate and significantly increased the moment to cause PE debonding. It is, therefore, recommended that CDC debonding, IC debonding and PE debonding can be treated independently in the design, and that the design procedure must ensure that IC and PE debonding do not occur in the same region as do both the hinge and anchorage approaches.

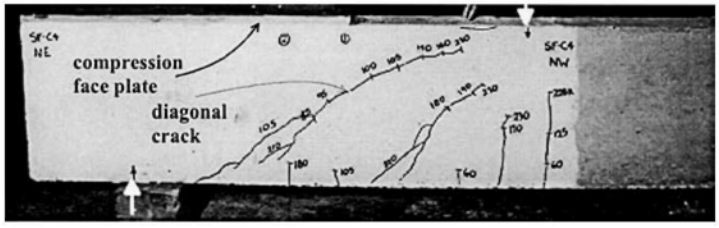

Figure 6.12 Relief of curvature in compression face plate

6.7 Examples

The plated structures first analysed in Chapters 3, 4 and 5 for IC and CDC debonding are now analysed for PE debonding. In this chapter, we will only compare the PE moment capacity with the ultimate flexural capacity of the plated beam $(M_u)_{pl}$ to illustrate the circumstances when PE debonding does and does not affect plating. The full analyses, including the extent of plating are given in Chapter 7. Some of the material and geometric properties of the beam, slab and plates used in the subsequent calculations are constant and are given by the following: E_c = 25.5 GPa; f_{cb} = 2.9 MPa; t_p = 1.2 mm for CFRP plates and 3 mm for steel plates so that they yield prior to IC debonding; and E_p = 160 GPa for CFRP plates and 200 GPa for steel plates.

Table 6.1 summarises the results of the PE debonding analysis for the slabs in Sections 3.5.1.4 and 4.6.2, which were strengthened with CFRP and steel tension face plates respectively in the sagging region. The mean and characteristic PE debonding moment $(M_{PE})_{tfp}$ was calculated using Eq. 6.12 and it can be seen that the characteristic PE debonding moment is less than the flexural moment capacity of the plated section $(M_u)_{pl}$ in both cases. This means that the plate end must be terminated where the applied moment is less than the characteristic PE debonding moment. The axial stiffness E_pA_p of the steel plate is substantially larger than that of the CFRP plate, so that the flexural rigidity $EI_{cr,pl}$ of the steel plated beam is larger than that of the CFRP plated beam. Hence the steel plated beam is stiffer than the CFRP plated beam and more resistant to PE debonding as can be seen in Eq.6.12. However because the steel plate is thicker than the CFRP, this makes it more prone to PE debonding.

Table 6.2 gives the results of the PE debonding analysis for the beams in Sections 4.6.1 and 3.5.2.2, which were strengthened with CFRP tension face plates and underside of flange plates respectively in the hogging moment region. Also included in Table 6.2 are the beams with full depth steel side plated beams in the hogging and sagging moment regions analysed in Sections 3.5.2.3 and 5.6 respectively. Recall that a plate is attached to each side of the web for the full depth

steel side plated beams. Equation 6.12 was used to calculate M_{PE} for the first tension face plated beam, Eq. 6.13 for the underside of flange plated beam, and Eq. 6.10 for the two side plated beams.

Table 6.1 PE debonding analysis of tension face plated slabs

Section	Plate material	$b_p x t_p$ [mm]	$I_{cr,pl}$ x10^6 [mm^4]	$(M_{PE})_{tfp}$ [kNm/m]		$(M_u)_{pl}$ [kNm/m]
				mean	5% char	
3.5.1.4	CFRP	211x1.2	73.5	59.6	31.6	47
4.6.2	Steel	140x3	95.9	24.9	13.2	47

Table 6.2 PE debonding analysis of strengthened beams

Section	Plate mat.'l	Plate location	$b_p x t_p$ [mm]	$I_{cr,pl}$ x10^9 [mm^4]	(M_{PE}) [kNm]		$(M_u)_{pl}$ [kNm]
					mean	5% char	
4.6.1	CFRP	tfp – hog	600x1.2	2.30	1868	990	450
3.5.2.2	CFRP	ufp – hog	795x1.2	2.06	1674	887	436
3.5.2.3	Steel	sp – hog	370x3	2.05	1107	897	403
5.6	Steel	sp – sag	370x3	2.62	200	162	277

The results for the two CFRP plated beams are similar with the tension face plated beam having a higher second moment of area and flexural moment capacity for a smaller cross-sectional area of plate because the plates are farther from the neutral axis maximising the efficiency. However, the underside of flange plated beam will have an improved ductility as the strain in the tension reinforcement will be higher. The mean PE debonding strength for both of these beams is very high and even though the characteristic strength is substantially lower due to the scatter of experimental results, both are much greater than $(M_u)_{pl}$. Hence, for these two beams PE debonding will never govern the location of the plate end.

The situation is different for the two steel full depth side plated beams. The PE debonding resistance in the hogging region will never govern the location of the plate end. However, both the mean and characteristic PE debonding strength in the sagging region are less than $(M_u)_{pl}$ hence, the plate end must be located where the applied moment is less than the characteristic PE debonding moment so that this form of debonding is prevented. The primary factor resulting in the difference in PE debonding resistance in side plated beams is d_{sp}. In the hogging region, where the neutral axis of the fully cracked plated section is in the web, d_{sp} was only 7 mm. However, in the sagging moment region the neutral axis was in the flange and because the centroid of the plates is still in the web, d_{sp} increased to 232 mm.

6.8 References

Oehlers, D. J. and Moran, J. P. (1990). "Premature failure of externally plated reinforced concrete beams." Journal of the Structural Division of the ASCE, Vol. 116, No. 4, 978-995, April.

Oehlers, D.J., Nguyen, N.T., and Bradford, M.A. (2000) "Retrofitting by adhesive bonding steel plates to the sides of R.C. beams. Part 1: Debonding of plates due to flexure." Journal of Structural Engineering and Mechanics, An International Journal, Vol.9, No.5, May, 491-504.

Nguyen, N.T., Oehlers, D.J., and Bradford, M.A. (1998) "Models for the flexural peeling of angle plates glued to R.C. beams." J. of Advances in Structural Engineering. Vol. 1 No.4, pp 285-298.

Chapter 7: Design Examples

7.1 Introduction

This book on the *Design of FRP and Steel Plated RC Structures* deals with a unique and new form of structure, as it has numerous failure mechanisms that other existing codes, such as RC and composite steel and concrete codes, do not address. It is not the aim of this book to promote specific plating techniques nor to promote specific plating materials, as we believe that this can severely restrict the use of plating. The aims of this book are to: explain the fundamental behaviour of plated structures so that the designer develops a feel for plating and, hence, the confidence to apply the plating technique; illustrate the huge variety of plating options that are available and should be considered in addressing a retrofitting problem; provide a generic approach for debonding design that is independent of the design equations available; and to provide comprehensive analysis tools, for those plating options, that not only illustrate what can be done but also what cannot be done, so that they can be applied with confidence. It is hoped that these aims will allow designers to develop their own individual forms of plating, and allow them the freedom to combine different techniques and materials in order to find an efficient solution to their specific plating problem.

It is felt that the debonding failure mechanisms are now well understood and generally agreed upon and these have to be designed for. Design equations, and specifically characteristic or lower bound values, have been provided that can be used in design. No doubt, and hopefully, these design equations will be improved with time, and as more accurate equations become available these can be substituted into the general design procedure. It is felt that a major improvement in quantifying the IC debonding strain will help considerably. For example, if we could reduce the scatter and start designing for IC debonding at strains that are closer to their mean resistances in pull tests then this would allow us to use much thicker plates and higher stresses. There is really little need to improve the PE debonding equations as any refinement will only lead to nominal savings in material, particularly as this form of debonding can be easily prevented by simply terminating the plate in a region of low curvature. The CDC debonding equations are fairly accurate and allow a range of approaches from complex iterative techniques that can be applied to any combination of plates to simpler and direct approaches which may require a larger volume of plates. The fact that the CDC debonding equations have been tied to prestressed code rules suggest that they are more than adequate.

The examples used in this chapter are not meant to reflect the most efficient choice but to simply illustrate and provide some feel for the design procedure. Furthermore, they have not been restricted to within the range of test results from which the design equations were derived. This chapter starts with a summary of the debonding design approaches and design steps, and an illustration of the occurrence of the different forms of debonding. The first structure to be plated is a continuous slab in an internal bay. As slabs are usually designed without stirrups and, therefore, for the concrete shear capacity, CDC debonding is rarely a problem. Hence this design has been used to concentrate on IC debonding of tension face plates and, importantly, the moment redistribution that the IC debonding resistance allows. PE debonding is checked, just to illustrate how it affects the extent of plating. The second structure to

be plated is a continuous beam with stirrups which allows us to go beyond the restriction of just using tension face plates and instead adhesively bond plates to any surface of the beam. This beam is designed without moment redistribution, so that the analysis can concentrate on all the forms of debonding and in particular CDC debonding, where it is shown that CDC debonding may prevent the use of adhesively bonded plates in some regions of a beam. To overcome this problem of premature CDC debonding in beams, plates are bolted to the sides of a continuous beam in the final structure considered.

7.2 Summary of design procedure

The choice of the design philosophy to be used is first discussed, these are then followed by the items that need to be considered in the design steps, and this section is then completed by considering the prevalence of the different debonding modes.

7.2.1 *Design philosophies available*

7.2.1.1 Anchorage approach

The anchorage approach (Section 2.5.1) is illustrated in Fig. 7.1. To induce the maximum strain in the plate, the plate ends are anchored in regions, shown shaded in Fig. 7.1, that need to be uncracked through flexural cracks, flexural/shear cracks, and critical diagonal cracks. This anchorage allows the IC force in the plate to accumulate throughout the plate length. The behaviour is similar to stud shear connectors in composite steel and concrete beams where each individual shear connector contributes to the overall axial force in an element of the composite beam (Section 2.3.2). In tension face plated beams, the *concrete teeth* between flexural and flexural/shear cracks, Fig. 7.1, act as shear connectors, and there is also an additional force at the *end anchorage* that is similar to that obtained from pull tests (Section 2.3.1). The sum of all these shear forces is the maximum force in the plate at mid-span.

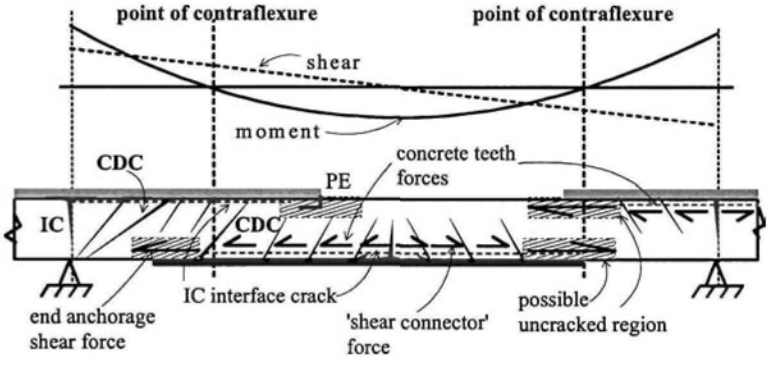

Figure 7.1 Anchorage approach

The anchorage approach requires the IC interface crack, shown as a broken line in Fig. 7.1, to spread over most of the plate. In order to prevent the interaction between IC and PE debonding, the plate end is anchored in an uncracked region where the curvature is small. Hence PE debonding should be checked, or at least

detailed against, by carefully choosing the position of the plate end, to ensure that the plate end is in a position where PE debonding is well designed against. The anchorage approach was developed for tension face plates and it is felt that this design approach should be restricted to tension face plates, as it is unclear whether the shear connector behaviour, through the *concrete teeth*, has the same effect with side plates, particularly when part of the side plate is in the compression zone of the beam. A problem may occur in trying to find a suitably uncracked zone, particularly for beams subjected to longitudinally moving loads where there is no stationary point of contraflexure, or for regions of the beam subjected to high vertical shear forces where critical diagonal cracks may occur near the points of contraflexure.

The anchorage approach is important because it achieves the maximum strains in the plate and, hence, minimises the cross-section area of plate required. Furthermore and just as importantly, by maximising the plate strains, the anchorage procedure also maximises the ductility of the structure and the capacity for moment redistribution.

7.2.1.2 Hinge approach

The hinge approach (Section 2.5.2) is illustrated in Fig. 7.2 and differs from the anchorage approach in Fig. 7.1 by allowing the plate to be terminated short of the point of contraflexure. As the plate in the hinge approach is terminated short of the point of contraflexure, that is in a region where there is curvature, PE debonding can occur at the plate end. Therefore, and in order to prevent the interaction between PE and IC debonding, the IC interface cracks must be restricted to a small region, or *hinge,* in the vicinity of the position of maximum moment, as shown hatched in Fig. 7.2. This is achieved by limiting the strain in the plate to that determined directly from pull tests (Section 2.4.3). Hence, the hinge approach restricts the force in the plate to the *end anchorage shear force* in the anchorage approach in Fig. 7.1 without the additional *shear connector forces* from the *concrete teeth*.

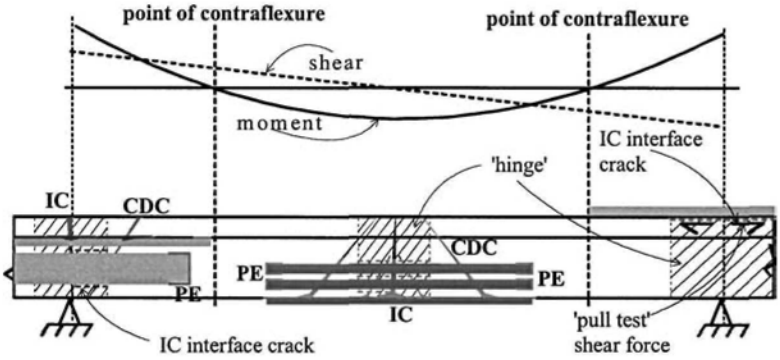

Figure 7.2 Hinge approach

In the hinge approach, the plate end can be terminated short of the point of contraflexure so that the hinge approach tends to concentrate the plate to where it is required for flexure. CDC and PE debonding have still to be checked. Because of the reduced strains allowed in the hinge approach, the hinge approach requires a greater cross-section of plate than the anchorage approach but over a shorter length. The anchorage approach is restricted to tension face plates, whereas the hinge approach

can be applied to plates on any surface such as those shown in Fig. 7.2. In the anchorage approach, the plate strains depend on the *shear connector force* in Fig. 7.1 and, making the analogy with shear connectors in composite steel and concrete beam, this would infer that the plate strains depend on the distribution of the applied loads and beam properties. In contrast, the plate strains in the hinge approach can be determined directly from pull tests. As the IC design strains in the hinge approach are smaller than those in the anchorage approach, the hinge approach will lead to less ductile beams with less ability to redistribute moment.

7.2.2 *Design steps*

The issues and items that may be worth considering in the design procedure are listed in the following design steps.

1) Stress resultants

- Require envelopes of the applied design moments and design vertical shear forces as in Fig. 7.3(a). In developing these envelopes, it may be necessary to consider moment redistribution.
- For flexural strengthening, there may be a need to further consider moment redistribution (Section 3.3.4.2) and its changes to the envelopes, as moment redistribution may allow greater increases in the overall capacity.

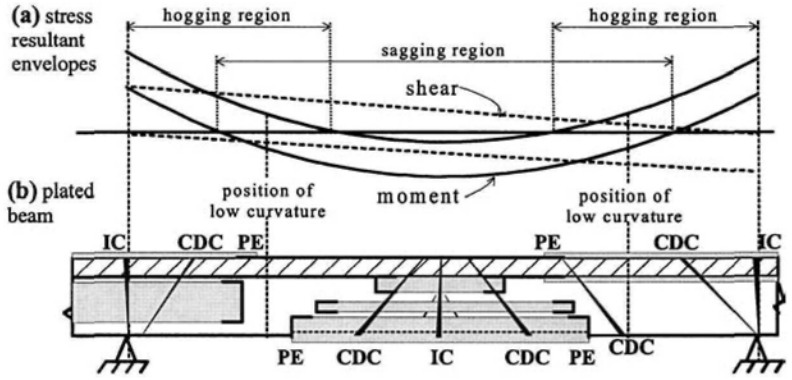

Figure 7.3 Design options

2) Plate material

- Choose type of plate material (Section 1.5) in the hogging and sagging regions in Fig. 7.3.
- For durability and ease of application, FRP may be the preferred option.
- Metal plates may be preferred for ductility and moment redistribution at a joint (Section 3.3.2) and for reducing deflections at serviceability.
- Combinations of plate materials can be considered. For example metal plates at potential plastic hinges where rotation is required (Section 3.3.2) and FRP plates where rotation is not required.

3) Plate position
- Consider plating any face and level of the beam (Section 1.2.2) in Fig. 7.3(b).
- Plate position may be chosen for convenience of adhesive bonding or bolting plate (Section 1.2.1).
- Position may be chosen for mechanical considerations such as flexural strengthening, shear strengthening (Section 1.2.2), increase in flexural rigidity for deflection; maximising ductility and moment redistribution (Section 3.3.4.2); and ensuring reinforcing bars yield prior to plate debonding.

4) Plate cross-sectional area
- Determine for flexural strength (Section 3.4) and sometimes the cross-sectional area for shear strength (Chapter 5).
- For serviceability such as deflections, metal plates may be the preferred option as thick plates may be used which can significantly increase the flexural rigidity.

5) Design philosophy
- Anchorage approach for tension face plates only (Section 2.5.1).
- Hinge approach for all positions of plates (Section 2.5.2).

6) Plate thickness
- Plate thickness governed by IC debonding at positions of maximum moment (Chapter 2).
- IC debonding strain depends on design philosophy (Section 2.5).

7) Plate extent
- Chapter 2: for each individual plate, check for IC debonding at position of maximum moment.
- Chapter 3: extend plate to cover region where flexural increase in strength required.
- Chapters 4 and 5: check for CDC debonding and extend plate to encompass critical diagonal crack.
- Chapter 6: check for PE debonding and extend plate if required.
- For the anchorage approach, extend plate into uncracked region and check for PE debonding if curvature exists at the plate end.

7.2.3 *Occurrence of IC, CDC and PE debonding*

Let us consider the possible debonding modes that can occur in a partially plated beam, as the plate end is extended along the length of the beam as shown in Fig. 7.4(a). The shear load at the point of contraflexure V_{dat} at which debonding occurs is the ordinate in Fig. 7.4(b) and the abscissa is the position of the plate end x.

The typical failure envelope for CDC debonding which was developed in Section 5.2.1.5 and illustrated in Fig. 5.9 has been reproduced in Fig. 7.4(b). Also included in Fig. 7.4(b) are families of individual failure envelopes for IC and PE debonding. The individual IC debonding failure envelopes have been shown as parabolas with a debonding strength of zero when the plate end is adjacent to the position of maximum moment, as the anchorage length is zero, and which increases to a maximum value when the plate end is anchored at a point of contraflexure. This shape was chosen because beam tests and analyses in Section 2.3.2.2 have shown that flexural cracks increase the strain at which IC debonding occurs so that extending the

plate way beyond the effective length of Eq. 2.3 will increase the strains in the plate at debonding. The PE debonding moment capacity is finite and independent of the position of the plate end, so that the shape of the failure envelope is governed by the shear at the datum point to induce that finite moment at the plate end. Hence, the individual PE failure envelopes tend to infinity as the plate end tends to the point of contraflexure.

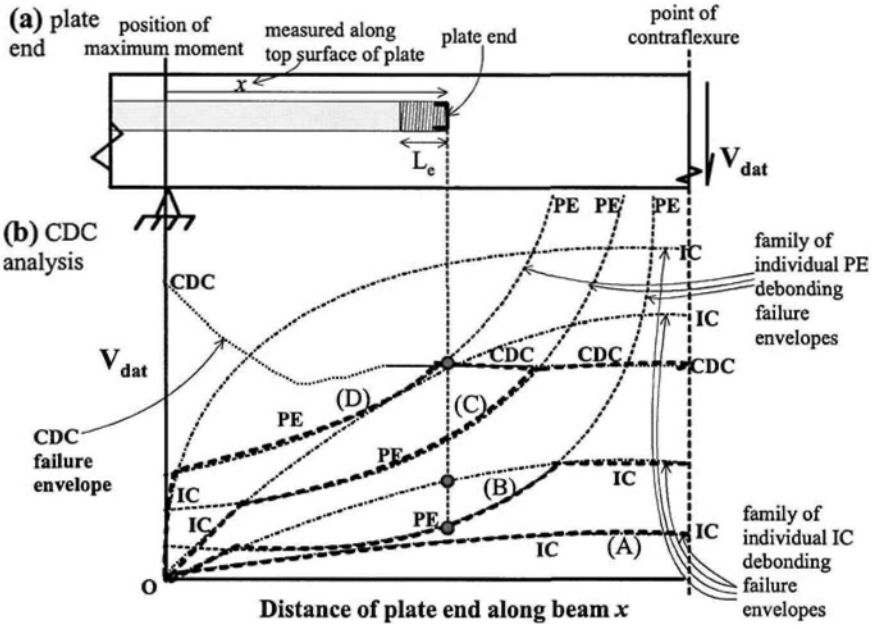

Figure 7.4 Interaction between IC, CDC and PE debonding

For a specific plate cross-section, one individual CDC failure envelope, one individual IC failure envelope, and one individual PE failure envelope control design. For a specific plate end position such as that shown in Fig. 7.4(a), there are three debonding resistances shown as dots in Fig. 7.4(b) which lie on the three individual failure envelopes. The lower bound to these three individual failure envelopes gives the typical shapes of the overall failure envelopes which are shown as thick broken lines in Fig. 7.4(b). The overall failure envelopes marked (A) and (B) fall below the individual CDC envelope and, hence, can be considered to apply to plated slabs where CDC failure rarely occurs. IC debonding will always govern when the plates are ludicrously short, which will never happen in practice. IC debonding can occur at any position of the plate end but PE debonding is more likely to occur when the plates are terminated in the middle regions. It is felt that failure envelopes (C) and (D) are more typical of plated beams where CDC debonding tends to govern fully plated beams and PE and IC debonding govern partially plated beams.

7.3 Continuous slab structure with adhesively bonded plates

This section deals with the strengthening of a slab across one of its spans. The same approach can be applied to the other span as, in practice, slabs have been plated in both directions. As we are dealing with a slab, CDC debonding is of minor importance. As the neutral axis depth factor k_u in a slab is usually quite small this usually allows substantial moment redistribution which will be covered in detail. To help in the analysis, a detailed slab specification is first given. This is then followed by examples of plating just one of the regions, so that moment redistribution is required from the unplated region based on the neutral axis depth approach in Section 3.3.1. After which both regions are plated. The ability to redistribute moment is first based on the neutral axis depth factor approach but then it is checked using the flexural rigidity approach in Section 3.3.2 to ensure that the IC debonding strain capacity can allow the required moment redistribution from the neutral axis depth factor approach.

7.3.1 *Detailed slab specifications*

The slab structure and some of its specifications have already been described in Section 3.5.1.1 and these details are repeated here and considerably expanded to include information useful in the analysis procedure.

7.3.1.1 Slab structure

(a) Slab strength

The internal continuous slab shown in Figs. 7.5(a) and (d) has been chosen to be retrofitted. For ease of calculation, we will assume that it is encastre, subjected to uniformly distributed loads, and we will deal with a 1 m width of slab. The slab has a hogging moment capacity of 41 kNm and a sagging capacity of 31 kNm, so that the distribution of moment at ultimate flexural failure is given by the *strength* curve in Fig. 7.5(b) where the static moment is 72 kNm. If the beam remained elastic, then for the static moment of 72 kNm, the *elastic* distribution in Fig. 7.5(b) would occur, where the hogging moment is twice the sagging moment (for this case of an encastre beam with uniformly distributed loads). The *strength* line differs from the *elastic* distribution, requiring a moment redistribution of 15% from the hogging region.

(b) Applied loads

The static moment capacity is 41+31=72 kNm which implies a uniformly distributed load of 22.9 kN/m to cause failure, and which induces the vertical shear distribution shown in Fig. 7.5(c) with a maximum shear of 57 kN. Of the 22.9 kN/m applied uniformly distributed ultimate load, we will assume that 10.4 kN/m is due to dead load and the remainder of 12.5 kN/m is due to live load. For serviceability, we will assume the unfactored dead load is 6.7 kN/m and this load will be used to determine the residual stresses prior to plating.

(c) Distribution of moment

To assist in the ensuing plating calculations, for a continuous beam with uniformly distributed load, the distance of the point of contraflexure from the nearest support L_{poc} in Fig. 7.5(b) is given by

$$wL_{poc}^2 - wL_{poc}L - 2M_h = 0 \qquad 7.1$$

where w is the applied uniformly distributed load, L is the span of the beam and M_h is the hogging moment at the support which is input as a negative value. Furthermore, the variation of the applied moment along the length of the beam M_x is given by

$$M_x = M_h - \frac{wx^2}{2} + \frac{wLx}{2} \qquad 7.2$$

where x is the distance from the nearest support, hogging moments are negative and sagging moments are positive.

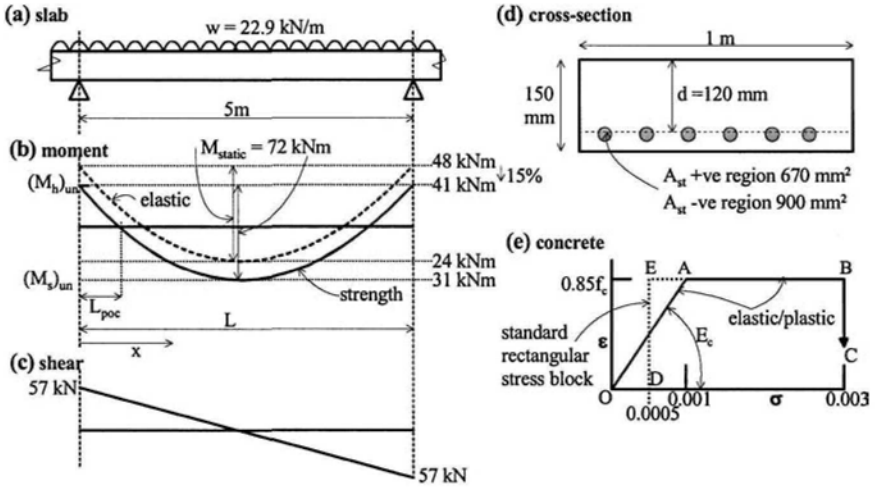

Figure 7.5 Slab structure

7.3.1.2 Reinforced concrete material properties

Concrete cylinder compressive strength f_c = 30 MPa; short term Young's modulus of concrete E_c = 25.5 GPa; long term Young's modulus of concrete = 13 GPa; tensile strength of concrete f_t = 2.2 MPa; indirect or Brazilian tensile strength of concrete f_{cb} = 2.7 MPa; depth of concrete rectangular stress block at concrete crushing = 84% of the effective depth of the slab; elastic/plastic concrete stress/strain distribution shown in Fig. 7.5(e); short term modular ratio (E_s/E_c) m_{short} = 7.8; long term modular ratio m_{long} =15.4; yield strength of reinforcing bars f_y = 400 MPa; Young's modulus of reinforcing bars E_s = 200 GPa. The shrinkage strain after plating is negligible, that is $\varepsilon_{sh} \rightarrow 0$.

7.3.1.3 Unplated slab mechanical properties

(a) Hogging section

Hogging moment capacity $(M_h)_{un}$ = 41 kNm; rigid plastic neutral axis depth as a proportion of the effective depth k_u = 0.14; concrete shear capacity from national standard $(V_c)_{code}$ = 119 kN; short term second moment of area of cracked section transformed to concrete $(I_{cracked})_{short}$ = 65.0x10^6 mm^4; elastic neutral axis depth of cracked section short term $(n_{crack})_{short}$ = 34.6 mm; $(EI_{cracked})_{short}$ = 1.66x10^{12} Nmm^2; long term second moment of area of cracked section transformed to concrete

$(I_{cracked})_{long}$ = 108x10^6 mm^4; elastic neutral axis depth from compression face of cracked section long term $(n_{crack})_{long}$ = 45.5 mm; $(EI_{cracked})_{long}$ = 1.41x10^{12} Nmm^2; static moment to cause residual strains $(M_{static})_{res}$ = 20.9 kNm based on dead load only; support moment to cause residual strains $(M_{hog})_{res}$ = 14.0 kNm; residual strain at tension face using unpropped construction and based on dead load moment of 14.0 kNm and long term properties ε_{res} = 0.00103.

(b) Sagging section

Sagging moment capacity $(M_s)_{un}$ = 31 kNm; rigid plastic neutral axis depth as a proportion of the effective depth k_u = 0.10; concrete shear capacity from national standard $(V_c)_{code}$ = 108 kN; $(I_{cracked})_{short}$ = 51.3x10^6 mm^4; elastic neutral axis depth from compression face of cracked section short term $(n_{crack})_{short}$ = 30.6 mm; $(EI_{cracked})_{short}$ = 1.31x10^{12} Nmm^2; $(I_{cracked})_{long}$ = 87.4x10^6 mm^4; elastic neutral axis depth of cracked section long term $(n_{crack})_{long}$ = 40.5 mm; $(EI_{cracked})_{long}$ = 1.14x10^{12} Nmm^2; static moment to cause residual strains $(M_{static})_{res}$ = 20.9 kNm based on dead load only; support moment to cause residual strains $(M_{hog})_{res}$ = 14.0 kNm; residual strain at tension face using unpropped construction and based on dead load moment of 7.0 kNm and long term properties ε_{res} = 0.00067.

7.3.1.4 Plate material properties

(a) Typical IC debonding strains

Examples and ranges of IC debonding strains are given in Table 7.1. Chen and Teng's results are based on the α values in columns 4 and 7 in Table 2.1 and use a value of b_p/b_c = 0.5 in Eq. 2.2. Chen and Teng's results tend to be on the low side. Hence in order not to be too restrictive in the following calculations, a value of α = 0.5 has been chosen for the pull test strengths, furthermore and in order to remove the iterations from the analysis, it has been assumed that b_p/b_c = 0.5; for example, for the CFRP plate this gives a debonding strain of 0.00267 which is close to Neubauer and Rostasy's (2001) recommendations in Table 7.1. Table 7.1 is also used in the ensuing flexural rigidity moment redistribution analyses to determine whether the plate has the required strain capacity.

Table 7.1 Typical IC debonding strains

Source	IC debonding strains
(1) Chen and Teng pull: 1.2 mm CFRP characteristic	0.0012-0.0019
(2) Chen and Teng pull: 1.2 mm CFRP mean	0.0016-0.0026
(3) Neubauer and Rostasy pull: 1.2 mm CFRP characteristic	0.0026
(4) Chen and Teng beam: 1.2 mm CFRP characteristic	0.0014-0.0023
(5) Chen and Teng beam: 1.2 mm CFRP mean	0.0036-0.0053
(6) Adelaide beam tests: 1.2 mm CFRP plates	0.0025-0.0052
(7) Adelaide beam tests: 3 mm steel plates	0.0044-0.0213
(8) Adelaide beam tests: 2 mm steel plates	0.0059
(9) Adelaide beam tests: 1 mm steel plates	0.0149

(b) Pultruded CFRP plate

Plate thickness t_p = 1.2 mm; Young's modulus of plate E_p = 160 GPa; effective length (Eq. 2.3) L_e = 187 mm; pull test stress at debonding $\sigma_{IC} = \sigma_{db}$ = 427 MPa; pull test strain at debonding $\varepsilon_{IC} = \varepsilon_{db}$= 0.00267; assume ultimate debonding strain in beams for *anchorage approach* is 75% greater i.e. $(\varepsilon_{db})_{anch} = 1.75\varepsilon_{db}$ = 0.00467, which is similar to the strains achieved in the beam tests at Adelaide in Table 7.1.

(c) Steel plate
Yield strength of plate f_{yp} = 300 MPa; Young's modulus of plate E_s = 200 GPa; stress at debonding for a 3 mm plate σ_{db} = 302 MPa from pull tests, that is it yields prior to debonding; effective length for 3 mm thick plate L_e = 331 mm.

(d) Aluminium plates
Yield strength of plate f_{yp} = 125 MPa; Young's modulus of plate E_{al} = 63 GPa; transition thickness between debonding and yield, i.e. when $\sigma_{db} = f_{yp}$, t_p = 5.52 mm; for t_p = 5.52 mm the effective length is L_e = 252 mm.

(e) Prefabricated FRP plates for bolting
Glass/carbon FRP plates have a fracture strength 600 MPa and a Young's modulus of 51 GPa. Glass FRP plates have a fracture strength of 390 MPa and a Young's modulus 25 GPa.

7.3.2 *Plating +ve region only (redistribution from unplated –ve region)*

Let us assume, that for practical reasons such as accessibility, we are only allowed to plate the tension face of the sagging region of the slab as in Fig. 7.6(a). The question is how much can we increase the overall capacity, that is how much can we increase the applied load on the structure. For comparison, we will look at plating the sagging region with FRP plates using the hinge approach, then with FRP plates using the anchorage approach, and finally with steel plates using the hinge approach.

7.3.2.1 Strengthening option based on moment redistribution

(a) Moment redistribution
The distribution at failure of the unplated beam, the *strength* curve in Fig. 7.5(b), is shown in Fig. 7.6(b) as the *unplated strength* curve A. As the maximum hogging moment in the *unplated strength* curve is less than twice the maximum sagging moment (which is the ratio required for an elastic distribution for this encastre beam with a uniformly distributed load), on loading the hogging capacity will be reached first. Therefore, hinges will first occur in the hogging regions which will then redistribute moments to the sagging region. From Section 7.3.1.3(b) for the sagging region, k_u = 0.1. From Fig. 3.14, it can be seen that for k_u =0.1 most national standards will allow 30% redistribution which is what we will use. We will also use the benefit of unpropped construction.

For the hogging region to achieve 30% redistribution from the *elastic* distribution, curve B in Fig. 7.6(b), and end up at $(M_h)_{un}$ = 41 kNm, the elastic moments at the hogging regions must be 41/0.7 = 58.6 ≈ 59 kNm as shown. Those are just two points (both hogging regions) on the elastic distribution, but it is enough to fix the elastic distribution as the sagging moment is half the elastic hogging moment; this gives a static moment of 1.5(58.6) ≈ 88 kNm. Hence, we can in theory increase the static moment from the original unplated static capacity of 72 kNm to 88 kNm, that is by 22%. Reducing the hogging elastic moment by 30%, that is reducing it by 18 kNm from 59 kNm to 41 kNm, drops the *elastic* moment distribution by 18 kNm to the *redistributed for plated beam* curve C in Fig. 7.6(b), so that the sagging moment has increased from 31 kNm to 88-41 = 47 kNm.

There is no point in making the sagging region any stronger. For example, if we attempt to increase the sagging capacity to say 57 kNm instead of the 47 kNm, then the static moment at failure would increase to 57+41 = 98 kNm. So that the elastic hogging moment for this static moment of 98 kNm would be two-thirds of 98

kNm, that is 65 kNm. The percentage redistribution required at the hogging region would be (65-41)/41 = 59% which is greater than the 30% redistribution capacity of the hogging region, that is the hogging region does not have the rotational capacity or ductility required for this 59% moment redistribution. There is no problem in making the sagging region weaker than 47 kNm, as this simply implies that the hogging regions have to redistribute less than their maximum capacity of 30%.

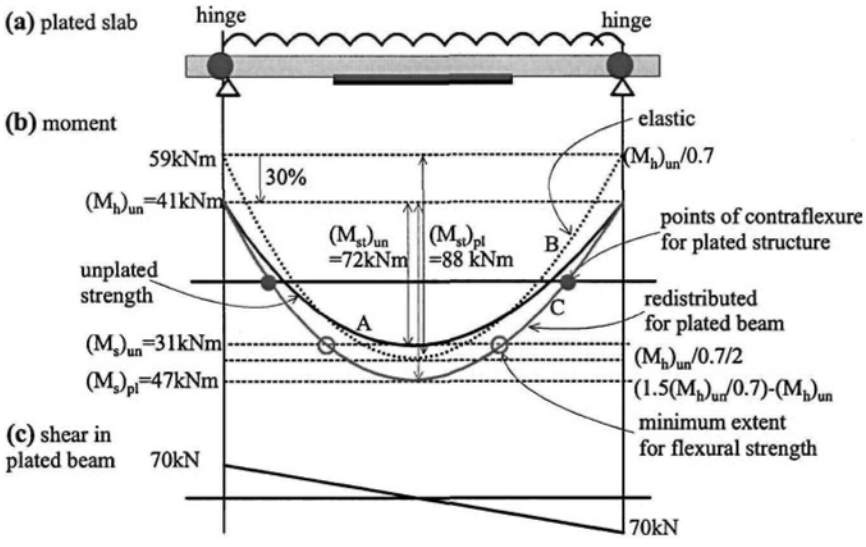

Figure 7.6 Plating sagging region only

To conclude, the analysis in this section has shown how the moment redistribution capacity has restricted the maximum increase in strengthening for the beam where plating is limited to the sagging region. The next step in the analysis is to determine whether plating can increase the sagging capacity by 47-31=16 kNm, that is by 52%. Any plate material can be used for the sagging region, as the sagging region is not required to redistribute moment and, hence, does not have to behave in a ductile fashion. However, FRP plates are often the preferred option due to their durability and ease of application.

(b) Applied loads

The plating proposal discussed in Section 7.3.2.1(a) increases the static moment from the original unplated static capacity of 72 kNm to 88 kNm, that is by 22%, which means that the applied loads can be increased by 22% from 22.9 kNm (Section 7.3.1.1(b)) to 27.9 kN/m. We will assume that this 22% increase in the overall capacity is due to an additional live load. Hence at failure of the plated beam, the dead load remains at 10.4 kN/m (Section 7.3.1.1(b)), whereas, the live load increases to 27.9-10.4=17.5 kN/m, that is the live load is 62% of the total load at ultimate. It is also worth noting that the increase in live load is 40%.

7.3.2.2 Option 1: Hinge approach, FRP plates in sagging region

(a) Flexural capacity (IC debonding)

We need to increase the sagging capacity from 31 kNm to 47 kNm (Section 7.3.2.1(a)). We are using the hinge approach so that the IC debonding strains are restricted to those from pull tests which are ε_{db} = 0.00267 (Section 7.3.1.4(b)). The beam is to be plated as unpropped, in which case the residual stresses due to the dead load are ε_{res} = 0.00067 (Section 7.3.1.3(b)). The concrete material properties are given in Fig. 7.5(e) where the crushing strain of the concrete ε_c = 0.003.

The flexural analysis (Section 3.4.2.1 and Fig. 3.36) is illustrated in Fig. 7.7 where the pivotal point in Fig. 7.7(b) is taken to be the strain in the RC beam at plate debonding $(\varepsilon_{pivot})_{RC}$ = 0.00267+0.00067 = 0.00334. The depth of the neutral axis d_n is varied in the analysis. For each position of d_n, the strain profile Fig. 7.7(b) and consequently the stress profile Fig. 7.7(c) is fixed. Hence, the force in the concrete F_c and reinforcing bars F_s are now known. Therefore as the sum of the forces equals zero, from longitudinal equilibrium, the required force in the plate F_p can be determined. Taking moments of the forces in Fig. 7.7(d) about any convenient axis gives the moment capacity. The neutral axis depth d_{na} is varied until the required capacity of 47 kNm is achieved. From the analysis in which the moment capacity is achieved F_p is known and as ε_{db} and, hence, σ_{db} is fixed, the cross-sectional area of the plate required can be determined.

The results of the flexural analysis are given in row 1 of Table 7.2. The bars have yielded, as the strain in the reinforcing bars ε_{bar} = 0.00249 is greater than the yield strain of 0.002. The maximum strain in the concrete $(\varepsilon_c)_{max}$ = 0.00091 is much less than the crushing strain of 0.003. In fact, the depth of the rectangular stress block, d_y in Fig. 7.7(c), is negative in Table 7.2, which shows that the concrete remains in the pseudo elastic range. It can be seen that plate debonding can occur well before the concrete crushes.

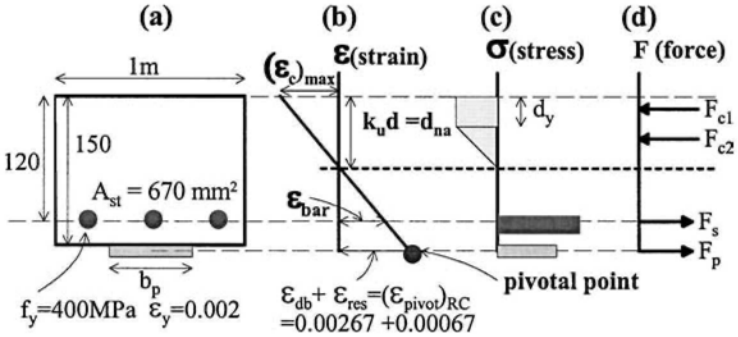

Figure 7.7 Flexural analysis of FRP plated slab in sagging region

From Table 7.2, the width of CFRP plate required is b_p = 198 mm, say 200 mm, for every meter width of slab. This plate has to extend between the points marked O in Fig. 7.6(b) which is the zone where the moment capacity has to be greater than that of the unplated section. The length of the plate required for flexure can be determined from Eq. 7.2, with M_x = +31 kNm, M_h = -41 kNm and w = 27.9 kN/m, and the plate extended at least a further effective length L_e = 187 mm (Section 7.3.1.4(b)) to ensure the plate is fully anchored as shown in Fig. 7.8(c).

Table 7.2 Plating sagging region only - unpropped

Details	$(\varepsilon_{pivot})_{RC}$	$k_u d$ [mm]	ε_{bar}	$(\varepsilon_c)_{max}$	d_y [mm]	F_p [kN]	b_p [mm]	M_{cap} [kNm]
1) FRP hinge	0.00334	32	0.00249	0.00091	-3.33	102	198	47.9
2) FRP anch.	0.00534	27	0.00404	0.00117	3.97	127	141	47.6
3) Steel hinge	0.02067	19	0.0159	0.00291	12.1	123	136	47.6

Figure 7.8 shows the sagging region of the plated beam. The length of the sagging region can be derived from Eq. 7.1 with w = 27.9 kN/m and M_h = -41 kNm. The stress resultants in Fig. 7.8(a) are from the *redistributed for plated beam* curve C in Fig. 7.6. The plate has to extend to where the applied moment is equal to the unplated strength of 31 kNm and then extended an effective length for anchorage as shown in Fig. 7.8(c). It can be seen that 69% of the sagging region has to be plated for flexure, this percentage includes the effective length required for full anchorage.

(b) Shear capacity (CDC debonding)

As the uniformly distributed load at failure of the plated beam is 27.9 kN/m (Section 7.3.2.1(b)), the maximum shear load in the sagging region of the plated beam at flexural failure is 51 kN as shown in Fig. 7.8(a). The concrete shear capacity of the unplated sagging region from a national standard is $(V_c)_{code}$ = 108 kN (Section 7.3.1.3(b)). As the concrete shear capacity of 108 kN is much greater than the maximum applied shear of 51 kN in Fig. 7.8(a), a critical diagonal crack will not form in the plated structure, that is CDC debonding will not occur. Hence, the extent of plating for CDC debonding required in the sagging region is shown as zero in Fig. 7.8(d). It is worth bearing in mind that plating will increase the concrete shear capacity above that of the unplated section of $(V_c)_{code}$ = 108 kN, which further increases the safety factor against CDC debonding. It may also be worth noting that if CDC debonding did control the extent of plating, then the plate may have to be extended by h/2 + L_e as shown in Fig. 5.10(e) or by just h/2 as in Fig. 5.10(f); the latter is the preferred option. However in this example, CDC debonding does not control the extent of plating but the additional lengths are represented in Fig. 7.8(d) just to remind the reader.

(c) Plate extent (PE debonding)

Unlike CDC and IC debonding which depend on the total load being applied at a section, PE debonding only depends on the load or shrinkage applied after plating. In this example, the beam is being plated as unpropped, so it will be assumed that the additional load after plating is only due to the live load of 17.5 kN/m which is 62% of the total applied load (Section 7.3.2.1(b)); this live load induces a moment which is shown as the curve *ultimate live load moment in plated beam* in Fig. 7.8(a). It will also be assumed that there is negligible concrete shrinkage after plating; if shrinkage had occurred after plating then it could have been allowed for using Eq. 6.5.

From Eq. 6.12, the moment at the plate end to cause debonding is M_{PE} = 29.0 kNm. Hence, it is a simple procedure to extend the plate in Fig. 7.8(e) until the applied moment at the plate end due to the live load only is less than or equal to M_{PE}. The position of M_{PE} can be derived from Eq. 7.2 where w is the live load w = 17.5 kNm, and the hogging moment M_h is due to the live load only, hence, M_h=(-0.62x41) The sagging moment is 0.62x47 = 29.1kNm, which is basically M_{PE}; theoretically, PE debonding will not occur so that the plate can be terminated anywhere along the sagging region. It may be worth noting that if the plate extent for PE debonding, $L_{PE}/2$, had been greater than zero there is no need to extend the plate an additional effective length of L_e as the plate end does not have to be anchored for PE debonding.

Furthermore, it is felt that it is not necessary to extend the plate a further distance h/2 as we are not dealing with the vagaries of the position or shape of critical diagonal cracks. From a comparison of the extent of plating required in Figs 7.8(c), (d) and (e), it can be seen that the length of plate required is controlled by the flexural strength requirements in Fig. 7.8(c).

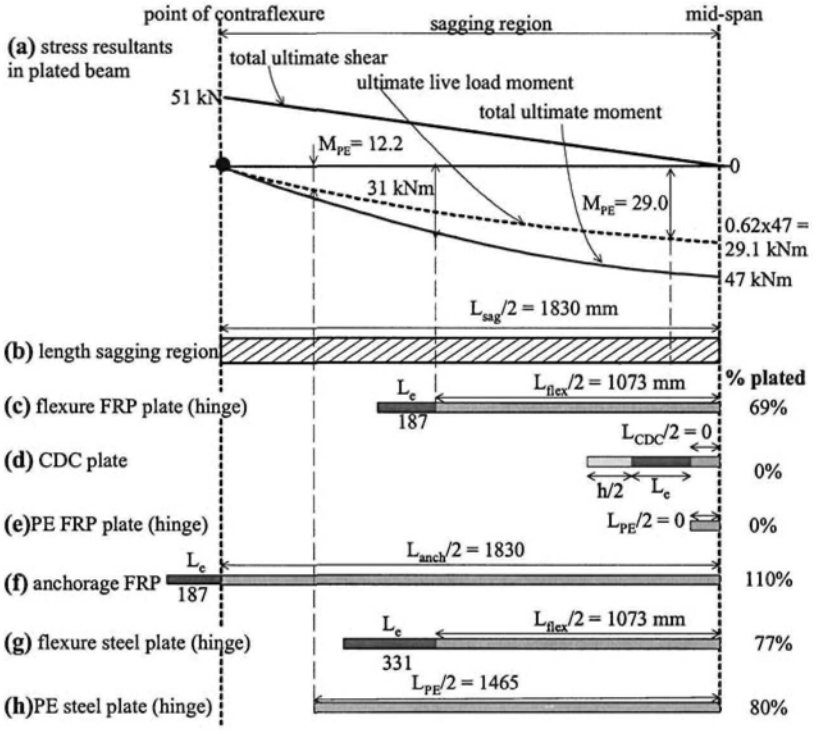

Figure 7.8 Extent of plating in sagging region – plated slab

It may be worth noting that in deriving M_{PE} from Eq. 6.12, the short term flexural rigidity for the cracked plated section was calculated as 1.85×10^{12} Nmm^2. This can be compared with that of the unplated section of 1.31×10^{12} Nmm^2 (Section 7.3.1.3(b)). Hence, the plating has increased the flexural stiffness by 41% which is an indication of the effect of plating on the deflections.

7.3.2.3 Option 2: Anchorage approach, FRP plates in sagging region

(a) Flexural capacity (IC debonding)

It is required to increase the sagging capacity from 31 kNm to 47 kNm (Section 7.3.2.1). As we are using the anchorage approach, the IC debonding strain can be increased to ε_{db} = 0.00467 (Section 7.3.1.4(b)). The beam is also to be plated as unpropped, in which case the residual stresses due to the dead load are ε_{res} = 0.00067 (Section 7.3.1.3(b)).

The flexural analysis is the same as in Fig. 7.7 except that the pivotal point now occurs at $(\varepsilon_{pivot})_{RC}$ = 0.00467+0.00067 = 0.00534. The results for this anchorage approach are given in row 2 of Table 7.2 and are worth comparing with those in row 1

which are the results for the hinge approach. It can be seen that using a larger plate debonding strain in the anchorage approach has substantially increased the strain in the reinforcing bars ε_{bar} so that there is little chance of IC debonding prior to the reinforcing bars yielding. There is a marginal increase in the concrete strains $(\varepsilon_c)_{max}$ but they are still well below the crushing strain of 0.003. The width of plate required has reduced from 198 to 141 mm per meter width of slab. The extent of plating required for flexure would be the same as that in the previous example shown in Fig. 7.8(c), as both the distribution of applied moment and the increase in the flexural strength are the same. However, this is irrelevant for the anchorage approach as, to achieve the increased plate strains, the plate has to be anchored beyond the point of contraflexure as shown in Fig. 7.8(f).

(b) Shear capacity (CDC debonding)

Even though the plate has been extended beyond the point of contraflexure in Fig. 7.8(f) and into the hogging region, the shear at the plate end of 56 kN is still considerably less than the concrete shear capacity $(V_c)_{code}$ of the hogging region of 119 kN (Section 7.3.1.3(a)). Hence CDC debonding will not occur.

(c) Plate extent (PE debonding)

The plate end has been terminated slightly beyond the point of contraflexure on the compression face of the hogging region to allow the plate to be fully anchored. Hence the plate end is now subject to some curvature, so Eq. 6.14, for compression face plates, could be used to determine the moment at the plate end to induce PE debonding. However, the combination of thin FRP plates, termination in a region of low curvature and in a compression face would suggest that PE debonding is very unlikely to occur.

As confirmation of the assumption above. From Eq. 7.2, the moment at the plate end is –6.3 kNm. A lower bound to the resistance to PE debonding can be derived by using the flexural rigidity of the cracked unplated section of 1.66×10^{12} Nmm^2 (Section 7.3.1.3(a)) into Eq. 6.14; this is a lower bound as plating will increase the flexural rigidity. This gives a PE capacity of –59 kNm which is much greater than the applied moment of –6.3 kNm. Hence PE debonding will not occur and, more importantly, there should be no interaction between PE and IC debonding in the anchorage zone.

7.3.2.4 Option 3: Hinge approach, steel plates in sagging region

(a) Flexural capacity (IC debonding)

It is required to increase the sagging moment capacity from 31 kNm to 47 kNm (Section 7.3.2.1).

Based on pull test results (as this is a hinge approach), a steel plate thickness of 3 mm was chosen so that the plate yields prior to IC debonding (Section 7.3.1.4 (c)). This means that if this steel plate was bonded to a concrete block and tested in a pull test as in Fig. 2.11, the plate above the block would yield and eventually fracture at very high strains without IC debonding, so that the strain at failure could be considered to be very large. However, this does not always occur in beams, as it has been found in beam tests that the plates do detach after yielding has occurred due to IC debonding. The beam test results in row 7 of Table 7.1 show that, in beams with 3 mm thick steel plates, IC debonding does occur after yield at strains that ranged from 0.0044 to 0.0213. To demonstrate the effect of very high debonding strains, we will

assume in this analysis that the debonding strain is 0.02. The residual stress remains at $\varepsilon_{res} = 0.00067$ (Section 7.3.1.3(b)).

The flexural analysis is also depicted by Fig. 7.7 expect that the pivotal point is now at $(\varepsilon_{pivot})_{RC} = 0.020 + 0.00067 = 0.02067$ and the results are given in row 3 of Table 7.2. The reinforcing bars have now well and truly yielded and it is also interesting to note that the maximum strain in the concrete has almost achieved the crushing strain of 0.003. However, even with such a large pivotal strain of 0.02067, the concrete has not crushed which suggests that it will rarely crush prior to debonding in practice. The plate width required is 136 mm per meter width of slab. The extent of plating for flexure is shown in Fig. 7.8(g) and is the same as for the FRP plate in Fig. 7.8(c) except that the anchorage length has increased from 187 mm for the FRP plate to 331 mm for the steel plate.

(b) Shear capacity (CDC debonding)

As in Options 1 and 2 in Sections 7.3.2.2 and 7.3.2.3, the shear load to cause a critical diagonal crack is much larger than the applied shear so that CDC debonding will not occur.

(c) Plate extent (PE debonding)

It can be seen in Eq. 6.12, that because the steel plate is thicker than the FRP plates in Options 1 and 2 and because the Young's modulus of the steel plate is larger than that of the FRP plate, the moment to cause PE debonding reduces for the steel plate in comparison to that of the FRP plate. Hence, the steel plate will have to be terminated closer to the point of contraflexure. From Eq. 6.12, $M_{PE} = 12.2$ kNm which requires a half plated length of 1465 mm, that is 80% of the length of the sagging region as shown in Fig. 7.8(h). A comparison of the extent of plating required in Figs 7.8(d), (g) and (h) shows that PE debonding now controls the extent of steel plating which is in contrast to Option 1 shown in Figs 7.8 (c), (d) and (e) where PE debonding did not control the extent of FRP plating.

The 3 mm steel plate increased the flexural rigidity of the cracked section from 1.31×10^{12} Nmm^2 (Section 7.3.1.3(b)) to 2.42×10^{12} Nmm^2 which is an 85% increase as compared with the 41% increase with the FRP plates in Options 1 and 2.

7.3.2.5 Comparison of plating procedures

The three options to plating the sagging region only, in Sections 7.3.2.2 to 7.3.2.4, are compared in Table 7.3. In row 5, is the volume of plate material required which could be considered to be a measure of the material and handling costs; in row 6, this volume is given in terms of the volume in the first option in column 2. In row 7, is the surface area of the interface between the plate and the slab which can be considered to be a measure of the surface preparation required and also the amount of adhesive required; this is given in row 8 as a proportion of the interface area in column 2.

The hinge approach with FRP plates in column 2 in Table 7.3 can be compared with the anchorage approach with FRP in column 3. The hinge approach requires a greater cross-sectional area of plate than the anchorage approach, but the hinge approach requires a shorter length of plate than the anchorage approach. The outcome is that the anchorage approach needs a slightly greater volume of FRP and volume of adhesive and area of surface preparation.

Let us compare the hinge approach with FRP plates in column 2 with the hinge approach with steel plates in column 4. The volume of steel plates is about twice that required for FRP plates which suggests that the handling costs are greater.

However, the steel plates are probably still less expensive than FRP plates, but they do need more surface preparation such as sand blasting. The steel plates have a smaller interface area suggesting less concrete preparation and adhesive.

Table 7.3 Results of plating sagging region only

(1)	(2) Option 1	(3) Option 3	(4) Option 3
(1) Design approach	Hinge	Anchorage	Hinge
(2) Plate	1.2 mm FRP	1.2 mm FRP	3 mm steel
(3) b_p [/m]	200 mm	145 mm	140 mm
(4) L_p (length of plate)	2520 mm	4034 mm	2930 mm
(5) V_p [/m] (plate volume)	604,800 mm^3	701,900 mm^3	1,230,600 mm^3
(6) ratio of V_p	1	1.16	2.03
(7) A_{int} [/m] (interface area)	0.504 m^2	0.585 m^2	0.410 m^2
(8) ratio of A_{int}	1	1.16	0.81

The differences between all three options in Table 7.3 are not great, which suggests that other considerations such as durability, application and ductility may have a much greater influence on choosing the material and design procedure.

7.3.3 *Plating -ve region only (redistribution from unplated +ve region)*

In this example, we will assume that access is only available to plate the hogging regions of continuous slabs. We will assume that further increases in shrinkage after plating will be minimal and that FRP plates are the preferred option as well as unpropped construction. The hinge and anchorage approaches will be applied.

7.3.3.1 Strengthening option based on moment redistribution

(a) Moment redistribution

The FRP plated slab is shown in Fig. 7.9(a). We will assume that FRP plated regions cannot redistribute moment (Section 3.3.1). Therefore, a hinge can only form in the unplated sagging region. The question is how much can we increase the overall capacity of the slab.

The moment distribution in the unplated beam at failure is shown as curve A in Fig. 7.9(b). On loading the unplated beam and because the hogging moment capacity of 41 kNm is less than twice the sagging moment capacity of 31 kNm, a hinge will first form in the hogging region. The only way to prevent a hinge first forming in the hogging region after it has been plated with FRP is to plate the hogging region so that the strength of the plated hogging region is at least twice the strength of the sagging region, that is 62 kNm; this is shown as curve B in Fig. 7.9(b). Curve B represents the minimum strengthening option for the hogging region. If the hogging region were strengthened to less than the minimum requirement of 62 kNm, then a hinge would first form in the FRP plated hogging section whose rotational capacity would not be sufficient to allow the sagging region to reach its ultimate capacity. Hence plate debonding would occur before the theoretical overall capacity of the beam was achieved. Curve B is the minimum strengthening requirement which will achieve a static moment of 31+62 = 93 kNm which is a 29% increase over the unplated static moment capacity.

The strength of the hogging region can be increased above the minimum requirement of 62 kNm in Fig. 7.9(b), as making it stronger will ensure that the hinge first forms in the sagging region. The question is what is the maximum theoretical capacity. The neutral axis depth factor for the unplated sagging region is $k_u = 0.10$ (Section 7.3.1.3(b)) and for which, from Fig. 3.14, most national standards will allow

30% redistribution, which is what we will use here. For the sagging region to redistribute 30% of its moment, will require the elastic moment at the sagging region to be 31/0.7 = 44 kNm. This is one point on the elastic distribution curve C in Fig. 7.9(b) but it also fixes the curve as the maximum hogging moment capacity must be twice the sagging capacity, that is 88 kNm. The static moment capacity of curve C is 44+88 = 132 kNm. Moving curve C upwards to allow for the 30% redistribution from the sagging region gives curve D.

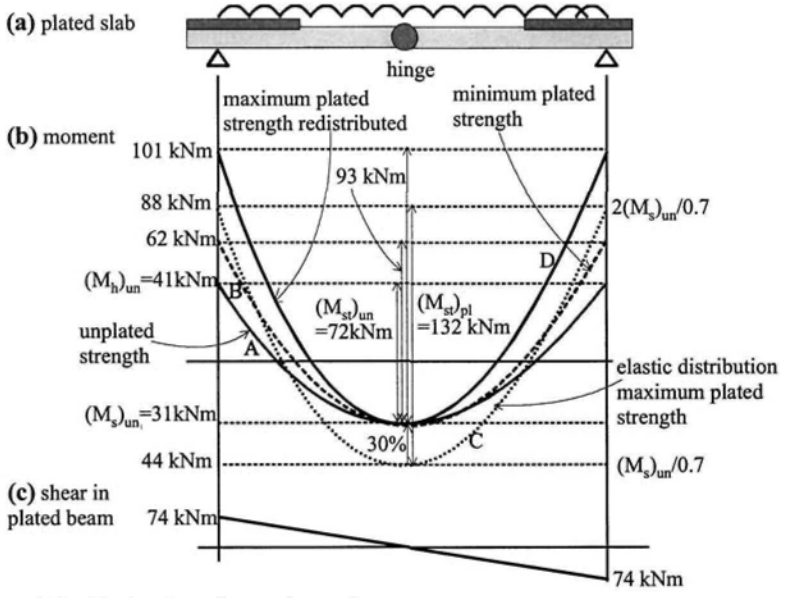

Figure 7.9 Plating hogging region only

Curve D in Fig. 7.9(b), where the hogging capacity is 101 kNm, represents the maximum strengthening that can occur. To verify this statement, let us consider what would happen if the hogging capacity had been increased from 101 kNm to say 122 kNm. The static moment is now 122+31 = 153 kNm, so that the elastic sagging moment is now 153/3 = 51 kNm. To go from the elastic sagging moment of 51 kNm to the sagging strength of 31 kNm requires (51-31)/31 = 65% moment redistribution in the sagging region, which is greater than its capacity of 30%.

The maximum theoretical increase in the static moment of the slab that can be achieved by plating is, therefore, 132-72 = 60 kNm, which is an 83% increase in the static capacity; this requires the hogging capacity to be increased by plating by 101-41 = 60 kNm, that is by 146%. This maximum increase of 83% can be compared with the minimum increase in strengthening of 29% which requires the hogging capacity to be increased by 88-41 = 47 kNm that is by 114%. In this example, we will increase the strength by the minimum requirement of 29% as at this stage of the design it is felt that it would be impractical to increase the hogging strength by 146% as will be discussed later.

(b) Applied loads

The plated static moment of 93 kNm in Fig. 7.9(b) requires a uniformly distributed load of 29.8 kN/m. As the dead load is 10.4 kN/m (Section 7.3.1.1(b)), this plating

option will allow an ultimate live load of 29.8-10.4 = 19.4 kN/m which is 65% of the total load and which is a 55% increase in the live load which may be considered to be substantial.

7.3.3.2 Option 4: Hinge approach, FRP plates in hogging region

(a) Flexural capacity (IC debonding)

The aim is to increase the hogging capacity from 41 kNm to 62 kNm using 1.2 mm thick carbon FRP plates and unpropped construction. The IC debonding strain is ε_{db} = 0.00267 (Section 7.3.1.4(b)) and the residual stress in the hogging section is ε_{res} = 0.00103 (Section 7.3.1.3(a)). The analysis is illustrated in Fig. 7.10 where for a specific depth of neutral axis the required force in the plate F_p is first established and then the moment in the cross-section determined; the neutral axis depth is varied until the required moment capacity is achieved. A detailed description of the analysis procedure is given in Section 7.3.2.2(a).

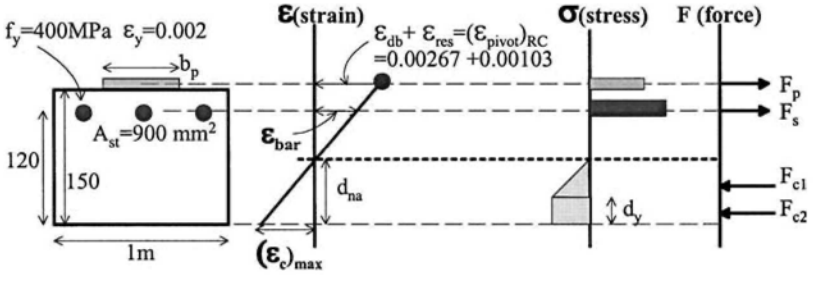

Figure 7.10 Flexural analysis of FRP plated slab in hogging region

The results of the analyses are given in row 1 in Table 7.4 where it can be seen that the reinforcing bars have yielded and the maximum strain in the concrete is well below its crushing strain. The width of plating required is 328 mm per meter width, say 330 mm, and this is required to increase the flexural capacity of the slab from 41 to 62 kNm per meter width in Fig. 7.9(b). Extrapolating this increase in strength would suggest that to increase the capacity to the maximum theoretically allowable of 101 kNm would require thicker plates and hence would be very inefficient and impractical.

Table 7.4 Plating hogging region only - unpropped

Details	$(\varepsilon_{pivot})_{RC}$	$k_u d$ [mm]	ε_{bar}	$(\varepsilon_c)_{max}$	d_y [mm]	F_p [kN]	b_p [mm]	M_{cap} [kNm]
1) FRP hinge	0.00370	36	0.00273	0.00117	5.3	168	328	62.0
2) FRP anch.	0.00570	31	0.00426	0.00149	10.1	164	183	62.1

The extent of plating required for flexural strengthening is illustrated in Fig. 7.11(c). The plate is extended to where the applied moment is equal to the moment capacity of the unplated section of 41 kNm as shown in Fig. 7.11(a) and extended a further distance of the effective length to ensure that it is fully anchored.

(b) Shear capacity (CDC debonding)

The total vertical shear force in the plated beam at failure varies from 43 kN to 74 kN in the hogging region as shown in Fig. 7.11(a). This shear force is considerably less

than the concrete shear capacity of the unplated slab from a national standard $(V_c)_{code}$ = 119 kN (Section 7.3.1.3(a)). Hence CDC debonding will not occur.

(c) Plate extent (PE debonding)

From Eq. 6.12, the moment at the plate end to cause PE debonding is M_{PE} = 38.8 kNm. This is the moment induced in the beam after plating. The ultimate live load to cause failure is 29.8-10.4 = 19.4 kN/m (Section 7.3.3.1(b)), which is 65% of the total load, and is shown as the *live load moment* in Fig. 7.11(a). It is this *live load moment* that occurs after plating which induces PE debonding and, hence, the plate should be terminated where M_{PE} is equal to this live load moment as shown in Fig. 7.11(a). The maximum live load moment is 0.65x62 = 40 kNm and, hence, for all intents and purposes PE debonding will not occur. From Eq. 7.2, the extent of plating required is 16mm. A comparison of Figs 7.11(c), (d) and (e), indicates that the extent of plating is governed by the flexural strengthening requirements.

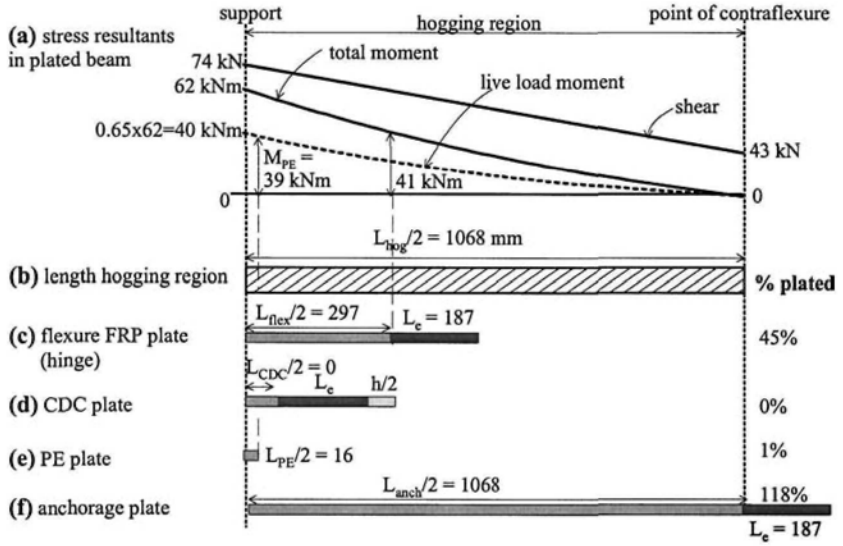

Figure 7.11 Extent of plating in hogging region – FRP plated slab

7.3.3.3 Option 5: Anchorage approach, FRP plates in hogging region

(a) Flexural capacity (IC debonding)

The aims are the same as in Section 7.3.3.2(a) except that the anchorage approach is now being applied, so that an IC debonding strain of 0.00467 (Section 7.3.1.4(b)) can be used with the residual strain of 0.00103 to give a pivotal strain of 0.00570 in Fig. 7.10. The results of the analyses are given in row 2 of Table 7.4. It can be seen that the use of an increased debonding strain has substantially increased the reinforcing bar strain when compared with the hinge approach in row 1 but has only a minor effect on the maximum concrete strain which is still well below its crushing capacity. The anchorage approach has reduced the width of plate required from 328 mm, in the hinge approach, to 183 mm, in the anchorage approach. Because of the narrower width of plate required in the anchorage approach, the anchorage approach is much more capable of achieving, or at least getting closer to, the theoretical maximum increase in the capacity of 101 kNm in Fig. 7.9 than the hinge approach.

(b) Shear capacity (CDC debonding)
The same conclusions as in Section 7.3.3.2(b); CDC debonding will not occur.

(c) Plate extent (PE debonding)
Plate end debonding is unlikely to occur because of the use of thin FRP plates, termination on a compression face, and termination adjacent to point of contraflexure as in Fig. 7.11(f).

7.3.3.4 Comparison of plating procedures
The amount of plating required in the hinge and anchorage approaches in Options 4 and 5 are compared in Table 7.5. The anchorage approach tends to require a larger volume of FRP and adhesive and a greater area of surface needs to be prepared. However the quantities we are dealing with are quite small as the hogging region itself is quite small.

Table 7.5 Results of plating hogging region only

(1)	(2) Option 4	(3) Option 5
1) Design approach	2) Hinge	3) Anchorage
2) Plate	1.2 mm FRP	1.2 mm FRP
3) b_p [/m]	330 mm	185 mm
4) L_p (length of plate)	968 mm	2510 mm
5) V_p [/m] (plate volume)	383,330 mm^3	557,220 mm^3
6) ratio of V_p	1	1.45
7) A_{int} [/m] (interface area)	0.319 m^2	0.464 m^2
8) ratio of A_{int}	1	1.45

7.3.4 ***Plating -ve and +ve regions (redistribution from -ve region)***
In the previous five options in Sections 7.3.2.2 to 7.3.2.4, 7.3.3.2 and 7.3.3.3, plating was deliberately restricted to one region, that is either the hogging region or the sagging region. This allowed a hinge to form in the unplated region so that the neutral axis depth factor approach in national standards (Section 3.3.1) could be used to control the amount of moment redistribution that could occur.

We will now look at plating both the hogging and sagging regions. In this example in this section, we will use steel plates in the hogging region where moment redistribution is required and FRP plates in the sagging region where it is not. We will design the steel plated regions so that the steel plates yield before debonding and make the assumption that these steel plated regions can be treated as ordinary RC sections where the neutral axis depth factor controls moment redistribution (Section 3.3.1). Then in Section 7.3.4.4 we will check, using the flexural rigidity approach (Section 3.3.2), whether the moment redistribution allowed using the neutral axis factor can be achieved.

7.3.4.1 Strengthening option based on moment redistribution
(a) Moment redistribution
The plated slab is shown in Fig. 7.12(a). It will be assumed that the use of FRP plates in the sagging region precludes the formation of a hinge in this region. Steel plates will be used in the hogging region and will be designed to yield before debonding and, hence, it will be assumed that hinges can form in the hogging regions and that the neutral axis depth approach for moment redistribution can be used.

In theory, virtually any amount of strengthening can be achieved by simply adding more and more plates to each region. The following suggesting is, therefore,

one of numerous solutions. The question is, what would be considered to be an efficient form of plating. As we are going to treat the steel plated hogging region as an RC section, then it may be a good idea to minimise the strengthening of the hogging regions so that they can still redistribute 30% of their elastic moment. Using Fig. 3.14 as a guide, we will assume that we can get 30% redistribution if the neutral axis depth factor $k_u = 0.2$. The analysis based on $k_u = 0.2$ is given in Section 7.3.4.2(a). From this analysis, the capacity of the steel plated hogging region is $(M_h)_{pl} = 61$ kNm which is shown in Fig. 7.12(b).

As the plated hogging capacity in Fig. 7.12(b) is $(M_h)_{pl} = 61$ kNm and as it is assumed that this plated hinge can redistribute by 30%, then the elastic moment at the hogging region is 61/0.7 = 87 kNm. This requires an elastic sagging moment of 87/2 = 44 kN and an elastic static moment of 87+44 = 131 kNm as shown in curve B. Allowing the hogging region to redistribute by 30% drops curve B to curve C where the maximum sagging strength is 70 kNm. Hence, plating both regions and using metal plates where moment redistribution is required increases the static moment by 82% from 72 kNm to 131 kNm. This large increase is feasible as the increase is shared fairly uniformly between the two regions; the hogging strength increasing by 49% from 41 kNm to 61 kNm and the sagging strength by 125% from 31 kNm to 70 kNm.

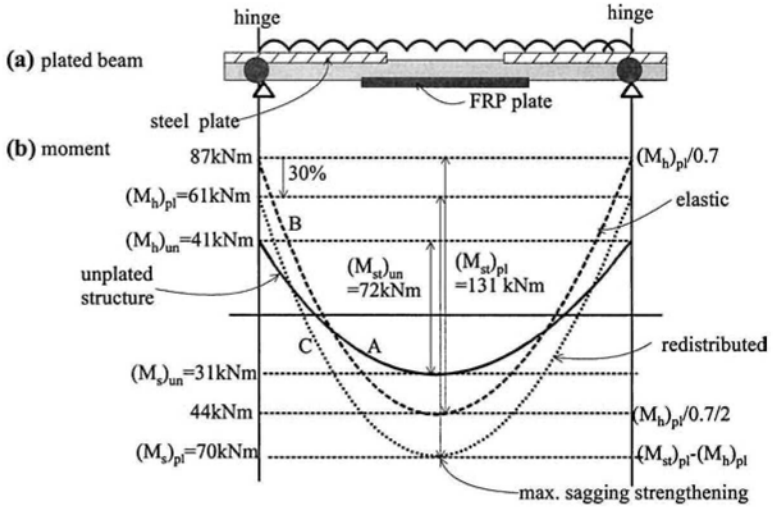

Figure 7.12 Plating hogging and sagging regions – hinge at hogging region

(b) Applied loads

A static moment of 131 kNm requires an ultimate uniformly distributed load of 41.9 kNm. As the ultimate dead load is assumed to be 10.4 kNm (Section 7.3.1.1(b)), the live load is 41.9-10.4 = 31.5 kNm which is 75% of the total load, hence, plating has increased the live load by 152%.

7.3.4.2 Option 6: Steel plating hogging region - hinge approach

(a) Flexural capacity (IC debonding)

The IC debonding strain and residual strain is shown in Fig. 7.13. We are specifically designing for a neutral axis depth of 0.2d to allow 30% redistribution. Hence d_{na} in

Fig. 7.13 is now fixed at 0.2x120 = 24 mm as shown. At this stage we do not know whether concrete crushing will precede plate debonding or vice versa so that both options need to be checked. If we assume debonding occurs first, then the strain profile in Fig. 7.13 goes through the debonding strain at point A and the fixed neutral axis depth at B; extrapolating this strain to the concrete compression face gives the maximum strain in the concrete of 0.00383 which is given in row 1 in Table 7.6. As the theoretical maximum concrete strain 0.00383 is larger than the concrete crushing strain of 0.003, this means that concrete crushing will precede plate debonding. Therefore, the strain profile needs to go through points C and B in Fig. 7.13.

Having now found the correct strain profile in Fig. 7.13, the stress profile is now known, bearing in mind the strain in the plate is the strain in the strain profile less the residual strain of 0.00103. From the stress profile, can be determined the force in the reinforcing bars F_s, and that in the concrete F_c; the latter can be determined using a standard rectangular or plastic stress block because the maximum compression strain is 0.003 although the elastic/plastic distribution shown will give almost identical results. As the longitudinal forces must sum to zero, this gives the force in the plate F_p that is required. As the stress in the plate is known, we can derive the area and width of plate required. The results of the analyses are given in row 2 in Table 7.6 and the extent of plating required in Fig. 7.14(c).

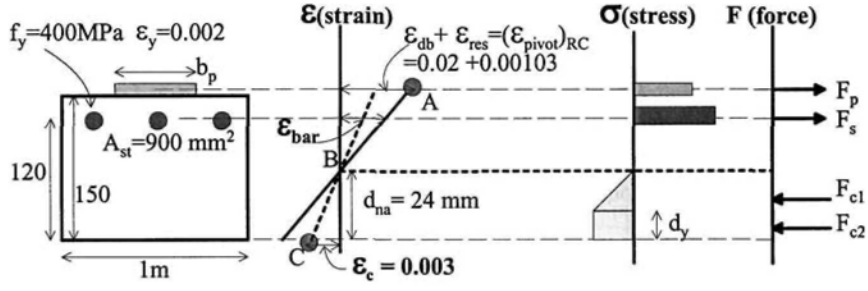

Figure 7.13 Flexural analysis of steel plated slab in hogging region

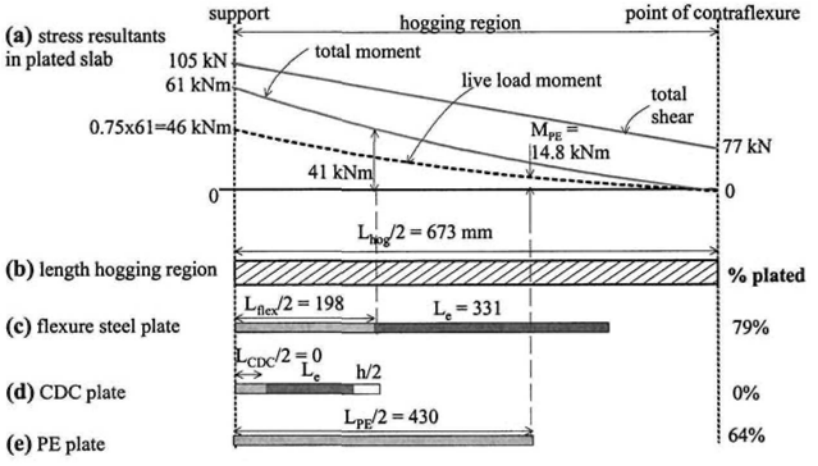

Figure 7.14 Extent of plating in hogging region – steel and FRP plated slab

Table 7.6 Steel plate hogging, FRP plate sagging

Details	$(\varepsilon_{pivot})_{RC}$	$k_u d$ [mm]	ε_{bar}	$(\varepsilon_c)_{max}$	d_y [mm]	F_p [kN]	b_p [mm]	M_{cap} [kNm]
1) Steel hog.	0.02103	24	-	0.00383	-	-	-	-
2) Steel hog.	ε_c=0.003	24	0.0121	0.003	N/A	152	169	61
3) FRP sag.	0.00334	39	0.00243	0.00117	5.7	301	588	70.0

(b) Shear capacity (CDC debonding)

The maximum shear load in the hogging region of 105 kN, as shown in Fig. 7.14(a), is less than the concrete shear capacity of $(V_c)_{code}$ = 119 kN of the unplated section (Section 7.3.1.3(a)). However, as the shear load is approaching the shear capacity of the unplated section, it may be worth determining the increase in the shear capacity due to plating. The simplest approach for estimating the effect of plating is the prestressed code approach in Section 5.2.2.2. For $P_{plate} = F_p$ = 152 kN (Table 7.6), the increase in the concrete component of the vertical shear capacity due to plating is $(V_{incr})_{pp}$ = 0.13(152) = 19 kN (Eq. 5.17), which is a 15% increase in $(V_c)_{code}$. From Eq. 5.18, the vertical shear load to cause CDC debonding is $V_{c\text{-}plate}$ = 119+19 = 138 kN, which is 31% greater than the maximum applied shear load in the hogging region. Hence, it is confirmed that CDC debonding will not occur.

(c) Plate extent (PE debonding)

From Eq. 6.12, M_{PE} = 14.8 kNm. The live load to cause PE debonding of 31.5 kNm is 75% of the total load (Section 7.3.4.1(b)). From Eq. 7.2, the extent of plating is 430 mm as shown in Fig. 7.14(e). Hence the flexural requirement in Fig. 7.14(c) just controls the extent of plating.

7.3.4.3 Option 7: FRP plating sagging region - hinge approach

(a) Flexural capacity (IC debonding)

It is required to increase the sagging capacity from 31 kNm to 70 kNm, as shown in Fig. 7.12(b), using 1.2 mm FRP plates with a pull-test debonding strain of ε_{db} = 0.00267 and on a beam with residual stresses of ε_{res} = 0.00067. The flexural analysis is illustrated in Fig. 7.7 and the steps described in Section 7.3.2.2(a). The results of the analysis are given in row 3 of Table 7.6. The width of FRP plate required is 588 mm per meter width of slab which is not unreasonable as the strength is being more than doubled. The extent of plating for flexure is shown in Fig. 7.15(c).

(b) Shear capacity (CDC debonding)

The vertical shear load within the sagging region, shown in Fig. 7.15(a), is well within the concrete vertical shear capacity of $(V_c)_{code}$ = 108 kNm so CDC debonding will not occur.

(c) Plate extent (PE debonding)

From Eq. 6.12, M_{PE} = 43.7 kNm. The total live load of 31.5 kN/m is 75% of the total load (Section 7.3.4.1(b)). From Eq. 7.2, the extent of plating is 747 mm, as shown in Fig. 7.15(e). It can be seen in Figs. 7.15(c) to (e) that the flexural strengthening requirement determines the extent of plating.

7.3.4.4 Moment redistribution based on flexural rigidity approach

Having designed the plated continuous beam for 30% redistribution from the steel plated hogging region to the FRP plated sagging region, it is now necessary to

determine whether the steel plated hogging region has the rotational capacity or ductility to shed 30% of its elastic moment. The *flexural rigidity approach* of Section 3.3.2 will be used. In the analysis, the sagging FRP region stays linear elastic, that is it follows the path O-A_s-B_s-C_s in Fig. 3.17, whereas the steel plated region moves along the path B_h - C_{deb}. The analysis is fully explained in Section 3.5.4, in which the flexural rigidity in the sagging region in Fig. 3.45(c) is that of O-Cs in Fig. 3.17, and that of the hogging region is the secant flexural rigidity of O-C_{dcb} in Fig. 3.17, that is the flexural rigidity at plate debonding.

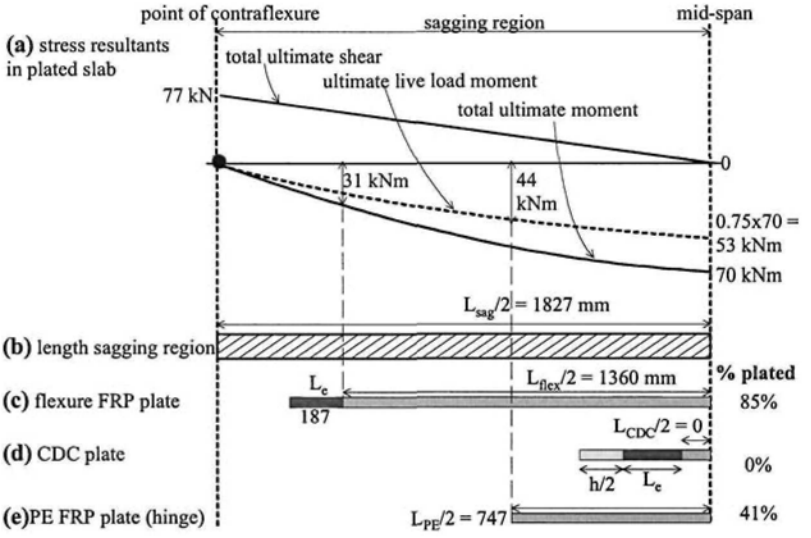

Figure 7.15 Extent of plating in sagging region – steel and FRP plated slab

For any magnitude of applied load, a stiffness analysis program was used to vary the length of the hogging region L_h in Fig. 3.45(c) until it coincided with the position of the point of contraflexure, from which the hogging moment M_h, sagging moment M_s and static moment $M_{static} = M_h + M_s$ is derived. Hence for this continuous beam with a uniformly distributed load, the percentage moment redistribution, %MR, is $(2/3\ M_{static}–M_h)/(2/3\ M_{static})$. The plate strain at debonding ε_{db} was varied; a flexural analysis, such as that depicted by Fig. 7.13, was performed for each debonding strain from which the curvature and moment and, hence, flexural rigidity could be determined for use in the *flexural rigidity approach* of the moment redistribution analysis. The results of the analyses are shown in Fig. 7.16. It can be seen that a debonding strain of about 0.011 is required to achieve 30% redistribution which steel plates can achieve as shown in Table 7.1.

7.3.5 Summary of all plated slab options

The various options for strengthening the slab are summarised in Table 7.7 where L_{pl} = length of plate required; A_{int} = surface area required; ΔM_{st} is the increase in the static moment due to plating. It can be seen that if both regions are plated, then large increases in the overall strength can be achieved particularly if FRP plates are combined with steel plates. The last column, which is the increase in the static

moment divided by the interface area, is an attempt at quantifying the efficiency. Plating the hogging region turns out to be the most efficient simply because the hogging region is shorter than the sagging region so that less plates are required.

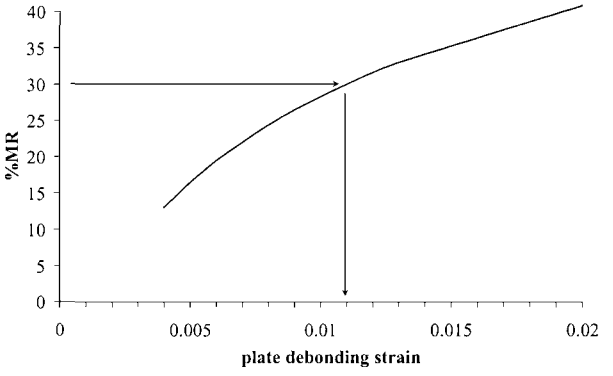

Figure 7.16 Variation in moment redistribution with plate debonding strain

Table 7.7 Results of retrofitting the slab

	Approach	b_p (mm)	$L_{pl}/2$ (mm)	t_p (mm)	$A_{int}/2$ (m^2)	ΔM_{st} /A_{int}
Option 1-3: plating sagging region only with redistribution from hogging ΔM_{static} = 16 kNm (22% increase)	Hinge	200	1260	1.2 FRP	0.274	63
	Anch.	145	2017	1.2 FRP	0.292	55
	Hinge	140	1465	3 steel	0.205	78
Option 4-5: plating hogging region only without redistribution from sagging ΔM_{static} = 21kNm (29% increase)	Hinge	330	484	1.2 FRP	0.160	131
	Anch.	185	1255	1.2 FRP	0.232	91
Option 6-7: plating both regions with redistribution from hogging ΔM_{static} = 59 kNm (82 % increase)	Hinge/hog	170	529	3 steel	0.090	
	Hinge/sag	590	1547	1.2 FRP	0.913	
	Total				1.003	59

7.4 Continuous beam structure with adhesively bonded plates

Section 7.3 dealt with slabs, so that retrofitting was restricted to adhesive bonding tension face plates. As slabs are relatively strong in shear, that is they are much more likely to fail in flexure than form a critical diagonal crack and fail in shear, CDC debonding was shown not to be a problem, which allowed us to concentrate on moment redistribution. Section 7.3 also dealt with residual stresses present prior to plating and their effect on IC debonding, and also on PE debonding and the additional curvature after plating that induces PE debonding.

Section 7.4 will now deal with adhesive bonding plates to RC beams. In contrast to Section 7.3 on slabs: we will assume the beams are propped prior to plating so that there are no residual stresses, which also means that the total applied load will now induce PE debonding; we will retrofit according to the elastic distribution of moment, so that there will be no moment redistribution; dealing with

beams, will allow us to plate the sides of beams as well as their tension faces; as most beams have stirrups, beams are much more likely to form critical diagonal cracks prior to flexural failure, so that CDC debonding can now become a problem and will be dealt with in detail.

The detailed beam specifications are first given. The hinge approach will be used throughout, as plates are adhesively bonded to the sides of the beam and the anchorage approach, as yet, cannot be applied to side plates. The first example uses FRP plates and these are compared with steel plates in the second example.

7.4.1 *Detailed beam specifications*

7.4.1.1 Beam structure

(a) Beam strength

The internal continuous beam is shown in Figs 7.17(a) and (d). We will assume that it is encastre and subjected to uniformly distributed loads. The beam has a hogging capacity of 339 kNm and a sagging capacity of 173 kNm, so that the distribution of moment at ultimate flexural failure is given by the *strength* curve in Fig. 7.17(b) where the static moment is 512 kNm. For all intents and purposes, the *elastic* distribution in Fig. 7.17(b) can be considered to be identical to the strength distribution as the moment redistribution is only 0.6%. Hence, the unplated beam has been designed without moment redistribution.

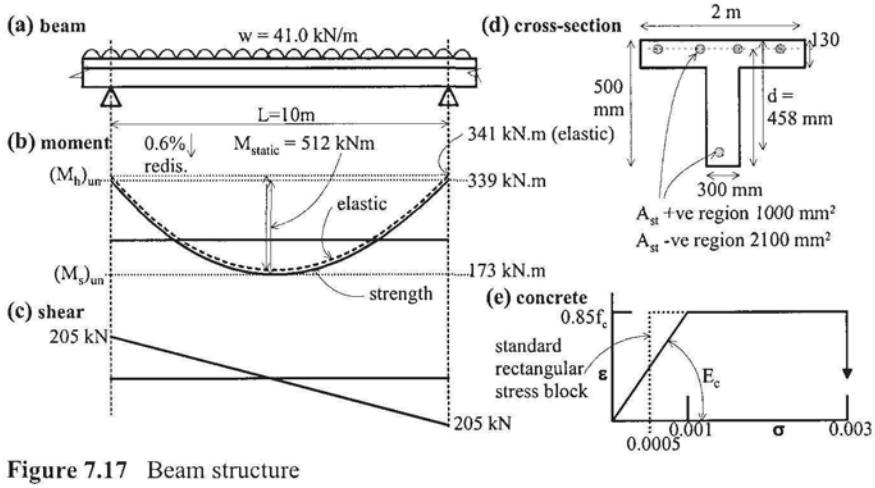

Figure 7.17 Beam structure

(b) Applied loads

The static moment is 512 kNm, which requires a uniformly distributed load of 41.0 kN/m. In the following calculations, there is now no need to break down the ultimate load into live and dead as we are assuming that the beam is propped prior to plating, so that all of the load acts after plating in the PE debonding analyses. Furthermore, as it is propped prior to plating, we can assume that there are no residual stresses to affect the IC debonding calculations, so that there is no need to determine the serviceability loads.

7.4.1.2 Reinforced concrete material properties
These are the same as for the slab in Section 7.3.1.2

7.4.1.3 Unplated beam mechanical properties
(a)Hogging section
Hogging moment capacity $(M_h)_{un}$ = 339 kNm; rigid plastic neutral axis depth as a proportion of the effective depth k_u = 0.29 which for most national standards would not allow much moment redistribution (Fig. 3.14); shear capacity from national standard $(V_c)_{code}$ = 134 kN; assume sufficient stirrups so that $V_s+(V_c)_{code}$ can resist any shear load required; $(I_{cracked})_{short}$ = 1848x10^6 mm^4; $(EI_{cracked})_{short}$ = 4.71x10^{13} Nmm^2.

(b) Sagging section
Sagging moment capacity $(M_s)_{un}$ = 173 kNm; rigid plastic neutral axis depth as a proportion of the effective depth k_u = 0.14 which would allow substantial moment redistribution if so required; shear capacity from national standard $(V_c)_{code}$ = 104 kN; assume sufficient stirrups so that $V_s+(V_c)_{code}$ can resist any shear load required; $(I_{cracked})_{short}$ = 1378x10^6 mm^4; $(EI_{cracked})_{short}$ = 3.51x10^{13} Nmm^2.

7.4.1.4 Plate material properties
These are the same as for the slab in Section 7.3.1.4.

7.4.2 *Hinge approach: FRP side plates in +ve and tension face plates in -ve regions*
7.4.2.1 Strengthening option
We will try and increase the static capacity by 30% from 512 kNm to 666 kNm. As we are maintaining the 2:1 elastic distribution ratio, this will mean increasing the hogging capacity by 30% from 339 kNm to 441 kNm and the sagging moment capacity by 30% from 173 kNm to 225 kNm. To achieve a static moment of 666 kNm, will require an applied load of 53.3 kN/m. As the elastic distribution of moment is being maintained, moment redistribution is not required so that FRP plates can be used anywhere.

7.4.2.2 Option 8: Hinge approach, FRP side plates in sagging region
(a) Flexural capacity (IC debonding)
It is required to increase the sagging capacity from 173 kNm to 225 kNm using 1.2 mm carbon FRP plates with a debonding strain of ε_{db} = 0.00267. As the debonding strain is usually much less than the fracture strain of the FRP plate, the pivotal point is taken as the debonding strain at the level of the bottom of the plate where the strain is the greatest, as shown in the flexural analysis in Fig. 7.18.

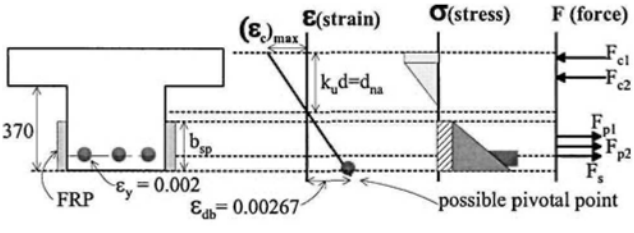

Figure 7.18 Flexural analysis of side FRP plated beam in sagging region

The results of varying the height of the plate, b_{sp} in Fig. 7.18 whilst maintaining the bottom of the plate at the level of the beam soffit, is shown in Table 7.8, where $\varepsilon_{p(top)}$ is the strain at the top level of the plate. A height of plate of 150 mm is required to achieve the moment capacity of 225 kNm which is shown in the row in bold in Table 7.8. The reinforcing bars have yielded but the maximum concrete strain is well below its crushing capacity. The strain at the top of the plate is 66% of the debonding strain. The extent of plating required for flexure is shown in Fig. 7.19(c).

Table 7.8 Results of varying depth of FRP side plate

b_{sp} [mm]	$k_u d$ [mm]	$\varepsilon_{p(top)}$	$(\varepsilon_c)_{max}$	ε_s	M_{cap} [kNm]
50	54.2	0.00237	0.00032	0.00242	198
100	56.6	0.00207	0.00034	0.00242	215
150	**58.5**	**0.00176**	**0.00035**	**0.00242**	**227**
200	60.1	0.00146	0.00036	0.00242	237
250	61.3	0.00115	0.00037	0.00241	243

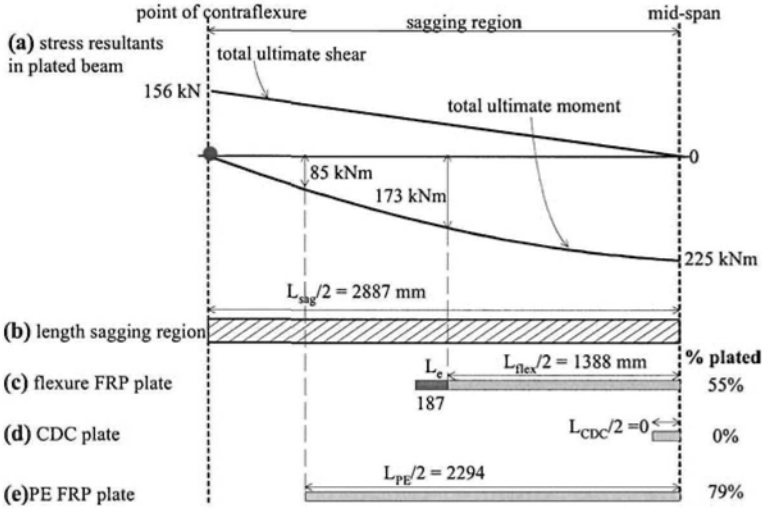

Figure 7.19 Extent of plating in sagging region – FRP side plated beam

(b) Shear capacity (CDC debonding)

The concrete shear capacity for the unplated section from national standards $(V_c)_{code}$ = 104 kN (Section 7.4.1.3(b)) is less than the maximum shear force in the sagging region of 156 kN as shown in Fig. 7.19(a). Hence there is a possibility of CDC debonding.

The results of the iterative CDC analysis are shown in Fig. 7.20 for varying focal point locations z from the point of contraflexure because the location of the CDC in the sagging region is not easily defined with a uniformly distributed load; a more detailed explanation of this type of analysis is described in Section 4.6.2 and Fig. 4.26. It can be seen in Fig. 7.20 that $(V_{dat})_{c\text{-}plate}$ is greater than $(V_{dat})_{applied}$ hence, CDC debonding will not occur in the plated structure. Furthermore, as $(V_{dat})_{c\text{-}unpl}$ is also greater that $(V_{dat})_{applied}$, the CDC analysis suggests that the formation of a CDC will not occur in the unplated beam. This is further demonstrated by comparing the

shear strength of the concrete component of the unplated beam from the CDC analysis, $V_{c\text{-}unpl}$ in Fig. 7.20 and $(V_{max})_{Lo}$, which is the distribution of shear due to the applied load. $V_{c\text{-}unpl}$ exceeds $(V_{max})_{Lo}$ everywhere confirming that a CDC will not occur in the unplated beam. It is interesting to note that $V_{c\text{-}unpl}$ increases near the point of contraflexure where the moment is small. This phenomenon is often indirectly allowed for in national standards by designing for the maximum shear at an effective depth d from the support; whether this should apply to points of contraflexure is debatable. It can be seen that $(V_c)_{code}$ = 104 kN, which is assumed to be constant over the entire sagging region, is less than the applied shear $(V_{max})_{Lo}$ near the point of contraflexure but greater than that near mid-span.

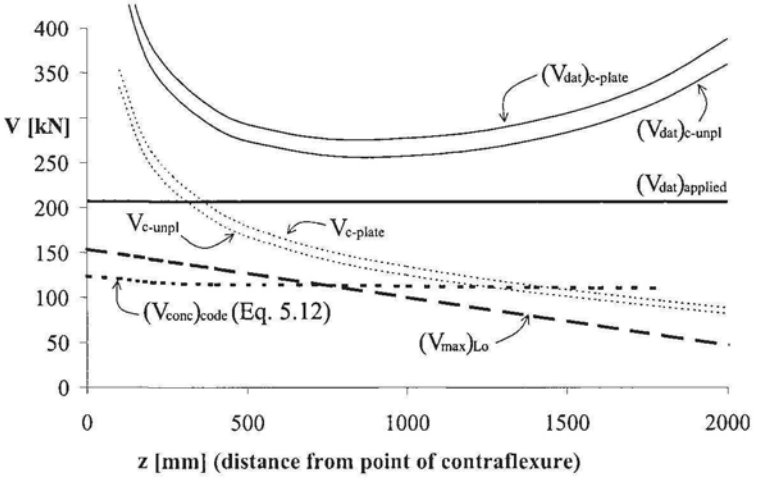

Figure 7.20 Results of CDC analysis for sagging region

The difference between $V_{c\text{-}plate}$ and $V_{c\text{-}unpl}$ in Fig. 7.20 is the increase in the concrete component of the shear capacity due to plating, which can be added to $(V_c)_{code}$ as in Eq. 5.12 to give $(V_{conc})_{code}$ in Fig. 7.20, which shows that CDC debonding would occur as $(V_{conc})_{code}$ is exceeded by $(V_{max})_{Lo}$ near the point of contraflexure. However, at an effective depth d (of approximately 500mm for this beam) from the point of contraflexure at z = 500 mm $(V_{conc})_{code} \approx (V_{max})_{Lo}$ so that CDC debonding may not occur.

To use the simplified *prestressed code approach* described in Section 5.2.2.2, P_{plate} is required. From Fig. 7.18 and Table 7.8, the strain distribution along the side plates is known so that P_{plate} = 128 kN. From Eq. 5.17 the increase in the concrete component of the shear capacity is $(V_{incr})_{pp}$ = 16 kN so that the vertical shear load to cause CDC debonding is 120 kN (Eq. 5.18), which is less than the maximum applied shear in the sagging region at the point of contraflexure (Fig. 7.20) but close to the applied shear at an effective depth from it.

For comparison, the increase in the shear capacity based on the passive prestress approach $(V_{incr})_{pp}$ is shown in Table 7.9 for the side plate depths b_{sp} given in Table 7.8. It can be seen that increasing the depth of a side plate is an effective way of increasing the CDC debonding resistance. In summary, based in particular on the more accurate iterative CDC analysis summarised in Fig. 7.20, CDC debonding will not occur as indicated by the extent of plating shown in Fig. 7.19(d).

Table 7.9 $(V_{incr})_{pp}$ with varying side plate depths

b_{sp} [mm]	P_{plate} [kN]	$(V_{incr})_{pp}$ [kN]	$V_{c\text{-}plate}$ [kN]	$V_{c\text{-}plate}/(V_c)_{code}$
0	0	0	104	1.0
50	48	6	110	1.06
100	91	11	115	1.11
150	**127**	**16**	**120**	**1.15**
200	158	20	124	1.19
250	183	23	127	1.22

(c) Plate extent (PE debonding)

Equation 6.10 gives the plate end debonding capacity for the side plates as 85.0 kNm. For this plated section: K = 0.81; $(EI)_{cr,pl} = 4.31 \times 10^{13}$ Nmm^2 which is a 23% increase over the unplated stiffness (Section 7.4.1.3(b)); $f_{cb} = 2.7$; $E_p = 160$ GPa; $t_{sp} = 1.2$ mm; and $d_{sp} = 362$ mm. Because this beam is propped prior to plating, all of the applied load acts on the plated section to induce PE debonding. Hence, the extent of plating is governed by the total moment as shown in Figs 7.19(a) and (e).

7.4.2.3 Option 9: Hinge approach, FRP tension face plates in hogging region

The aim is to increase the flexural capacity of the hogging region from 339 kNm to 441 kNm using 1.2 mm FRP plates on the tension face.

(a) Flexural capacity (IC debonding)

The flexural analysis is illustrated in Fig. 7.21 where the depth of the neutral axis was varied until the required moment capacity was achieved. When the depth of the neutral axis was $k_u d = 205$ mm in Fig. 7.21: the moment capacity was 449 kNm; this required a plate width of 600 mm; the strain in the reinforcing bars was 0.00229; and the maximum strain in the concrete was 0.00186. The extent of plating required is shown in Fig. 7.22(c).

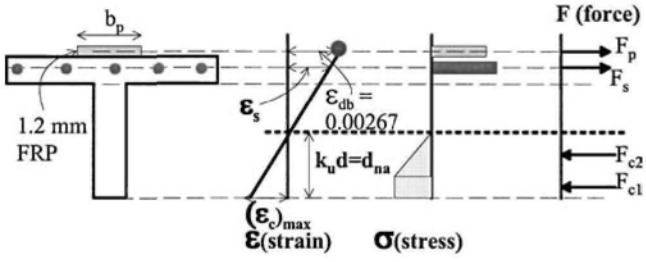

Figure 7.21 Flexural analysis of tension face plated beam in hogging region

(b) Shear capacity (CDC debonding)

The concrete shear capacity of the unplated section from national standards is $(V_c)_{code}$ = 134 kN (Section 7.4.1.3(a)) is less than the shear force in the hogging region as shown in Fig. 7.22. Hence there is a possibility of CDC debonding.

For convenience in the CDC analysis, the datum point will be taken at the point of contraflexure so that $M_{dat} = K_M = 0$, and $V_{dat} = 156$ kN from Fig. 7.22 and K_W is defined by Eq. 5.3, which varies depending on the orientation of the crack as illustrated in Fig. 5.3(c). In this calculation K_W can be taken as Eq. 4.17 and in this analysis the focal point is taken at the position of the support. From Eqs 5.1 and 5.5, the loads to cause cracking and crack sliding, respectively, are calculated using a

spreadsheet analysis and are given by the solid curves in Fig. 7.23 for the plated beam where P_{plate} = 128 kN based on the debonding strain shown in Fig. 7.21. Based on this analysis, $[(V_{dat})_{crit}]_{pl}$ = 112 kN, which is less than V_{dat} = 156 kN and hence, CDC debonding will occur prior to achieving the desired increase in flexural strength.

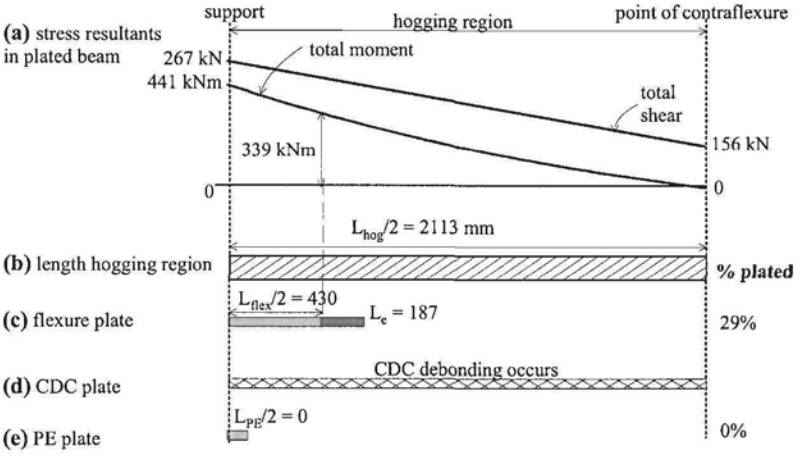

Figure 7.22 Extent of plating in hogging region – FRP tension face plated beam

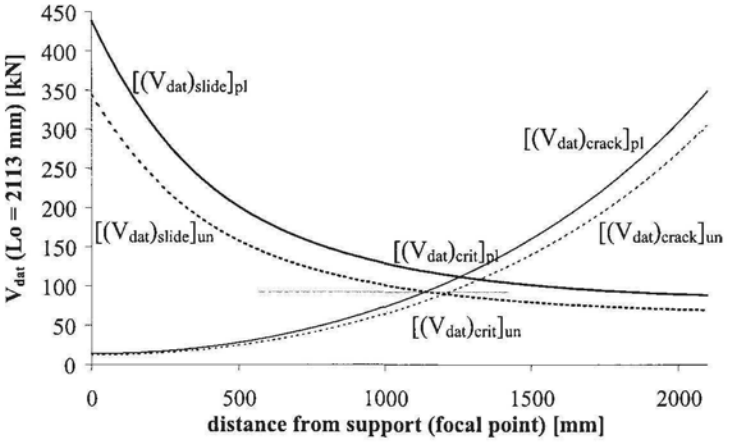

Figure 7.23 CDC analysis of FRP tension face plated beam in the hogging region

For the sake of comparison, Fig. 7.23 also shows the CDC analysis for the unplated beam, where it can be seen that $[(V_{dat})_{crit}]_{un}$ = 90 kN so that from Eq. 5.11 the increase in the concrete component of the shear capacity due to plating is $(\Delta V_{conc})_{pl}$ = 28 kN, which is a 20% increase in $(V_c)_{code}$ for the unplated beam given by national concrete standards. The increase in shear capacity is now compared with the direct approaches, which require the entire sagging region to be plated and fully anchored. Using the *mean approach* of Section 5.2.2.1 that assumes a crack inclination of 57° gives $(\Delta V_{conc})_{pl}$ = 28 kN using Eq. 5.16, which is the same as the increase predicted

using the iterative CDC analysis. From the *prestressed code approach* of Section 5.2.2.2, the increase in the concrete component of the shear capacity due to plating is 16.5 kN (Eq. 5.17), which is conservative compared to the other approaches.

In summary, all of the approaches demonstrated that the plating arrangement illustrated in Fig. 7.21 is not sufficient to increase the concrete component of the shear capacity of the beam in the hogging region to prevent CDC debonding. Hence, an alternative plating arrangement would need to be investigated to develop a valid solution.

(c) Plate extent (PE debonding)

The short term flexural rigidity of the cracked tension face plated beam is 5.87×10^{13} Nmm^2 which is 25% greater than that of the unplated section. From Eq. 6.12, the PE debonding capacity is 923 kNm which is much greater than the maximum moment capacity of 441 kN. Hence PE debonding will not occur.

As summarised in Figs 7.22(c) - (e), CDC debonding is restricting the use of this plating option. Other options must be investigated such as those described in the following sections.

7.4.3 *Hinge approach: steel side plates in +ve and –ve regions*

7.4.3.1 Strengthening option

In this example, we will determine the effect of adhesive bonding 3 mm steel plates over the full depth of the web and on both sides of the web. We will ignore moment redistribution and design for the elastic distribution of moment.

7.4.3.2 Option 10: Hinge approach, steel side plates in hogging region

(a) Flexural capacity (IC debonding)

The flexural analysis is illustrated in Fig. 7.24. Pivoting about the debonding strain of $\varepsilon_{db} = 0.02$ showed that the maximum concrete strain was greater than its crushing capacity of 0.003. Hence, the pivotal point was changed to that of the crushing strain. This gave a moment capacity of 403 kNm with a strain in the reinforcing bars of 0.0061 and that at the top of the plate of 0.0044. The extent of plating required is shown in Fig. 7.25(c).

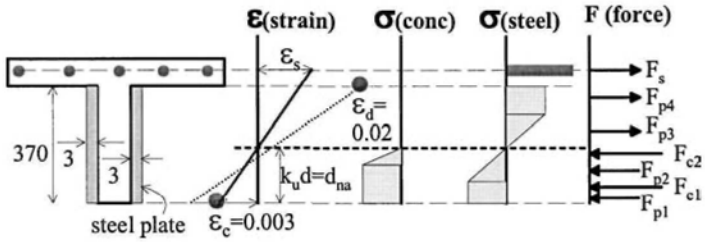

Figure 7.24 Flexural analysis of steel side plated beam in hogging region

(b) Shear capacity (CDC debonding)

As we are dealing with an elastic distribution of moment, the static moment is 1.5x403 = 605 kNm which requires an applied load of 48.4 kN/m. Hence the maximum shear force is 242 kN as shown in Fig. 7.25(a). The concrete shear capacity from a national standard is 134 kN (Section 7.4.1.3(b)) which is much less than the maximum applied shear so that there is a good chance that CDC debonding will occur.

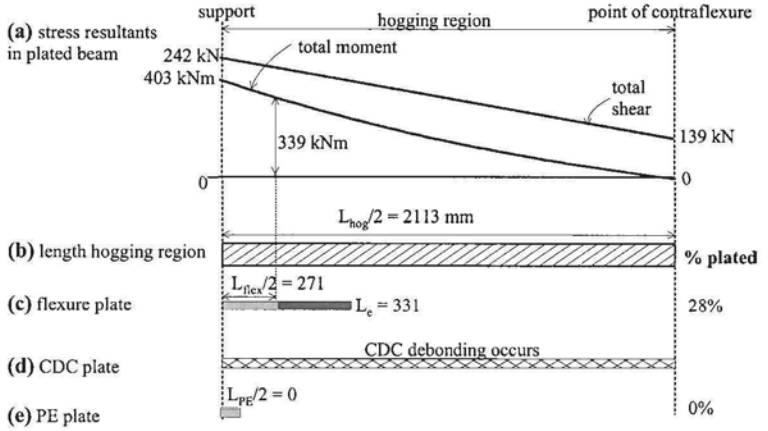

Figure 7.25 Extent of plating in hogging region – full depth steel plates

The CDC analysis procedure in Section 7.4.2.3(b) is used in this example and the results are summarised in Fig. 7.26. With P_{plate} = 666 kN, $[(V_{dat})_{crit}]_{pl}$ = 133 kN and is slightly less than V_{dat} = 139 kN, which was again taken at the point of contraflexure for convenience. Once again, CDC debonding is restricting the use of this plating option. The CDC analysis of the unplated beam is also shown in Fig. 7.26 and from this analysis, the increase in the concrete component of the shear capacity due to plating is found to be $(\Delta V_{conc})_{pl}$ = 54 kN, which is a 40% increase in $(V_c)_{code}$ of the unplated beam in the hogging region. Although the effectiveness of side plates in increasing $(V_c)_{code}$ is demonstrated in this example, it also shows the difficulty of preventing CDC debonding in the hogging region of continuous beams. One method of overcoming this difficulty is to bolt side plates, which is the topic of Section 7.5.

For comparison, the increase in the concrete component of the shear capacity of the beam in the hogging region due to plating is 50 kN using the *mean approach,* and 86 kN using the *prestressed code approach.*

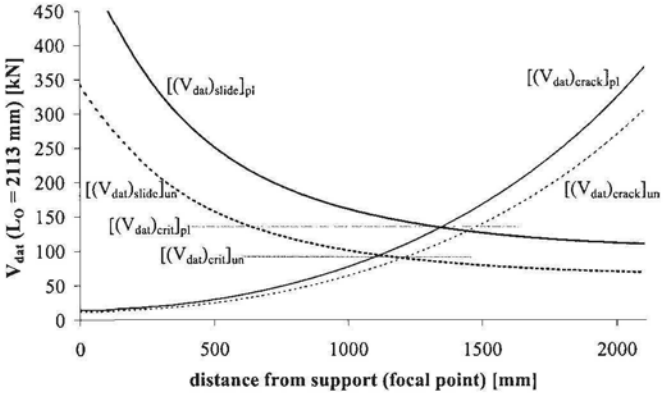

Figure 7.26 CDC analysis of full depth steel side plated beam in the hogging region

(c) Plate extent (PE debonding)
The short term flexural rigidity of the cracked tension face plated beam is 5.24×10^{13} Nmm^2. From Eq.6.10, the PE debonding capacity is 828 kNm which is much greater than the maximum moment capacity of 403 kN. Hence PE debonding will not occur.

As summarised in Figs 7.25(c) - (e), CDC debonding has once again restricted the use of this plating option in the hogging region.

7.4.3.3 Option 11: Hinge approach, steel side plates in sagging region
(a) Flexural capacity (IC debonding)
The flexural analysis is shown in Fig. 7.27. Pivoting about the debonding strain of ε_{db} = 0.02 gave a moment capacity of 277 kNm with a maximum concrete crushing strain of 0.00139. As we are dealing with an elastic distribution of moment, the maximum applied moment cannot be greater than half the maximum hogging moment (Section 7.4.3.2) of 403/2 = 202 kNm. Hence, the sagging flexural capacity is sufficient. The extent of plating is shown in Fig. 7.28(c).

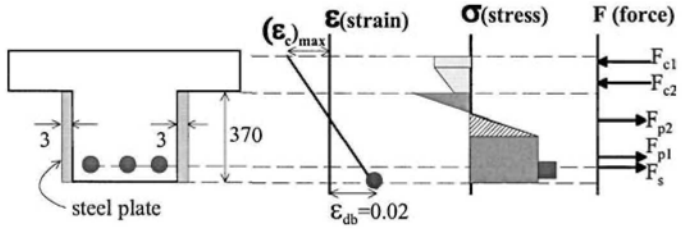

Figure 7.27 Flexural analysis of steel side plated beam in sagging region

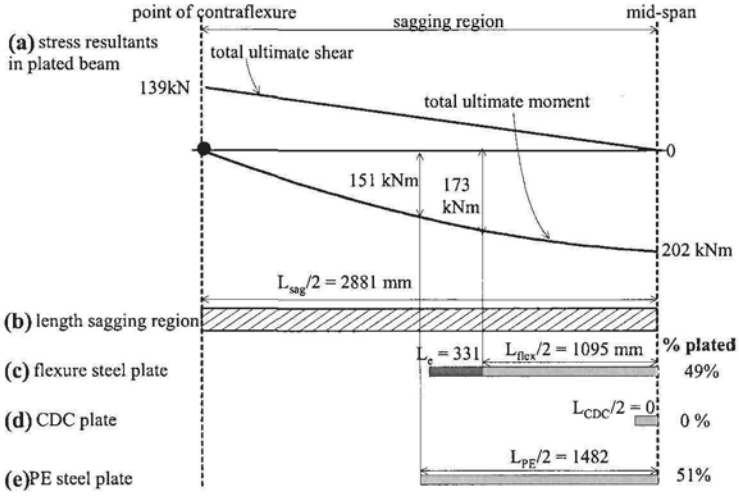

Figure 7.28 Extent of plating in sagging region – full depth steel plates

(b) Shear capacity (CDC debonding)
The CDC debonding analyses for this plating option in the sagging region is the same as that in Section 5.6.1 hence, it is not repeated here. The analyses using the indirect

CDC analysis and direct prestressed code approach demonstrated that CDC debonding will not occur. As the applied load is less in this example, the same conclusion can again be made.

(c) Plate extent (PE debonding)
The short term flexural rigidity of the cracked tension face plated beam is 5.24×10^{13} Nmm^2. From Eq. 6.10, the PE debonding capacity is 151 kNm which requires the extent of plating shown in Fig. 7.25(e).

From Figs 7.28(c) - (e) it can be seen that PE debonding governs the extent of plating for this option in the sagging region. Contrary to the hogging regions, CDC debonding was shown not to occur as the applied shear is less in the sagging region.

7.5 Continuous beam structure with bolted plates

7.5.1 *Detailed beam specifications*

In the retrofitting example of Option 10 in Section 7.4.3.2, it was found that plates could not be adhesively bonded to the hogging regions because of CDC debonding. To overcome this problem, plates will be bolted to these regions. The beam specifications are given in Section 7.4.1 and the properties of the plates are given in Section 7.3.1.4(c) for the steel plates, (d) for the aluminium plates and (e) for the prefabricated carbon/glass FRP plates.

7.5.2 Option 12: Side plates bolted to tension zone in hogging region

From Section 7.4.3.2, it is required to increase the flexural capacity to 403 kNm.

(a) Maximum flexural capacity
The analysis is illustrated in Fig. 7.29. The plate depths are fixed at 150 mm, as can be seen in Fig. 7.29(a), and the plate thickness is varied to achieve the required moment capacity. As the plates are bolted, IC debonding is no longer a problem, which leaves plate fracture and concrete crushing as possible pivotal points. As the strain capacity of steel and aluminium is vary large, the concrete crushing strain was chosen as the pivotal point in Fig. 7.29(b), and the maximum strain in the FRP plate checked to ensure that the FRP plate did not fracture prior to the concrete crushing. For a given plate thickness, the neutral axis depth d_{na} in Fig. 7.29(b) was varied until the longitudinal forces in Fig. 7.29(d) were in equilibrium. Then the resulting moment capacity was derived by taking moments of the forces in Fig. 7.29(d) about any convenient level. The plate thickness was varied until the required moment capacity was achieved. Figure 7.29(c) shows how the stress distributions are broken up into convenient shapes, such as triangles and rectangles, in which the resultant forces and their positions can be easily determined. For example, in the plate element, the stress distribution is broken into two rectangular elements and one triangular element, and the resultant forces from these three stress distributions are shown as F_{p1} to F_{p3} in Fig. 7.29(d).

Having obtained the required moment capacity in the analysis in Fig. 7.29, it is necessary to determine the stress resultants in the plate in Fig. 7.29(e) so that the bolts can be designed to transfer these stress resultants across the plate/beam interface. The sum of the plate forces F_{p1} to F_{p3} is equal to the resultant axial force in both plates P_{plate}, that is both side plates of combined thickness $2t_p$, and the moment of these plate forces about the plate centroid is equal to the moment in both plates M_{plate}.

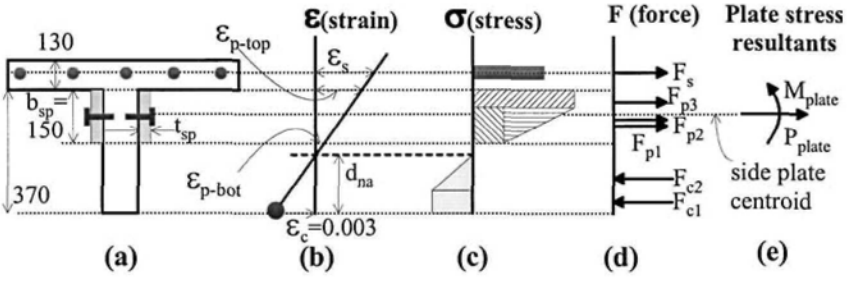

Figure 7.29 Flexural analysis of bolted side plated beams in sagging region

The results of the analyses are shown in Table 7.10. The required plate thicknesses vary from 10 mm for the steel plates to 25 mm for the carbon/glass FRP plate; the multiple 2 in the column for t_p is to remind the reader that in the analysis we are dealing with the combined thickness of plate and, therefore, the remaining values in Table 7.10 refer to a plate of thickness $2t_p$. These plates are much thicker than the 1 mm or 3 mm thick plates typically used in adhesive bonding. They need to be thicker to allow the bolts to bear against the plate to transfer the shear by dowel action and they also need to be thicker in order to resist buckling should the plate be extended into the compression zone which is not the case in this example. The strains in the reinforcing bars, ε_s in Table 7.10, show that they have yielded.

Table 7.10 Results of varying plate material

	t_{sp} mm	ε_s	$\varepsilon_{p\text{-}top}$	$\varepsilon_{p\text{-}bot}$	$(M_{cap})_{fi}$ [kNm]	ΔM_{cap} [kNm]	$(M_{cap})_{pi}$ [kNm]	P_{plate} [kN]	M_{plate} [kNm]
steel	2x10	0.0032	0.0020	0.0000	435	96	421	570	12
alum.	2x20	0.0037	0.0024	0.0002	424	85	411	486	10
FRP	2x25	0.0036	0.0024	0.0002	424	85	411	490	10

The strains at the bottom of the plate, $\varepsilon_{p\text{-}bot}$ in Table 7.10, are almost zero being close to the neutral axis. The strains at the top of the plate, $\varepsilon_{p\text{-}top}$ in Table 7.10, show that the top of the steel and aluminium plates have yielded and that the carbon/glass FRP plate is well below its fracture strain of 0.012. The moment capacities $(M_{cap})_{fi}$ are the moment capacities from the analyses illustrated in Fig. 7.29. This analysis assumes full interaction, that is the strain profile through the plate is the same as that through the RC beam as shown in Fig. 7.29(b). Because bolts require slip to resist shear, there is partial interaction and the true strain profile is illustrated in Fig. 3.33(b). It is recommended in Section 3.4.1.5 that the increase in strength due to plating, ΔM_{cap}, be reduced by 15% to allow for the reduction in strength due to partial interaction and this is shown as $(M_{cap})_{pi}$ in Table 7.10.

(b) Bolt shear connectors

Let us now determine the total shear force that has to be resisted by the bolts for the steel plate in Table 7.10 where P_{plate} = 570 kN and M_{plate} = 12 kNm; these are the stress resultants in both plates, that is the plates on either side of the RC beam as shown in Fig. 7.29(a). The derivation of the bolt shear forces is explained in Section 3.4.1.5 and illustrated Fig. 3.33(a) which is reproduced in Fig. 7.30(a) with the bolt forces for this steel plated example.

Figure 7.30(a) shows the hogging region on both sides of the position of maximum moment. The shear span lengths of 2113 mm were previously derived in Fig. 7.25(a). Because of the theoretically steep moment gradient in the hogging region, the extent of plating theoretically required is only 271mm as shown in Fig. 7.25(c); this is shown once again in Fig. 7.30(a) between the points A. Any length of plate can be chosen just as long as it is longer than 271 mm. For a comparison, the left plate has been chosen as just over 2 m long, with the distance from the position of maximum moment to the furthest bolts, which is the effective length of the plate, being 2 m. The right hand plate has an effective length of 1 m.

From Table 7.10, the axial longitudinal force P_{plate} on one shear span is 570 kN; this is the force in both plates on either side of the RC beam in that shear span. For the left shear span, the lever arm between the vertical transverse forces is 0.7x2 = 1.4 m. From Table 7.10, the moment M_{plate} = 12 kNm, therefore, the transverse force is 12/1.4 = 9 kN. Hence, the total bolt shear force in the left shear span is 570+(2x9) = 588 kN. This is the shear force transmitted by the bolts in both plates in a shear span. Therefore, the shear force per plate is 588/2 = 294 kN. If we assume that the bolt shear connectors have a shear capacity of 20 kN, then the number of bolts required is 294/20 = 14.7. Let us use 2 rows of bolts with 8 bolts per row. Then the longitudinal spacing would be 266 mm and with a transverse spacing of about 75 mm.

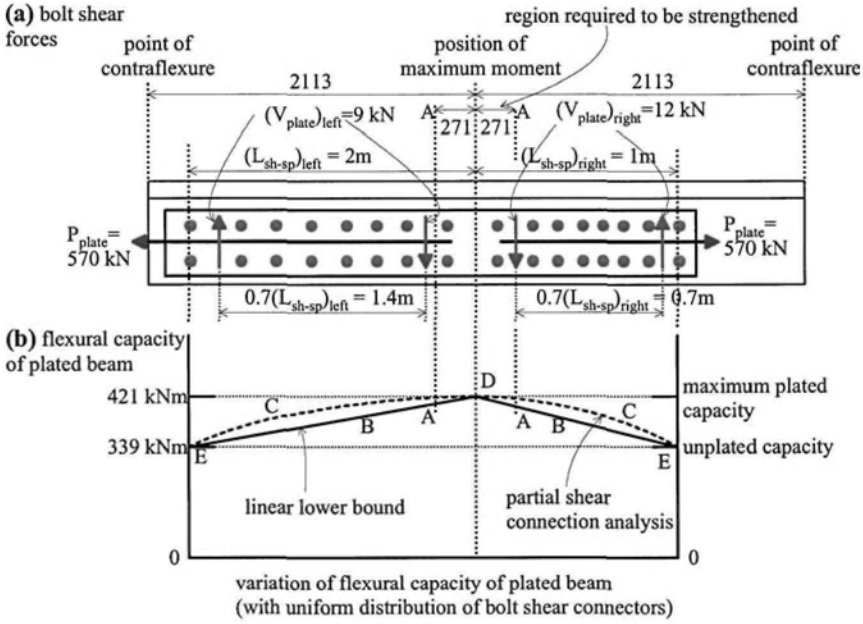

Figure 7.30 Dowel forces on bolt shear connectors

For the right hand shear span in Fig. 7.30, the total shear force is 570+(2x12/0.7) = 604 kN. This will require 604/2/20 = 15.1 bolts. Hence two rows of 8 bolts with a longitudinal spacing of 133mm. The total number of bolts required is 64. In this example, the transverse forces are relatively small compared with the longitudinal forces because the depth of the plate is quite shallow. This is not always

the case, as deeper plates can actually reduce the longitudinal force and attract more moment and hence increase the transverse force.

(c) Variation in flexural capacity

At the position of maximum moment, the moment capacity is that of the plated beam of 421 kNm from Table 7.10, which is shown as point D in Fig. 7.30. At the plate ends at point E, the moment capacity is that of the unplated beam of 339 kNm. Between these extremities, the moment capacity varies such as shown by the curves marked C. To determine the variation in curves C, partial shear connection theory has to be applied (Oehlers and Bradford 1995, 1999). However, a lower bound to the moment capacity is given by the linear variations marked B which can be used in design, just as long as there is a uniform distribution of the bolt shear connectors as shown in Fig. 7.30(a), otherwise, partial shear connection theory will have to be applied. It can be seen in Fig. 7.30(b) that extending the plates beyond the theoretical requirement of 271 mm given by the points A-A has ensured that the moment capacity at point A on curve B is greater than that required of 339 kNm.

7.5.3 Option 13: Deep side plates bolted in hogging region

In Option 12 in Section 7.5.2, shallow plates were used to strengthen the beam as this ensured that the plates remained in the tensile zone and, hence, buckling did not have to be considered. We will now plate the whole web, so that part of the plate goes into compression in order to illustrate the effect on the bolt shear connectors. We will ignore buckling although research has been published to position the bolts so that the plate does not buckle (Smith, Bradford and Oehlers 1999, 2000).

(a) Maximum flexural capacity

The flexural analysis is similar to that described in Section 7.5.2, the difference being that the side plates now extend to the compression face of the beam and hence, the compressive stresses in the plate must be considered as shown in Fig. 3.44. The flexural analysis has already been described in Section 3.5.3.1 and summarised in Table 3.5 and is not repeated here.

Comparing the full interaction results of the steel side plated beams in Tables 3.5 and 7.10, the 150 mm deep plate increased the moment capacity by 28%, whereas the 370 mm deep steel side plate increased the moment capacity by 59%. Furthermore, the curvature at failure for the 150 mm deep plate is $1.3\text{x}10^{-5}$ mm^{-1}, compared to $1.8\text{x}10^{-5}$ mm^{-1} for the 370 mm plate. Hence, the full depth steel plate is more effective in increasing the moment capacity of the beam and also improves the ductility.

It may be expected that the moment in the plates M_{plate} is bigger in the 370 mm deep side plates (190 kNm in Table 3.5) compared to that of the 150 mm deep plates (12 kNm in Table 7.10) because the moment capacity is bigger. However, it is interesting to note that the axial force in the plates P_{plate} is considerably less with the 370 mm deep side plates (220 kN in Table 3.5), because the resultant axial tensile and compressive forces in the plate (Fig. 3.44) tend to cancel each other out, compared with the 150 mm deep side plates (570 kN in Table 7.10). The influence this has on the number of bolt shear connectors required is described in the following section for the steel plated beam.

(b) Bolt shear connectors

From Table 3.5 for the 370 mm deep steel side plate, M_{plate} = 190 kNm and P_{plate} = 220 kN. For the sake of comparing the number of bolt shear connectors required with the 150 mm deep steel side plate, the same extent of plating shown in Fig. 7.30 will be used; that is, 2 m in the left shear span and 1 m in the right shear span.

The lever arm between vertical transverse forces in the left shear span is 1.4 m as shown in Fig. 7.29 and therefore, the transverse force is 190/1.4 = 136 kN. Hence, the total bolt shear force per plate in the left shear span is (220/2) + (2x136/2) = 246 kN. As in Section 7.5.2(b), a bolt shear connector shear capacity of 20 kN is assumed and therefore, the number of bolts required is 246/20 = 12.3. Hence, for strength requirements, 2 rows of 7 bolts per row are required, which is two bolts less than that required for the 150 mm deep plate in the left shear span.

Comparing with the right shear span, the total bolt shear force per plate is (220/2) + (2x190/0.7/2) = 381 kN. The total number of bolts required in the right shear span is 381/20 = 19.1, which can be arranged in 2 rows of 10 bolts per row, four more than that required for the right shear span of the 150 mm deep plate.

In summary, the total number of bolt shear connectors required in each arrangement is similar, with 68 for the 370 mm deep steel plates and 64 for the 150 mm deep steel plates, even though the moment capacity is increased significantly more using the 370 mm deep steel plate. Because the 370 mm deep steel plate extends into the compression region of the beam, the spacing of the bolts must also be designed to prevent buckling of the plate.

7.6 References

Ochlers, D. J. and Bradford, M. A. (1995)."Composite Steel and Concrete Structural Members: Fundamental Behaviour." Pergamon Press, Oxford.

Oehlers, D.J. and Bradford, M.A. (1999) "Elementary behaviour of Composite Steel and Concrete Structural Members". Butterworth Heinemann, Oxford, September.

Smith, S.T., Bradford, M.A. and Oehlers, D.J. (1999) "Local buckling of side-plated reinforced concrete beams. Part 1: Theoretical study. ASCE Structural division, Journal of Structural Engineering, June. 622-634.

Smith, S.T., Bradford M.A. and Oehlers, D.J. (2000) "Unilateral buckling of elastically restrained rectangular mild steel plates". Journal of Computational Mechanics, Vol.26, No.4, 317-324.

Index